

**This is an electronic reprint of the original article.  
This reprint *may differ* from the original in pagination and typographic detail.**

**Author(s):** Eronen, Tommi; Kankainen, Anu; Äystö, Juha

**Title:** Ion traps in nuclear physics : recent results and achievements

**Year:** 2016

**Version:**

**Please cite the original version:**

Eronen, T., Kankainen, A., & Äystö, J. (2016). Ion traps in nuclear physics : recent results and achievements. *Progress in Particle and Nuclear Physics*, 91, 259-293.  
<https://doi.org/10.1016/j.pnnp.2016.08.001>

All material supplied via JYX is protected by copyright and other intellectual property rights, and duplication or sale of all or part of any of the repository collections is not permitted, except that material may be duplicated by you for your research use or educational purposes in electronic or print form. You must obtain permission for any other use. Electronic or print copies may not be offered, whether for sale or otherwise to anyone who is not an authorised user.

## Accepted Manuscript

Ion traps in nuclear physics — recent results and achievements

Tommi Eronen, Anu Kankainen, Juha Äystö

PII: S0146-6410(16)30043-6

DOI: <http://dx.doi.org/10.1016/j.pnpnp.2016.08.001>

Reference: JPPNP 3619

To appear in: *Progress in Particle and Nuclear Physics*



Please cite this article as: T. Eronen, A. Kankainen, J. Äystö, Ion traps in nuclear physics — recent results and achievements, *Progress in Particle and Nuclear Physics* (2016), <http://dx.doi.org/10.1016/j.pnpnp.2016.08.001>

This is a PDF file of an unedited manuscript that has been accepted for publication. As a service to our customers we are providing this early version of the manuscript. The manuscript will undergo copyediting, typesetting, and review of the resulting proof before it is published in its final form. Please note that during the production process errors may be discovered which could affect the content, and all legal disclaimers that apply to the journal pertain.

# Ion Traps in Nuclear Physics — Recent Results and Achievements

Tommi Eronen, Anu Kankainen and Juha Äystö

*University of Jyväskylä, P.O. Box 35 (YFL), FI-40014 University of Jyväskylä, Finland*

## Abstract

Ion traps offer a way to determine nuclear binding energies through atomic mass measurements with a high accuracy and they are routinely used to provide isotopically or even isomerically pure beams of short-living ions for post-trap decay spectroscopy experiments. In this review, different ion-trapping techniques and progresses in recent nuclear physics experiments employing low-energy ion traps are discussed. The main focus in this review is on the benefit of recent high accuracy mass measurements to solve some key problems in physics related to nuclear structure, nuclear astrophysics as well as neutrinos. Also, several cases of decay spectroscopy experiments utilizing trap-purified ion samples are summarized.

*Keywords:* ion traps, atomic masses, trap-assisted spectroscopy

## 1. Introduction

Progress of ion manipulation technologies in ion traps has opened exciting opportunities for solving fundamental questions in atomic and nuclear physics. Calculation of electron binding energies in atoms using the well-known theory of QED (Quantum Electrodynamics) can be performed with accuracies of the order of a few eV for almost any atom. To be sensitive in this level in atomic mass itself, a relative mass uncertainty of the order of  $10^{-10}$  or better is required. Experimentally this precision is already reached for stable isotope masses [1–3].

The calculation of the nuclear binding, however, has to rely on less accurately quantifiable strong interaction derived from the theory of QCD (Quantum Chromodynamics). The mass  $M$  of a neutral atom can be expressed as

$$M = N \times m_n + Z \times m_p + Z \times m_e - (B_{\text{atom}} + B_{\text{nucleus}})/c^2, \quad (1)$$

where  $N$  and  $Z$  are the neutron and proton number and  $m_p$ ,  $m_n$  and  $m_e$  are free proton, neutron and electron masses, respectively.  $B_{\text{atom}}$  and  $B_{\text{nucleus}}$  are the total electron and nuclear binding energies, respectively. At best, the total mass (or binding energy, see Chapter 3.1) of an atom can presently be calculated to an accuracy

of the order of a few 100 keV which corresponds to a relative mass uncertainty  $\Delta m/m$  of the order of  $10^{-6}$  only, which is several orders of magnitude less precise than for atomic binding energies. Therefore in nuclear physics, in general, the required experimental accuracies are currently less stringent than in atomic physics. This is particularly true when comparing experimental data with theoretical model predictions for absolute masses and the effects of global correlations on masses.

However, the first- and second-order differentials of masses can serve as sensitive indicators of local behavior of collective or single particle structures with changing proton and/or neutron numbers. In fact, the measurement accuracy required for those observables is of the order of 10 keV or better, and is comparable to that routinely available in spectroscopy of nuclear excited states. This opens up interesting perspectives for studying the binding energy systematics for the excited states as well. The observables, for example, include nucleon or nucleon pair binding energies,  $Q$ -values for radioactive decays, isomer masses, pairing gaps and shell gaps. Some examples of differentials and their typically required accuracies are given in Table 1 together with related key physics topics.

In this review, we wish to introduce the newest developments in ion trapping techniques for nuclear physics. The emphasis in the review is in the use of Penning-

Table 1: Required accuracies for different nuclear physics motivations.

| Physics motivation                                     | Accuracy        |
|--|-----------------|
| <b>Nuclear structure</b>                               |                 |
| Global correlations                                    | a few 100 keV   |
| Local correlations                                     | $\leq 10$ keV   |
| Evolution of shell structure, pairing and collectivity | $\leq 10$ keV   |
| Drip-line phenomena, halos, isomers                    | $\approx 1$ keV |
| Nuclear astrophysics                                   | $\geq 1$ keV    |
| Charge symmetry in nuclei                              | $\leq 1$ keV    |
| <b>Fundamental symmetries</b>                          |                 |
| Tests of the Standard Model                            | $\leq 100$ eV   |
| $\beta$ decay and electroweak interaction              | $\leq 100$ eV   |
| CVC theory and the unitarity of the CKM matrix         | $\leq 100$ eV   |
| Double $\beta$ decay                                   | 10 – 1000 eV    |
| Neutrino mass and mass hierarchy problem               | $\ll 100$ eV    |

trap technique for high-precision mass measurements as well as in their use as high-resolution mass separators to produce high-purity isotopic or isomeric sources for decay spectroscopy of exotic nuclei. It will be shown that these techniques have opened up unique possibilities for high-precision measurements of rare isotopes of practically all chemical elements down to half-lives of few ms and production rates on the order of few ions per hour.

Then, we move on to present an update of recent progresses of direct mass measurements of neutron-rich nuclei covering a wide range of the chart of nuclei between mass numbers  $A = 10$  and  $A = 250$ . The mass data will mainly be discussed in the framework of mass differentials, such as nucleon and nucleon-pair binding energies, pairing gaps and shell gaps. A comparison with some selected theoretical models will be discussed. In addition, a special class of high-precision measurements of isobaric mass doublets and isotopic mass multiplets will be presented. Finally, a novel technique of trap-assisted decay spectroscopy is introduced with applications on beta, gamma, conversion electron and  $\beta$  delayed neutron studies.

## 2. Ion trap techniques

Every major radioactive ion beam facility in the world utilizes ion traps. Their role is not just in mass measurement and separation but also as ion beam preparatory devices like ion bunchers, which convert continuous ion beam into a sequence of ion packages (bunches) [4].

The traps can be categorized to electrostatic traps, electric radiofrequency (RF) traps and Penning traps that employ a combination of homogenous magnetic

field and electrostatic potential [5]. This section gives an overview of different trap types and their uses in nuclear physics studies.

### 2.1. Radiofrequency cooler-bunchers

It is quite common that radioactive ion beams after their production and extraction from the source have rather poor ion optical properties and commonly are continuous in nature. Both of these properties are rather unsuitable for ion traps that require ions almost at rest.

To meet the ever-increasing requirements of ion traps, gas-filled radiofrequency cooler-bunchers (RFQCBs) have been developed for this task. The ions from the source are first decelerated to  $\sim 100$  eV and then injected to an RF-multipole (most commonly a quadrupole) structure that keeps the ions confined between the rods. The space between the rods is filled with dilute gas (usually helium at pressure of about 0.1 mbar) to allow for the reduction of the width of the ions' kinetic energy distribution (ion cooling). The ions collide with gas atoms and consequently lose energy and are centered to the RF electric field axis. Finally, using additional fine (on the order of 0.1 V/cm) DC-gradients, the cooled ions are collected to a potential well, from where they are swiftly released by switching the trap potentials. This is illustrated in Fig. 1.

These devices allow ions to be released downstream to trap experiments as short, well cooled, bunches. These devices have existed for a while now (see for example Refs. [7–9]) and are still in active use. The new devices built after the first-generation experiments have been concentrating on improving throughput of ions like CARIBU buncher [10] at Argonne National laboratory or preparations for DESIR at SPIRAL2 [11].

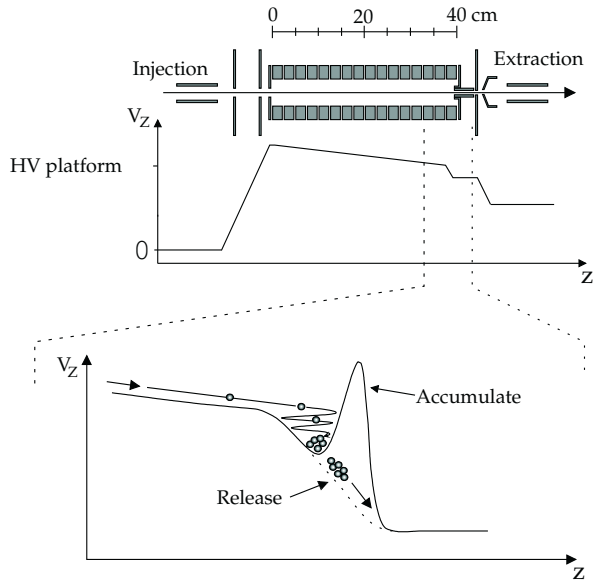


Figure 1: Schematic principle of an RFQCB (used at JYFLTRAP). The ions having  $30 \dots 60q$  keV of energy are electrostatically slowed down by setting the RFQ at a high voltage (HV) platform and injected into the gas-filled RF structure with about  $\sim 100$  eV of energy. Ion-atom collisions cool the ions. Finally the ions are collected into an axial potential well, from where they are released as a short bunch downstream. This figure is from Ref. [6].

RFQ cooler-bunchers are used in two rather distinctive modes of operation. One is preparation of ion bunches that, upon extraction, have extremely small energy spread (below 1 eV) but have rather long bunch size (typically few  $\mu$ s). Low energy spread is ideal for *e.g.* collinear laser spectroscopy [12, 13] and also is suitable even with long temporal length for Penning traps. The other RFQ operating mode is to provide temporally short (typically 10-100 ns) bunches but this comes with the expense of increased energy spread. This type of bunches are needed for multi-reflection time-of-flight separators [14–16].

## 2.2. Paul traps

Paul trap is a very simple type of ion trap, which utilizes radiofrequency (RF) electric fields to form a confining potential [17]. These type of traps are ideal for studying properties that require ions to be nearly "free floating". Such conditions are needed, *e.g.* for studying kinematics of radioactive decay. These type of studies require rather elaborate trap geometry designs to allow access for various types of detectors. A pioneering LPCTRAP serves as a good example, see Refs. [18, 19]. Schematic of the experiment is shown in Fig. 2.

The LPCTRAP at GANIL [18] and BPT at Argonne

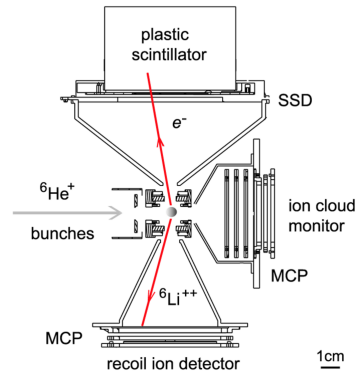


Figure 2: Schematic overview of the LPCTRAP. The ions under study are captured to a small volume of the trap, where the RF field keeps the ions confined. When a  $\beta$  decay occurs, the emitted electron or positron is detected with a position sensitive silicon strip detector (SSD) combined with a plastic scintillator. The recoiling ion is detected with a micro channel plate (MCP) detector. From the position of the  $\beta$  particle and the time-of-flight of the recoil the neutrino energy spectrum can be reconstructed. This figure is from Ref. [19].

National Laboratory [20] are Paul traps that have been developed to determine  $\beta$ - $\nu$  angular correlations in  $\beta$  decays and to study  $\beta$ -delayed neutron emission [21]. The decays will occur in a very small volume ( $\sim 1$  mm<sup>3</sup>) and since the decay occurs nearly at rest and in free space, the kinematics can be reconstructed rather accurately. In a  $\beta$  decay, the neutrino will go undetected but the momenta it carried away can be reconstructed from the detection of the emitted electron and the recoil daughter ion. Similarly, in case of a neutron emission, there is no need to detect the neutron but the energy carried away by the neutron can be reconstructed from the kinetic energy of the recoiling ion.

## 2.3. Penning traps

The best mass measurement accuracy and also the best mass resolving power is provided by Penning traps [22]. A Penning trap consists of a strong homogenous magnetic field and a weak quadrupolar electrostatic potential. Such a configuration confines a charged particle in all three spatial directions. In the absence of any electric field, ion undergoes cyclotron motion in a homogenous magnetic field with a so-called free-space cyclotron frequency

$$\nu_c = \frac{1}{2\pi} \frac{q}{m} B, \quad (2)$$

where  $q$  and  $m$  are the charge and mass of the particle and  $B$  the magnetic field. This relation gives a direct link between charge-over-mass and *frequency*. However, a homogenous magnetic field only offers ion confinement

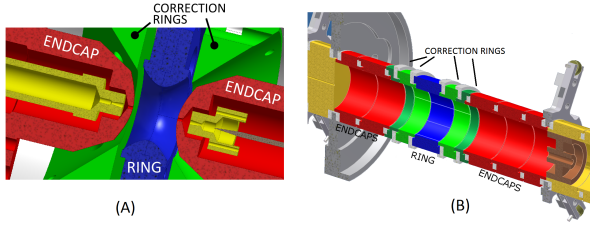


Figure 3: Hyperbolic (A) and cylindrical (B) Penning traps (Tritium-<sup>3</sup>He trap from Heidelberg, Germany [23] and JYFLTRAP [24], respectively). With both configurations a quadrupolar electric potential can be formed. In both cases additional compensation (correction) electrodes are needed to correct for the truncation of electrodes and unideal geometry. Some components have been stripped for clarity.

in two spatial directions. To achieve full confinement, a quadrupolar electrostatic potential is added in order to restrict ion movement along the magnetic field axis. Commonly hyperbolic or cylindrical electrodes are used as illustrated in Fig. 3.

With an added quadrupolar electrostatic potential, the ion will exhibit *axial motion* with frequency

$$\nu_z = \frac{1}{2\pi} \sqrt{\frac{qV_0}{md^2}} \quad (3)$$

and two *radial motions* with frequencies

$$\nu_{\pm} = \frac{1}{4\pi} \left( \nu_c \pm \sqrt{\nu_c^2 - 2\nu_z^2} \right). \quad (4)$$

The axial motion with frequency  $\nu_z$  along the magnetic field lines depends (in addition to ion  $q/m$ ) on the applied trapping potential  $V_0$  and the geometry described with the characteristic trap dimension  $d$ . The two radial motions are called cyclotron motion with frequency  $\nu_+$ , which is commonly called trap-modified cyclotron frequency, and magnetron motion with frequency  $\nu_-$  [25]. To get the free-space cyclotron frequency (Eq. (2)) out of these, one can utilize the invariance theorem [26]

$$\nu_c^2 = \nu_-^2 + \nu_z^2 + \nu_+^2 \quad (5)$$

or the radial sideband frequency

$$\nu_c = \nu_+ + \nu_-, \quad (6)$$

which is commonly used in nuclear physics measurements. The former, Eq. (5), is accurate even with small misalignments and inhomogeneity present and is commonly used in the most highest precision mass spectrometry reaching accuracies better than  $10^{-11}$  [1]. The latter, Eq. (6), requiring only the sum of the two radial frequencies to be determined, is commonly used in mass measurements for short-lived nuclei. Recently, mass-over-charge doublets have been measured at  $10^{-10}$  level [27] and non-doublets at  $10^{-8}$  level [28].

To measure an absolute atomic mass through Eq. (2), a well known calibration mass is needed since there is no way to otherwise determine  $B$  accurately enough. To this end, a Penning trap provides *frequency ratios* and, with proper treatment of the data, *atomic mass ratios*. Ideally, clusters of <sup>12</sup>C ions would be used [29], giving a calibration point every 12 mass units. There are also other suitable reference ions, whose masses have been determined very accurately, such as often used <sup>133</sup>Cs or <sup>85</sup>Rb.

If the ion of interest and reference ion masses are several mass units away, the frequency ratio is prone to so-called mass-dependent frequency shifts [30, 31]. These are due to imperfections in the electrostatic potential and homogenous magnetic field and depend on the motional amplitudes of the trapped ion.

### 2.3.1. Mass doublet technique

Especially in decay  $Q$ -value measurements where both parent and daughter have same mass number  $A$ , the aforementioned systematic shifts cancel out in the frequency ratio when both ions have equal starting conditions prior to ion motion excitations. Typically these shifts become small compared to statistical uncertainty [32]. To obtain a  $Q$ -value from a frequency ratio, a simple equation (for singly charged ions, omitting electron binding energies) can be used:

$$Q = (r - 1)(M_d - m_e)c^2, \quad (7)$$

where  $r$  is the daughter/parent ions' frequency ratio  $r = \nu_c^d/\nu_c^p$ ,  $M_d$  the atomic mass of the daughter and  $m_e$  the mass of an electron. Typically with  $Q$ -values of some MeV, the term  $r - 1 < 10^{-3}$ . This factor also reflects the cancellation of systematic shifts in the  $Q$ -value and the uncertainty contribution from the daughter mass. It is easy to generalize Eq. (7) for other charge states and to take electron binding energies into account.

This doublet technique has been extensively used in measurements of  $Q$ -values of superallowed  $\beta$  emitters (see Ref. [33] and references therein),  $Q$ -value measurements of double beta decay and double electron capture decays [34].

### 2.3.2. The time-of-flight ion-cyclotron resonance technique

To date, most of the atomic mass determinations for short-living ions with Penning traps are done with the so-called time-of-flight ion-cyclotron resonance technique (TOF-ICR) [35, 36]. Here, a radiofrequency (RF) electric field in quadrupolar configuration around the cyclotron frequency of Eq. (2) is applied for a certain

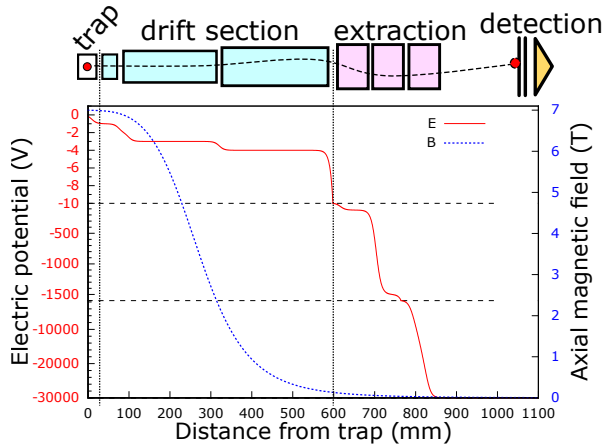


Figure 4: Extraction side of JYFLTRAP showing schematic extraction electrodes, electrostatic potential for extraction mode and the axial magnetic field. When the ions are extracted from the trap, they first pass the so-called drift section that has only few eV lower potential than the trap itself. Since the magnetic field has a rather big gradient there, the ions' radial energy gets converted to axial energy. After this slow drift section the ions are accelerated to 30 qkeV of energy and finally detected with a microchannel plate detector (MCP).

duration (usually dictated by the half-life of the ion-of-interest or for practical reasons capped to few seconds). With a given amplitude, such a field will periodically convert motion from cyclotron to magnetron and vice versa. The conversion is strongest at the sideband frequency of Eq. (6). Typically the amplitude is chosen so that only one full conversion happens at this frequency. Before this RF excitation, ions are prepared to have some amplitude in magnetron motion, e.g., by applying a dipolar RF electric field or using a Lorenz steerer [37].

After excitation, the ions are released from the trap towards a detector that is outside of the strong magnetic field of the trap (see Fig. 4). The radial energy gets converted to axial in the field gradient, and thus, the ions that have more radial energy (larger cyclotron motion orbit) will reach the detector earlier.

Repeating the measurement for different excitation frequencies, a TOF resonance curve is obtained as shown in Fig. 5. At resonance, the ions possess maximal radial energy, and thus, they are the first to reach the detector. At other frequencies, the conversion is only partial, defined by the excitation amplitude profile. The resonances shown in Fig. 5 is obtained with conventional excitation pulse, *i.e.* the excitation is switched on for a certain duration  $T_{RF}$  and off again while keeping the amplitude during the excitation constant.

The width of the resonance is inversely proportional to the excitation time, evident also from Fig. 5. With

longer excitation time the resonance becomes narrower and the frequency of the center can be obtained with better precision. In the resonances shown one can also see the motion damping gets worse with longer excitation times. That is, ions collide with rest gas molecules, and consequently, the resonance becomes less pronounced. With measurements of short-living nuclei, also the half-life imposes a limit to the excitation time.

#### Precision boosting methods

An advanced version of the conventional excitation is the **Ramsey's method of time-separated oscillatory fields**. Instead of applying a constant amplitude for the whole duration of the excitation, the application of the RF is split to two or more excitation pulses interleaved with waiting periods [38]. Usage of two pulses with a waiting period in between boosts the frequency determination precision by a factor of three when same total duration is used for the excitation pattern. The waiting period need to be much longer than the two excitation pulses (e.g. a pattern of 100-700-100 ms on-off-on) in order to get the full benefit of this technique. Ramsey's method has become the norm - nearly all mass measurements utilizing TOF-ICR technique have been performed using Ramsey's method of time-separated oscillatory fields in the recent past [39].

Other precision boosting methods have also been developed. One candidate is **octupolar excitation**. This method has been studied extensively (see e.g. Refs. [40, 41]) and also used in some mass measurements like in  $Q$ -value measurement of double-electron capture in  $^{164}\text{Er}$  at SHIPTRAP [42]. The experiment would have been impossible with the quadrupole excitation even when Ramsey-type excitation would have been used due to the very low mass difference of the two states.

Octupolar excitation utilizes an 8-pole RF field instead of the quadrupole. The gain factor in mass resolving power between quadrupolar and octupolar excitations is about a factor of ten - much larger than the naively expected factor of two due to doubling of the poles and hence the frequency. It was found out that the lineshape depends strongly on the initial phases and amplitudes of the ion motion and the octupolar field. For this reason, the octupolar excitation has not been used so extensively in experiments as it takes rather long to prepare the experiment for each particular case.

It is worth noting the full width at half maximum of the TOF-resonance is always constant independent of the mass-over-charge of the ion. A way to increase the frequency, and thus to improve the precision of the cyclotron frequency measurement, is to strip more electrons out from the ions. In principle, the precision in-



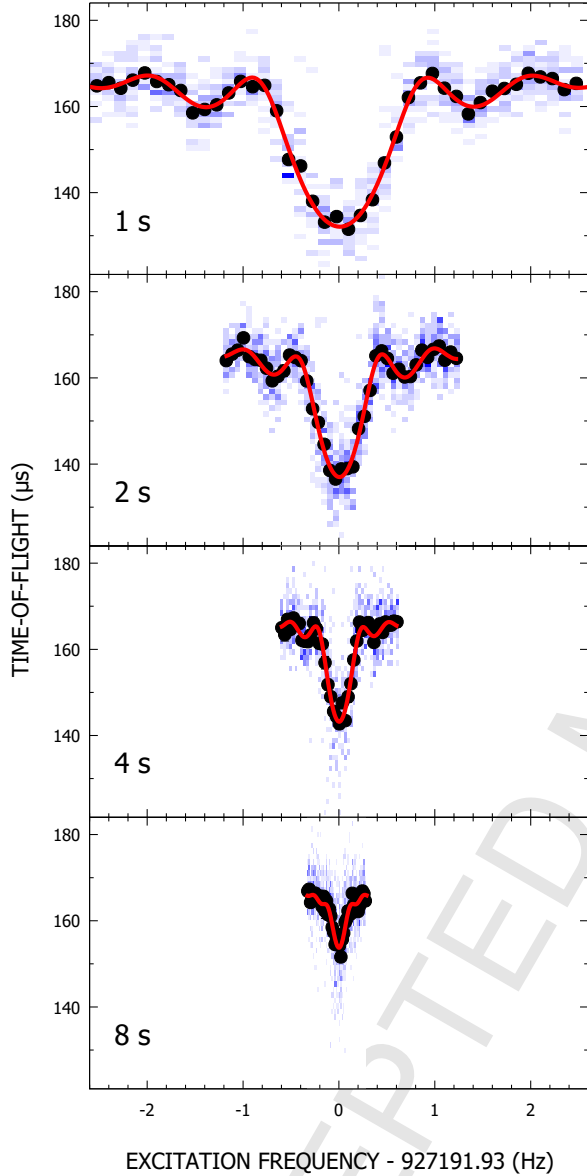


Figure 5: Time-of-flight resonance curves for different excitation ( $T_{RF}$ ) times as shown in the panels. Black points are the experimental TOF values and red curves are fit to the data. The blue pixels show the scatter of data; darker the pixel, more ions was observed. Each resonance were measured with  $^{116}\text{Sn}^{1+}$  ions at JYFLTRAP. One can see that the width of the resonance gets narrower when longer excitation times are used. Additionally, motional damping is evident from the decrease of TOF for ions in resonance. See text for more explanation.

329 creases proportionally to the charge of the ion but in  
 330 practice charge exchange reactions and difficulties in  
 331 preparing the ions becomes more and more difficult  
 332 with increased charge state. **Charge breeding** is cur-  
 333 rently pursued at TITAN trap [43]. Other limiting fac-  
 334 tors aside, at some point with high enough charge state  
 335 the precision of the binding energy of the stripped elec-  
 336 trons become the limiting factor in mass determination.  
 337 Or, put other way around, Penning traps can be used to  
 338 determine the binding energy.

#### 339 2.4. Phase-imaging cyclotron resonance technique

340 The most promising and already demonstrated Pen-  
 341 ning trap mass measurement technique at the moment  
 342 is the so-called *phase-imaging cyclotron resonance* (PI-  
 343 ICR) technique developed at SHIPTRAP [44, 45]. In-  
 344 stead of relying on the energy conversion like in the  
 345 TOF-ICR method, the new method is based on determi-  
 346 nation of ion motional phases with a spatially resolving  
 347 micro channel (MCP) plate detector. This technique is  
 348 thoroughly explained in Ref. [45].

349 In practice, the method is used to determine either  
 350 the magnetron  $\nu_-$  and modified cyclotron  $\nu_+$  frequency  
 351 separately, or alternatively the cyclotron frequency  $\nu_c$   
 352 (see section 5 of Ref. [45]) by determining the final  
 353 phase of the motion in question. Axial motion is not  
 354 measured but cooled to minimal amplitude to minimize  
 355 frequency shifts and ion scatter due to collisions with  
 356 rest gas molecules.

357 Only the magnetron motion phase can be directly pro-  
 358 jected to the MCP detector since the magnetron period  
 359 is much longer than the time-of-flight of the ions to the  
 360 MCP resulting in a well defined spot in the detector. In  
 361 the case of high-frequency cyclotron motion, direct de-  
 362 termination of the cyclotron phase is not possible. In-  
 363 stead of a well defined spot a ring is observed. To get the  
 364 phase of the fast cyclotron motion a short quadrupole  
 365 excitation pulse is applied to convert cyclotron motion  
 366 to slow magnetron motion and consequently its phase  
 367 can be determined. In addition, to obtain a distortion-  
 368 free phase image, the ion path from the trap to the MCP  
 369 detector needs to be electric field free.

370 Compared with the TOF-ICR technique using Ram-  
 371 sey excitation scheme, this technique is an astonishing  
 372 factor of 25 faster and provides a 40-fold gain in res-  
 373 solving power. Very recently mass difference of  $^{163}\text{Ho}$   
 374 and  $^{163}\text{Dy}$  was measured at SHIPTRAP with the new  
 375 method providing a mass ratio at  $10^{-10}$  precision level  
 376 surpassing any TOF-ICR measurements [27].

377 This technique is now being implemented in other  
 378 Penning trap experiments. It is clear that such precision  
 379 requires the ions in the trap to be prepared extremely



well in order to avoid amplitude-dependent frequency shifts. Although this method boosts the precision or reduces the frequency measurement time, preparation time for the measurement will be considerably longer than for TOF-ICR. Also, in order to utilize the method, the cyclotron frequency needs to be known to some precision so that the measured phase can be correctly assigned to the period preceded by *known* number of full periods. In case of short-lived ions of unknown mass, it is necessary to first obtain a rough frequency with the ordinary TOF-ICR technique. For example  $A/q = 100$  ions in 7 T field have about 1 MHz cyclotron frequency. In order to know the number of full periods the ions have circulated after phase accumulation time of 1 second, the mass needs to be known better than  $10^{-6}$  precision ( $100 \text{ keV}/c^2$ ).

### 2.5. Gas-filled Penning trap for beam purification

Perhaps the most used beam purification technique for short-lived rare ions is the sideband cooling technique developed nearly three decades ago at ISOLTRAP [46]. By filling a Penning trap with low-pressure gas ( $10^{-5}$  mbar), the amplitudes of the fast modified cyclotron and axial motions gets damped. The amplitude of the magnetron motion, on the other hand, slowly increases.

The recipe for mass-selective cleaning in a buffer-gas filled Penning trap is rather simple (example duration given in parenthesis, case dependent):

1. cooling (50 ms)
2. magnetron excitation (5 ms or simultaneously with quadrupole excitation)
3. mass-selective quadrupolar excitation (100 ms)
4. cooling (30 ms)
5. extract through narrow aperture ( $10 \mu\text{s}$ ).

The first step simply reduces the axial amplitude of the ions due to ion collisions with buffer gas atoms. The second step increases the magnetron motion diameter of all ions. The magnetron orbit diameter needs to become larger than the diameter of the extraction hole aperture in order for this cleaning technique to work.

The third step is where the mass selectivity comes into play. The excitation frequency is set to be the ion cyclotron frequency (Eq. (2)) and thus the magnetron motion for the ions of interest with some frequency bandwidth gets converted to cyclotron motion. The subsequent cooling period cools the cyclotron motion and thus ions of interest have now both their magnetron and cyclotron motion mostly removed. Once the bunch is extracted through an electrode having a narrow aperture

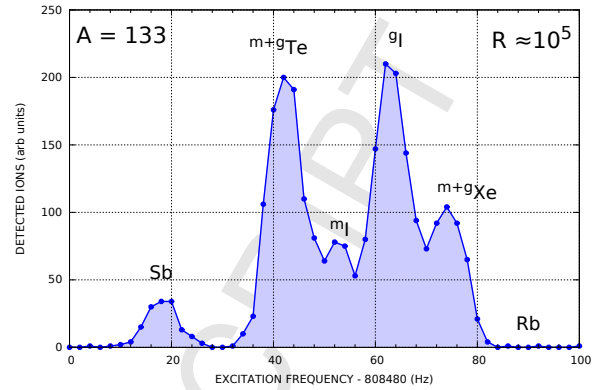


Figure 6: An example frequency scan utilizing sideband cooling method of Ref. [46] using JYFLTRAP’s gas filled purification trap [24]. The ions were produced in proton induced fission of uranium. The scan shows the various isotopes and isomers produced. A mass resolving power  $M/\Delta M$  of about  $10^5$  is obtained. Both  $^{133}\text{Te}$  and  $^{133}\text{Xe}$  have low-lying isomeric states, which can’t be fully separated with this method.

(see Fig. 3 (B), electrode on far left) only the ions of interest can pass and the contaminants hit the electrode.

The obtained resolving power depends on various factors like gas pressure, excitation times, amplitudes and durations. The resolving power is often tuned to “as low as necessary required” to gain in transmission and to properly cool the ions. The purity of the used gas (typically helium) and the background pressure plays an important role. The background gas molecules like water vapor can cause charge exchange to happen, *i.e.* the ion of interest getting neutralized (and subsequently lost) and the contaminant molecule ionized. An example of a rather high resolving power frequency scan of the quadrupolar electric field is shown in Fig. 6.

### 2.6. High-resolution Penning trap cleaning techniques

In absence or in addition to the cleaning method described in the previous section, a Penning trap without buffer gas can be utilized for cleaning purposes. Without any cooling method, it is necessary to be very careful to not excite the ion of interest with a too short excitation pulse duration, especially when its mass is being measured, in order to avoid frequency shifts.

Most often the cleaning is accomplished by exciting the contaminant ions’ cyclotron motion with dipolar excitation near or at its  $\nu_+$  frequency. This frequency offers the most mass resolving power as it is directly proportional to  $\nu_c = \frac{1}{2\pi} \frac{q}{m} B$  with a small offset due to the almost-constant magnetron frequency  $\nu_-$ . One example of dipolar cleaning is described in Ref. [47], where states of  $^{70}\text{Cu}$  were separated using this

459 method at ISOLTRAP. It has been used in many Pen-  
 460 ning trap experiments, especially in the ones lacking  
 461 high-resolution pre-separation. It is quite easy to remove  
 462 known contaminants but with unknown ones it is rather  
 463 tedious to apply cleaning to every possible contaminant  
 464 (especially to identify every contaminant) as explained  
 465 well in Ref. [48], where a cleaning method based on  
 466 stored waveform inverse fourier transform (SWIFT) is  
 467 explained. In short, SWIFT excitation scheme is ap-  
 468 plied that ions beyond a narrow “no excitation gap” are  
 469 removed with rather large bandwidth.

470 For extremely high resolution cleaning, the dipolar  
 471 excitation can be used by scaling the excitation time  
 472 up. Alternatively, if cooling is available (not necessar-  
 473 ily in the trap where the cleaning is applied), also the  
 474 ion-of-interest can be, to some extent, excited. This  
 475 shortens the required excitation time considerably, es-  
 476 pecially if Ramsey-type excitation is used described in  
 477 Ref. [49]. This so-called Ramsey cleaning method  
 478 that is frequently used at JYFLTRAP and can provide  
 479 separation at the  $\sim 0.5$  Hz level. For singly charged  
 480 ions with mass of 100 u in 7 T field this corresponds to  
 481  $M/\Delta M \approx 2 \times 10^6$  ( $\approx 50$  keV/ $c^2$ ). A glimpse of the  
 482 available resolving power can be seen in Fig. 7.

483 The Ramsey cleaning method has enabled  
 484 contaminant-free mass measurements and decay  
 485 spectroscopy of various nuclei. It is possible to  
 486 determine mass when a contaminant is present but  
 487 in Penning trap mass spectrometry the measured  
 488 frequencies are prone to shifts, which might result  
 489 in a reduction of the measurement accuracy [52].  
 490 Especially  $Q_{EC}$ -values of several superallowed beta  
 491 emitters could be determined in absence of low-lying  
 492 isomeric contaminants [33] and masses near  $^{132}\text{Sn}$  for  
 493 nuclear structure studies [53].

494 Recently, other types of cleaning methods have  
 495 emerged. One promising is the so-called SIMCO  
 496 method (simultaneous magnetron and resonant con-  
 497 version), where simultaneous dipolar magnetron and  
 498 quadrupolar cyclotron excitation is applied [54]. Also  
 499 octupolar excitation has been studied for cleaning pur-  
 500 poses [55].

### 501 2.7. Multi-reflection time-of-flight separators

502 The long-awaited multi-reflection time-of-flight  
 503 (MR-TOF) separators [56] have finally entered to the  
 504 field of nuclear physics [14–16]. These devices can  
 505 provide similar or even better [57] mass resolving  
 506 power in much shorter time than a buffer gas filled  
 507 purification Penning trap.

508 The principle of an MR-TOF separator is rather sim-  
 509 ple. A well-focused bunch of ions is injected inside the

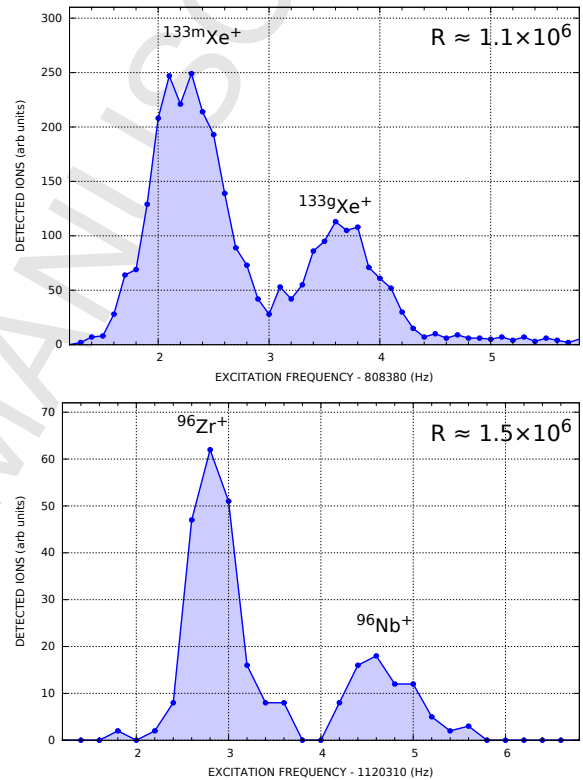


Figure 7: (Top) Separation of the isomeric states of  $^{133}\text{Xe}$  having mass difference 233 keV [50]. (Bottom) Separation of  $^{96}\text{Nb}$  and  $^{96}\text{Zr}$  having mass difference 163.96(13) keV [51].

device and let freely drift between two electrostatic mirrors. The geometry and potential of the mirror electrodes are chosen such that ions retain isochronicity: Ions can have tens of eV of energy spread and this is what the mirrors have to compensate for to keep the “lap time” constant. With each turn there is dispersion in mass. It has been shown that MR-TOFs can obtain and even surpass the mass resolving power of a gas-filled purification trap and reach resolving power beyond  $10^5$  in as little as 10 ms. This has enabled purification of ion beams with much worse ion-of-interest to contamination ratios and shorter half-lives [58].

Since the interest is to go further out from the valley of stability towards more exotic ions, the relative amount of accompanying contaminating ions is dramatically increasing. Buffer gas filled purification traps and other preseparators can do only that much and this is where MR-TOFs come in need. At the moment MR-TOFs are being built in many facilities, see Table 2.

### 2.8. Summary of ion-trap facilities in the world

Currently, there are seven operating Penning-trap facilities dedicated to high-precision mass measurements in the world (see Table 2, REXTRAP has not been used for mass measurements). With respect to the number of measured ground or isomeric states in nuclei, ISOLTRAP [59] at the ISOLDE facility at CERN has been the most productive Penning trap in the world. JYFLTRAP [24] holds the second place, thanks to the universal ion-guide technique employed at the IGISOL facility in the JYFL Accelerator Laboratory in Jyväskylä. The CPT Penning trap [60] has performed a massive number of mass measurements of neutron-rich fission fragments at the CARIBU facility in the Argonne National Laboratory. SHIPTRAP [61] at GSI has specialized in measuring masses of superheavy elements (see e.g. [62–64]). TITAN [65] at TRIUMF utilizes highly-charged ions in their experiments, and has measured many light, neutron-rich isotopes. LEBIT [66] employs exotic ions produced via fast beam fragmentation and in-flight separation at the National Superconducting Cyclotron Laboratory (NSCL). TRIGA-TRAP [67] in Mainz is also operating, and has been mainly dedicated to very high-precision  $Q$ -value measurements.

### 3. Overview of recent mass measurements employing ion traps

Over the years, Penning-trap measurements have yielded more than thousand mass or  $Q$ -values that have

improved our knowledge of e.g. evolution of shell closures, onset of deformation, and nucleosynthesis in stars (see Fig. 8). Most of the mass values have been compiled in the Atomic Mass Evaluation 2012 (AME12) [68]. After AME12, around 100 mass values from experiments with ion traps have been published. Twelve nuclei ( $^{52,53}\text{K}$  [58],  $^{53,54}\text{Ca}$  [69],  $^{82}\text{Zn}$  [70],  $^{100}\text{Rb}$  [71],  $^{129,131}\text{Cd}$  [72],  $^{141}\text{I}$  [73],  $^{198}\text{At}$ [74],  $^{232,233}\text{Fr}$  [75]) have been measured for the first time. The new measurements have revealed large deviations from the adopted or extrapolated mass values in the AME12 (see Fig. 9). For example,  $^{52,53}\text{K}$  and  $^{53,54}\text{Ca}$  are 400-1000 keV lower than the AME12 values. On the other hand, in the  $^{132}\text{Sn}$  region,  $^{129,130,131}\text{Cd}$  [72] all yield 100-360 keV higher values than in the AME12. The CPT results for  $^{130,131}\text{In}$  [73] also differ by more than 100 keV from the AME12. However, the results are for an unknown mixture of isomeric and ground states which can explain the deviations to AME12 and JYFLTRAP [53, 76]. Discrepancies at  $^{140}\text{Te}$  [73, 76] and  $^{146}\text{Cs}$  [73] are intriguing and call for new measurements.

The recent Penning-trap measurements have focused on a couple of regions on the chart of nuclides. Firstly, several measurements of nuclei in the vicinity of doubly magic  $^{132}\text{Sn}$  have been performed [53, 72, 73, 76, 80]. These nuclei are also important not only for studying the evolution of the  $Z = 50$  and  $N = 82$  shell-gap energies but also for modeling the astrophysical  $r$  process [81]. Secondly, the evolution of  $N = 28$  and  $N = 32$  shell closures in neutron-rich K and Ca nuclei have been studied at ISOLTRAP [82, 83] and TITAN [82, 83]. A third region of recent interest is located around the  $Z = 82$  shell closure, which has been explored via measurements of Tl, Pb, Fr, Ra isotopes at ISOLTRAP [74, 75, 84]. In addition, new measurements of neutron-rich Sr and Rb nuclei have probed the nuclear structure changes in the midshell region [71, 85], and extended these studies towards more neutron-rich regions than in previous works [86, 87]. Islands of inversion at  $N = 40$  and  $N = 20$  have been explored via measurements of neutron-rich Mn and Fe [88] and Mg [89] isotopes. In the neutron-deficient side, several measurements have focused on the isobaric multiplet mass equation at  $A=9$  [90],  $A=20$  and  $A=21$  [91] and  $A=31$  [92]. Studies of mirror nuclei  $^{21}\text{Na}$  [93],  $^{23}\text{Mg}$  [94],  $^{25}\text{Al}$  [95],  $^{29}\text{Na}$  [93],  $^{45}\text{V}$  [96], and  $^{49}\text{Mn}$  [96] have improved the precisions of the  $Q_{EC}$  values considerably (see Table 6). Also many stable nuclei have been studied, such as Zr and Mo isotopes at LEBIT [97] and JYFLTRAP [98, 99], or  $^{184}\text{Os}$  at TRIGA-TRAP [100], which revealed a  $2.9\sigma$  deviation to the AME12. The recently published mass-excess values, which have not been included in the AME12, have

Table 2: Table of all ion traps that are currently in use, being commissioned or under planning at the radioactive beam facilities around the world.

| Location             | Facility          | Setup name      | Type          | Status        |
|----------------------|-------------------|-----------------|---------------|---------------|
| <b>North America</b> |                   |                 |               |               |
| USA                  | Argonne NL        | CPT             | PT (+ MR-TOF) | Operational   |
| USA                  | NSCL/MSU          | LEBIT           | PT            | Operational   |
| Canada               | TRIUMF            | TITAN           | PT (+ MR-TOF) | Operational   |
| USA                  | Texas A&M         | TAMUTRAP        | PT            | Commissioning |
| <b>Europe</b>        |                   |                 |               |               |
| Switzerland          | ISOLDE            | ISOLTRAP        | PT+MR-TOF     | Operational   |
| Finland              | JYFL              | JYFLTRAP        | PT (+ MR-TOF) | Operational   |
| Germany              | GS1               | SHIPTRAP        | PT            | Operational   |
| Germany              | Univ. Mainz       | TRIGATRAP       | PT            | Operational   |
| Switzerland          | ISOLDE            | REXTRAP         | PT            | Operational   |
| Germany              | GS1               | HITRAP          | PT            | Commissioning |
| Germany              | GS1/FAIR          | FRS Ion Catcher | MR-TOF        | Operational   |
| Germany/France       | Univ. Munich/ALTO | MLL-TRAP        | PT            | Commissioning |
| Germany              | GS1/FAIR          | MATS            | PT            | Planning      |
| France               | GANIL             | DESIR-TRAP      | PT            | Planning      |
| France               | GANIL             | PIPERADE        | PT            | Planning      |
| France               | GANIL             | PILGRIM         | MR-TOF        | Planning      |
| Russia               | PNPI              | PITRAP          | PT            | Planning      |
| <b>Asia</b>          |                   |                 |               |               |
| Japan                | RIKEN             | SLOWRI          | MR-TOF        | Operational   |
| China                | IMP Lanzhou       | Lanzhou-trap    | PT            | Planning      |
| China                | CIAE, BRIF        | BRIF-TRAP       | PT            | Planning      |
| China                | CIAE, CARIF       | CARIF-TRAP      | PT            | Planning      |
| India                | VECC              | VECC-TRAP       | PT            | Planning      |
| Japan                | RIKEN             | RIKEN-TRAP      | PT            | Planning      |
| South Korea          | RISP              | RISP-TRAP       | PT            | Planning      |

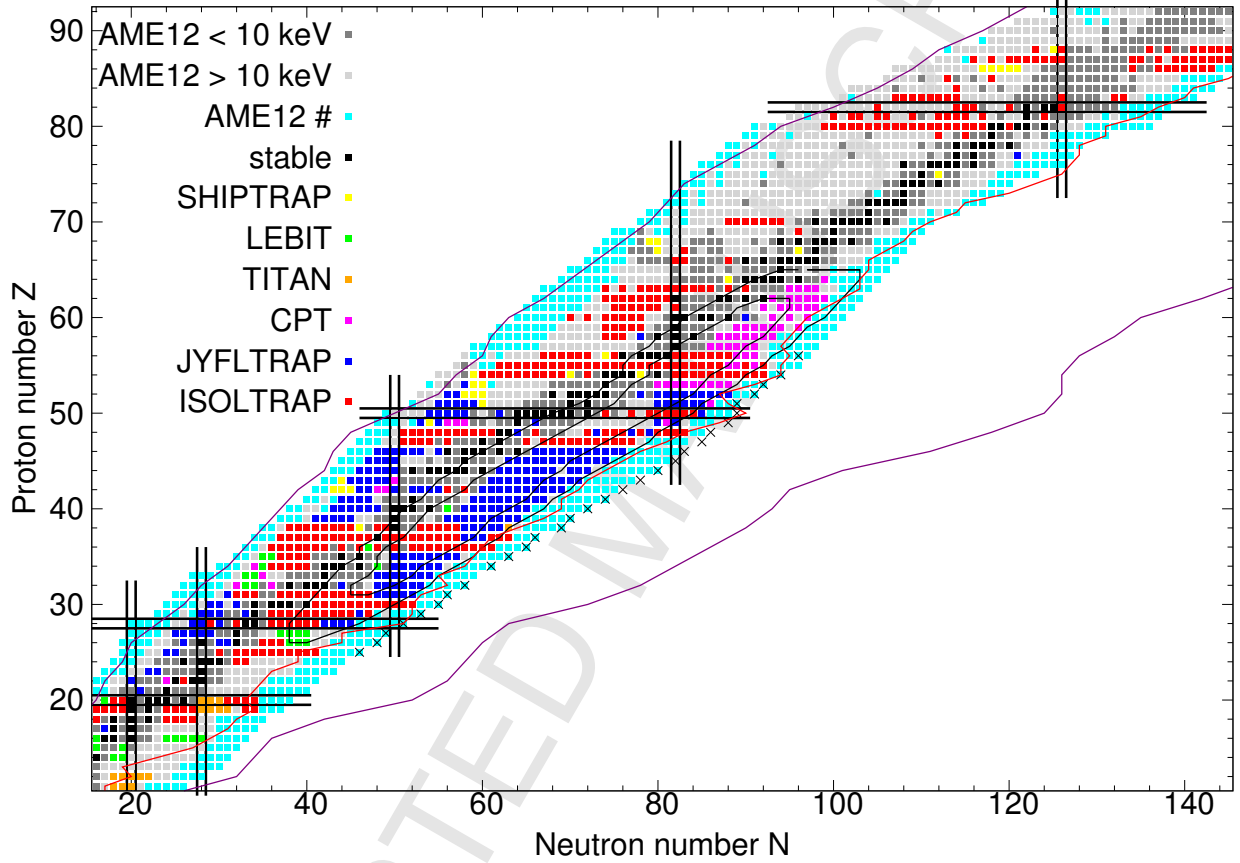


Figure 8: (Color online) Penning-trap measurements performed at ISOLTRAP, JYFLTRAP, SHIPTRAP, LEBIT, CPT and TITAN. Since many nuclei have been measured at several facilities, all data points are not visible in the figure. The nuclei whose mass-excess values in AME2012 [68] are known with a precision better than 10 keV (dark grey), worse than 10 keV (light grey) or have extrapolated mass values (cyan) are also shown. The average two-proton and two-neutron driplines from the energy-density functional calculations are plotted in purple [77]. The crosses highlight the most neutron-rich isotopes whose half-lives have been measured recently at RIKEN [78, 79]. A 100-ms contour for half-lives of neutron-rich isotopes (red line) and contours for calculated 1- $\mu$ b and 1-mb  $^{238}\text{U}$ (p 25 MeV,f) fission cross sections are also shown (black lines).

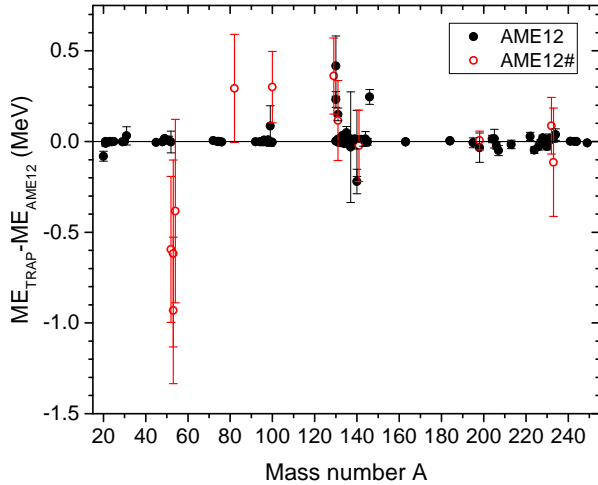


Figure 9: Comparison of recent ion-trap mass measurements to the AME12 [68]. The general agreement with the AME12 is rather good. However, several isotopes deviate significantly. The largest deviations are observed for nuclei around  $^{52}\text{Ca}$  and  $^{132}\text{Sn}$ .

610 been summarized in Tables 3, 4, and 5.

### 611 3.1. Comparison with theoretical mass models

612 The Penning-trap measurements provide a data pool  
613 for comparisons with different theoretical mass mod-  
614 els. We have now compared five different mass mod-  
615 els (FRDM2012 [108], Duflo-Zuker [109], WS4 [110],  
616 HFB-24 [111], and UNEDF0 [112]) to experimental  
617 mass-excess values in three different regions in the chart  
618 of nuclides. The regions,  $Z = 15 - 25$ ,  $Z = 45 - 55$   
619 and  $Z = 80 - 90$ , were selected due to their locations  
620 close to magic neutron and proton shells at  $^{48}\text{Ca}$ ,  $^{132}\text{Sn}$ ,  
621 and  $^{208}\text{Pb}$ , and since recently mass measurements have  
622 been performed in these regions (see Table 3). Most  
623 of the theoretical models selected are relatively new  
624 [108, 110–112], the only exception is the Duflo-Zuker  
625 formula. Three of the models, FRDM2012, Duflo-  
626 Zuker, and WS4 are macroscopic-microscopic models  
627 where the macroscopic part is based on the liquid drop  
628 model. The HFB-24 and UNEDF0 models are based  
629 on Hartree-Fock-Bogoliubov mass model with Skyrme  
630 forces. Of these, UNEDF0 is purely energy density  
631 functional without any additional procedures done to  
632 match the experimental data. Below, the different mod-  
633 els are shortly described.

634 FRDM2012 is a macroscopic-microscopic mass  
635 model. It is based on finite-range droplet macro-  
636 scopic and the folded-Yukawa single-particle micro-  
637 scopic nuclear-structure models. FRDM2012 employs  
638 the same model as its precursor, FRDM1995 [113], but  
639 with considerably improved treatment of deformation

640 and fewer approximations have been made thanks to  
641 more computing power available. The root-mean square  
642 (rms) error of the FRDM2012 model is 0.5595 MeV for  
643 the entire region of nuclei included in the adjustment,  
644 and only 0.3549 MeV for the nuclei with  $N \geq 65$  (0.669  
645 MeV and 0.448 MeV for the FRDM1995 model, respec-  
646 tively).

647 Duflo-Zuker is also a macroscopic-microscopic for-  
648 mula. Its six macroscopic monopole terms lead asymp-  
649 totically to a liquid drop form, three microscopic terms  
650 take into account configuration mixing (multipole) cor-  
651 rections to the monopole shell effects, and one term is  
652 for deformed nuclei. Duflo-Zuker, originally fitted to  
653 AME1995 values, performed outstandingly well com-  
654 pared to other mass models when AME2003 mass eval-  
655 uation was published [114] with a root-mean square er-  
656 ror of about 0.5 MeV.

657 WS4 (Weizsäcker-Skyrme 4) model [110] is a  
658 macroscopic-microscopic mass formula, where the  
659 macroscopic part is treated using the liquid drop  
660 model, and axially deformed Woods-Saxon potential is  
661 adopted to obtain the shell corrections using the Strut-  
662 nsky method. The latest WS model, WS4, has taken  
663 into account the surface diffuseness effect of nuclei near  
664 the drip lines for the first time. This resulted in a bet-  
665 ter prediction of neutron-rich masses, and the root-mean  
666 square to AME12 only 0.298 MeV.

667 The HFB-24 model [111] is based on the Hartree-  
668 Fock-Bogoliubov (HFB) mass model supplemented by  
669 the Skyrme forces with a microscopic pairing force,  
670 phenomenological Wigner terms and correction terms  
671 for the spurious collective energy. The model param-  
672 eters have been fitted to the AME12 [68] experimental  
673 mass values, and the Skyrme force has been simultane-  
674 ously fitted to the zero-temperature equation of state of  
675 infinite homogeneous neutron matter as determined by  
676 many-body calculations with realistic two- and three-  
677 nucleon forces. The HFB-24 model works rather well  
678 with about 0.55 MeV root-mean square deviation to the  
679 AME2012 [68] evaluation.

680 UNEDF0 [112] is a pure energy-density functional  
681 model relying on the nuclear energy density of Skyrme  
682 type in the framework of the Hartree-Fock-Bogoliubov  
683 theory. The energy-density functional was calibrated by  
684 fitting to a set of 72 nuclei at closed  $Z=20, 28, 50$ , and  
685 82 proton shells, from the mid-shell region with  $N \approx$   
686 100 and from the heavy region  $Z \geq 100$ . Only spherical  
687 or axially deformed nuclei are considered in UNEDF0.  
688 The root-mean square error, 1.45 MeV, is much better  
689 than for example for the SLy4 model [115, 116] with  
690 an rms error of 4.80 MeV. It has been suggested that  
691 the Sly4 model has an overemphasis on doubly-magic



Table 3: Summary of most recent Penning-trap measurements (not included in the AME12). The reference ions are singly-charged unless stated otherwise.

| Nuclide           | Ref.  | $ME_{trap}$ (keV) | $ME_{AME12}$ (keV) | Trap            | Ref.  |
|-------------------|---|-------------------|--------------------|-----------------|-------|
| <sup>21</sup> Na  | <sup>21</sup> Ne                                | -2184.63(10)      | -2184.64(28)       | LEBIT           | [93]  |
| <sup>20</sup> Mg  | <sup>23</sup> Na                                | 17477.7(18)       | 17559(27)          | TITAN           | [91]  |
| <sup>21</sup> Mg  | <sup>23</sup> Na                                | 10903.85(74)      | 10914(16)          | TITAN           | [91]  |
| <sup>23</sup> Mg  | <sup>23</sup> Na                                | -5473.50(16)      | -5473.3(7)         | TITAN           | [94]  |
| <sup>24</sup> Al  | <sup>23</sup> Na                                | -48.86(23)        | -47.6(11)          | TITAN           | [101] |
| <sup>25</sup> Al  | <sup>25</sup> Mg                                | -8915.962(63)     | -8916.2(5)         | JYFLTRAP        | [95]  |
| <sup>29</sup> P   | <sup>12</sup> C <sub>3</sub>                    | -16953.15(47)     | -16952.5(6)        | LEBIT           | [93]  |
| <sup>30</sup> P   | <sup>30</sup> Si                                | -20200.854(64)    | -20200.6(3)        | JYFLTRAP        | [95]  |
| <sup>31</sup> Cl  | <sup>31</sup> P                                 | -7034.7(34)       | -7070(50)          | JYFLTRAP        | [92]  |
| <sup>52</sup> K   | <sup>39</sup> K, <sup>52</sup> Cr               | -17138(33)        | -16540(400)#       | ISOLTRAP/MR-TOF | [58]  |
| <sup>53</sup> K   | <sup>39</sup> K, <sup>52</sup> Cr               | -12298(112)       | -11680(500)#       | ISOLTRAP/MR-TOF | [58]  |
| <sup>48</sup> Ca  | <sup>14</sup> N <sup>18</sup> O <sup>16</sup> O | -44224.45(27)     | -44224.76(12)      | TITAN           | [102] |
| <sup>51</sup> Ca  | <sup>39</sup> K                                 | -36332.07(58)     | -36339(22)         | ISOLTRAP        | [69]  |
| <sup>52</sup> Ca  | <sup>39</sup> K                                 | -34266.02(71)     | -342660(60)        | ISOLTRAP        | [69]  |
| <sup>53</sup> Ca  | <sup>39</sup> K, <sup>53</sup> Cr               | -29388(43)        | -28460(400)#       | ISOLTRAP/MR-TOF | [69]  |
| <sup>54</sup> Ca  | <sup>39</sup> K, <sup>54</sup> Cr               | -25161(49)        | -24780(500)#       | ISOLTRAP/MR-TOF | [69]  |
| <sup>48</sup> Ti  | <sup>14</sup> N <sup>18</sup> O <sup>16</sup> O | -48492.71(21)     | -48491.7(4)        | TITAN           | [102] |
| <sup>45</sup> V   | <sup>45</sup> Ti                                | -31885.3(9)       | -31881(8)          | JYFLTRAP        | [96]  |
| <sup>49</sup> Mn  | <sup>49</sup> Cr                                | -37620.3(24)      | -37637(10)         | JYFLTRAP        | [96]  |
| <sup>82</sup> Zn  | <sup>85</sup> Rb                                | -42314(3)         | -42610(300)#       | ISOLTRAP        | [70]  |
| <sup>74</sup> Ga  | <sup>85</sup> Rb <sup>9+</sup>                  | -68049.7(50)      | -68050(3)          | TITAN           | [103] |
| <sup>72</sup> Br  | <sup>85</sup> Rb                                | -59062.2(10)      | -59067(7)          | LEBIT           | [104] |
| <sup>74</sup> Rb  | <sup>85</sup> Rb <sup>9+</sup>                  | -51916.5(60)      | -51916(3)          | TITAN           | [103] |
| <sup>75</sup> Rb  | <sup>85</sup> Rb <sup>9+</sup>                  | -57218.7(17)      | -57218.7(12)       | TITAN           | [103] |
| <sup>76</sup> Rb  | <sup>85</sup> Rb <sup>9+</sup>                  | -60481.0(16)      | -60479.1(9)        | TITAN           | [103] |
| <sup>98</sup> Rb  | <sup>85</sup> Rb                                | -54309.4(40)      | -54318(3)          | ISOLTRAP        | [71]  |
| <sup>99</sup> Rb  | <sup>85</sup> Rb                                | -51120.3(45)      | -51205(110)        | ISOLTRAP        | [71]  |
| <sup>100</sup> Rb | <sup>85</sup> Rb                                | -46247(20)        | -46550(200)#       | ISOLTRAP        | [71]  |
| <sup>96</sup> Zr  | <sup>96</sup> Mo                                | -85437.5(4)       | -85445(2)          | JYFLTRAP        | [51]  |
| <sup>96</sup> Nb  | <sup>96</sup> Mo                                | -85601.5(4)       | -85607(3)          | JYFLTRAP        | [51]  |
| <sup>92</sup> Mo  | <sup>87</sup> Rb, <sup>12</sup> C <sub>8</sub>  | -86808.53(17)     | -86807.8 0,781     | LEBIT           | [97]  |
| <sup>94</sup> Mo  | <sup>87</sup> Rb, <sup>12</sup> C <sub>8</sub>  | -88413.96(25)     | -88412.8(4)        | LEBIT           | [97]  |
| <sup>95</sup> Mo  | <sup>87</sup> Rb, <sup>12</sup> C <sub>8</sub>  | -87711.51(26)     | -87710.6(4)        | LEBIT           | [97]  |
| <sup>96</sup> Mo  | <sup>87</sup> Rb, <sup>12</sup> C <sub>8</sub>  | -88794.53(30)     | -88793.6(4)        | LEBIT           | [97]  |
| <sup>97</sup> Mo  | <sup>87</sup> Rb, <sup>12</sup> C <sub>8</sub>  | -87544.44(25)     | -87543.6(5)        | LEBIT           | [97]  |
| <sup>98</sup> Mo  | <sup>87</sup> Rb, <sup>12</sup> C <sub>8</sub>  | -88115.95(38)     | -88114.8(5)        | LEBIT           | [97]  |
| <sup>100</sup> Mo | <sup>87</sup> Rb, <sup>12</sup> C <sub>8</sub>  | -86193.04(30)     | -86189.5(10)       | LEBIT           | [97]  |

Table 4: Table 3 continued.

| Nuclide           | Ref.                               | $ME_{trap}$ (keV) | $ME_{AME12}$ (keV) | Trap            | Ref. |
|-------------------|------------------------------------|-------------------|--------------------|-----------------|------|
| $^{129}\text{Cd}$ | $^{133}\text{Cs}$                  | -63148(74)        | -63510(200)#       | ISOLTRAP        | [72] |
| $^{130}\text{Cd}$ | $^{133}\text{Cs}$                  | -61118(22)        | -61530(160)        | ISOLTRAP        | [72] |
| $^{131}\text{Cd}$ | $^{131}\text{Cs}, ^{133}\text{Cs}$ | -55215(100)       | -55330(200)#       | ISOLTRAP/MR-TOF | [72] |
| $^{130}\text{In}$ | $^{133}\text{Cs}$                  | -69652(20)        | -69880(40)         | CPT             | [73] |
| $^{131}\text{In}$ | $^{133}\text{Cs}$                  | -67876(35)        | -68025.6(27)       | CPT             | [73] |
| $^{130}\text{Sn}$ | $^{133}\text{Cs}$                  | -80130.8(36)      | -80132.9(21)       | CPT             | [73] |
| $^{131}\text{Sn}$ | $^{133}\text{Cs}$                  | -77259.6(43)      | -77272(6)          | CPT             | [73] |
| $^{132}\text{Sn}$ | $^{133}\text{Cs}$                  | -76549.0(28)      | -76543.9(29)       | CPT             | [73] |
| $^{133}\text{Sn}$ | $^{133}\text{Cs}$                  | -70869.1(36)      | -70874.2(24)       | CPT             | [73] |
| $^{134}\text{Sn}$ | $^{133}\text{Cs}$                  | -66444(16)        | -66432(3)          | CPT             | [73] |
| $^{135}\text{Sn}$ | $^{133}\text{Cs}$                  | -60584(34)        | -60632(3)          | CPT             | [73] |
| $^{131}\text{Sb}$ | $^{133}\text{Cs}$                  | -81986(10)        | -81981.9(21)       | CPT             | [73] |
| $^{132}\text{Sb}$ | $^{133}\text{Cs}$                  | -79633.8(61)      | -79635.6(27)       | CPT             | [73] |
| $^{133}\text{Sb}$ | $^{133}\text{Cs}$                  | -78921.3(76)      | -78923(3)          | CPT             | [73] |
| $^{134}\text{Sb}$ | $^{133}\text{Cs}$                  | -74012(10)        | -74020.5(17)       | CPT             | [73] |
| $^{135}\text{Sb}$ | $^{133}\text{Cs}$                  | -69693.9(65)      | -69689.6(29)       | CPT             | [73] |
| $^{136}\text{Sb}$ | $^{133}\text{Cs}$                  | -64491(15)        | -64510(6)          | CPT             | [73] |
| $^{137}\text{Sb}$ | $^{133}\text{Cs}$                  | -60061(52)        | -60030(300)        | CPT             | [73] |
| $^{133}\text{Te}$ | $^{133}\text{Cs}$                  | -82899.8(65)      | -82932(4)          | CPT             | [73] |
| $^{135}\text{Te}$ | $^{133}\text{Cs}$                  | -77729.6(21)      | -77727.9(27)       | CPT             | [73] |
| $^{136}\text{Te}$ | $^{133}\text{Cs}$                  | -74423.3(37)      | -74425.8(24)       | CPT             | [73] |
| $^{137}\text{Te}$ | $^{133}\text{Cs}$                  | -69301.7(37)      | -69304.2(25)       | CPT             | [73] |
| $^{138}\text{Te}$ | $^{133}\text{Cs}$                  | -65695.3(76)      | -65696(4)          | CPT             | [73] |
| $^{139}\text{Te}$ | $^{133}\text{Cs}$                  | -60191(17)        | -60205(4)          | CPT             | [73] |
| $^{140}\text{Te}$ | $^{133}\text{Cs}$                  | -56577(62)        | -56357(28)         | CPT             | [73] |
| $^{133}\text{I}$  | $^{133}\text{Cs}$                  | -85858.2(64)      | -85887(5)          | CPT             | [73] |
| $^{134}\text{I}$  | $^{133}\text{Cs}$                  | -84040.8(64)      | -84059(6)          | CPT             | [73] |
| $^{135}\text{I}$  | $^{133}\text{Cs}$                  | -83778.9(20)      | -83789(5)          | CPT             | [73] |
| $^{139}\text{I}$  | $^{133}\text{Cs}$                  | -68470.7(40)      | -68459(29)         | CPT             | [73] |
| $^{140}\text{I}$  | $^{133}\text{Cs}$                  | -63606(13)        | -63600(180)        | CPT             | [73] |
| $^{141}\text{I}$  | $^{133}\text{Cs}$                  | -59927(16)        | -59900(200)#       | CPT             | [73] |
| $^{142}\text{Cs}$ | $^{133}\text{Cs}$                  | -70506.9(93)      | -70518(7)          | CPT             | [73] |
| $^{143}\text{Cs}$ | $^{133}\text{Cs}$                  | -67676.3(79)      | -67674(22)         | CPT             | [73] |
| $^{144}\text{Cs}$ | $^{133}\text{Cs}$                  | -63256(31)        | -63271(25)         | CPT             | [73] |
| $^{145}\text{Cs}$ | $^{133}\text{Cs}$                  | -60057(16)        | -60056(11)         | CPT             | [73] |
| $^{146}\text{Cs}$ | $^{133}\text{Cs}$                  | -55323.2(86)      | -55570(40)         | CPT             | [73] |

Table 5: Table 3 continued.

| Nuclide                          | Ref.                                 | ME <sub>trap</sub> (keV) | ME <sub>AME12</sub> (keV) | Trap       | Ref.  |
|----------------------------------|--------------------------------------|--------------------------|---------------------------|------------|-------|
| <sup>163</sup> Dy                | <sup>12</sup> C <sub>15</sub>        | -66381.7(8)              | -66379.9(19)              | TRIGA-TRAP | [105] |
| <sup>163</sup> Ho                | <sup>12</sup> C <sub>15</sub>        | -66379.3(9)              | -66377.3(19)              | TRIGA-TRAP | [105] |
| <sup>184</sup> W                 | <sup>12</sup> C <sub>15</sub>        | -45705.40(94)            | -45707.6(9)               | TRIGA-TRAP | [100] |
| <sup>184</sup> Os                | <sup>12</sup> C <sub>15</sub>        | -44251.47(113)           | -44256.6(13)              | TRIGA-TRAP | [100] |
| <sup>195</sup> Tl <sup>g</sup>   | <sup>133</sup> Cs                    | -28162(25)               | -28155(11)                | ISOLTRAP   | [84]  |
| <sup>195</sup> Tl <sup>g,m</sup> | <sup>133</sup> Cs                    | -28152(24)               |                           | ISOLTRAP   |       |
| <sup>198</sup> Tl <sup>g</sup>   | <sup>133</sup> Cs                    | -27528.7(75)             | -27490(80)                | ISOLTRAP   | [84]  |
| <sup>198</sup> At <sup>g</sup>   | <sup>133</sup> Cs                    | -6715(6)                 | -6721(51)#                | ISOLTRAP   | [74]  |
| <sup>204</sup> Rn                | <sup>133</sup> Cs, <sup>208</sup> Pb | -7969(15)                | -7983(15)                 | SHIPTRAP   | [106] |
| <sup>205</sup> Rn                | <sup>133</sup> Cs, <sup>208</sup> Pb | -7698(9)                 | -7710(50)                 | SHIPTRAP   | [106] |
| <sup>206</sup> Rn                | <sup>133</sup> Cs, <sup>208</sup> Pb | -9139(10)                | -9115(15)                 | SHIPTRAP   | [106] |
| <sup>207</sup> Rn                | <sup>133</sup> Cs                    | -8685(26)                | -8635(8)                  | SHIPTRAP   | [106] |
| <sup>222</sup> Fr                | <sup>133</sup> Cs                    | 16378(7)                 | 16350(21)                 | ISOLTRAP   | [75]  |
| <sup>224</sup> Fr                | <sup>133</sup> Cs                    | 21748(12)                | 21795(13)                 | ISOLTRAP   | [75]  |
| <sup>226</sup> Fr                | <sup>133</sup> Cs                    | 27513(15)                | 27541(12)                 | ISOLTRAP   | [75]  |
| <sup>227</sup> Fr                | <sup>133</sup> Cs                    | 29682(7)                 | 29686(13)                 | ISOLTRAP   | [75]  |
| <sup>228</sup> Fr                | <sup>133</sup> Cs                    | 33389(8)                 | 33369(13)                 | ISOLTRAP   | [75]  |
| <sup>229</sup> Fr                | <sup>133</sup> Cs, <sup>238</sup> U  | 35666(6)                 | 35674(14)                 | ISOLTRAP   | [75]  |
| <sup>230</sup> Fr                | <sup>133</sup> Cs                    | 39483(8)                 | 39511(16)                 | ISOLTRAP   | [75]  |
| <sup>231</sup> Fr                | <sup>133</sup> Cs                    | 42080(8)                 | 42064(25)                 | ISOLTRAP   | [75]  |
| <sup>232</sup> Fr                | <sup>133</sup> Cs                    | 46073(14)                | 45990(160)#               | ISOLTRAP   | [75]  |
| <sup>233</sup> Fr                | <sup>133</sup> Cs                    | 48920(20)                | 49030(300)#               | ISOLTRAP   | [75]  |
| <sup>213</sup> Ra <sup>2+</sup>  | <sup>133</sup> Cs                    | 342(11)                  | 358(21)                   | SHIPTRAP   | [106] |
| <sup>233</sup> Ra                | <sup>133</sup> Cs                    | 44339(12)                | 44322(16)                 | ISOLTRAP   | [75]  |
| <sup>234</sup> Ra                | <sup>133</sup> Cs                    | 46931(8)                 | 46890(30)                 | ISOLTRAP   | [75]  |
| <sup>244</sup> Pu                | <sup>12</sup> C <sub>22</sub>        | 59806.2(18)              | 59807(5)                  | TRIGA-TRAP | [107] |
| <sup>241</sup> Am                | <sup>12</sup> C <sub>22</sub>        | 52936.9(18)              | 52936.2(18)               | TRIGA-TRAP | [107] |
| <sup>243</sup> Am                | <sup>12</sup> C <sub>22</sub>        | 57176.2(14)              | 57176.3(23)               | TRIGA-TRAP | [107] |
| <sup>249</sup> Cf                | <sup>12</sup> C <sub>22</sub>        | 69718.1(13)              | 69726.0(22)               | TRIGA-TRAP | [107] |

692 nuclei during the optimization process which might ex-  
 693 plain the larger differences.

694 The mass-excess differences to the FRDM2012 have  
 695 been plotted for the first region of interest, from P ( $Z = 15$ ) to Mn ( $Z = 25$ ), in Fig. 10. Between  $N = 20$  and  
 696  $N = 28$ , the agreement between the experimental val-  
 697 ues and theoretical models seems to be rather good with  
 698 the exception of UNEDF0 for some chains. An inter-  
 699 esting feature is observed at  $N = 32$  where FRDM2012  
 700 predicts higher mass-excess values, i.e. smaller binding  
 701 energies, than experimental results. HFB-24 and WS4  
 702 follow the experimental trend in a better way. However,  
 703 when we enter the region where no experimental data  
 704 exist so far, WS4 model predicts much smaller binding  
 705 energies than FRDM2012 and the other models. As a  
 706 result, deviations on the order of several MeV are ob-  
 707 served between the models outside the experimentally  
 708 known region.  
 709

710 For the second region of interest, from Rh ( $Z = 45$ )  
 711 to Cs ( $Z = 55$ ), the largest deviations to the experimen-  
 712 tal values are observed at  $N = 50$  and  $N = 82$  (see  
 713 Fig. 11). The trend in the neutron-rich region, where no  
 714 experimental data are available, is the same as for the  
 715 lower mass region: WS4 predicts much smaller binding  
 716 energies than FRDM2012, whereas Duflo-Zuker and  
 717 HFB-24 tend to give higher binding energies than the  
 718 FRDM2012. The overall deviations are large asking for  
 719 more refined mass models and systematic studies in or-  
 720 der to obtain a better understanding for example on the  
 721 astrophysical rapid neutron capture process.

722 In the third region of interest, from Hg ( $Z=80$ ) to  
 723 Th ( $Z=90$ ), the UNEDF0 model seems to have difficul-  
 724 ties in producing the binding energies at the closed neu-  
 725 tron shell  $N = 126$  (see Fig. 12). The uncertainties in  
 726 the Skyrme energy-density functional model have been  
 727 studied e.g. in Refs. [117, 118]. The discrepancy at  
 728  $^{208}\text{Pb}$  cannot be removed by fit parameters as they are al-  
 729 ready quite rigidly constrained by other data. This sug-  
 730 gests that something is missing in the description of the  
 731  $^{208}\text{Pb}$  mass ( $N = 126$ ). This is most probably related to  
 732 a poor description of the ground-state collective correla-  
 733 tions in doubly-magic systems [117]. Otherwise, the  
 734 trends in the experimentally unknown region are rela-  
 735 tively similar as in the lower mass regions, except that  
 736 the Duflo-Zuker model predicts now smaller binding en-  
 737 ergies than the FRDM2012 model, and thus, has a simi-  
 738 lar trend to WS4.

739 To summarize, most of the mass models are in a rea-  
 740 sonable agreement where experimental data exist but  
 741 the deviations between the models become very large  
 742 outside the known region. None of the discussed mod-  
 743 els performs outstandingly well in all three regions dis-

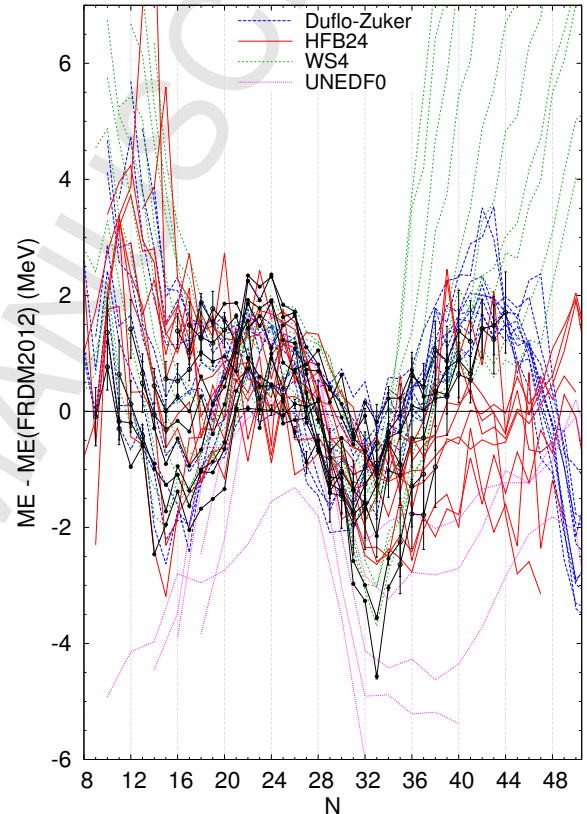


Figure 10: Comparison of experimental mass-excess values to different theoretical models for isotopic chains from P ( $Z=15$ ) to Mn ( $Z=25$ ) as a function of neutron number  $N$ . FRDM2012 has been used as a baseline. Black solid points are experimental values and hollow points are AME2012 extrapolated values.

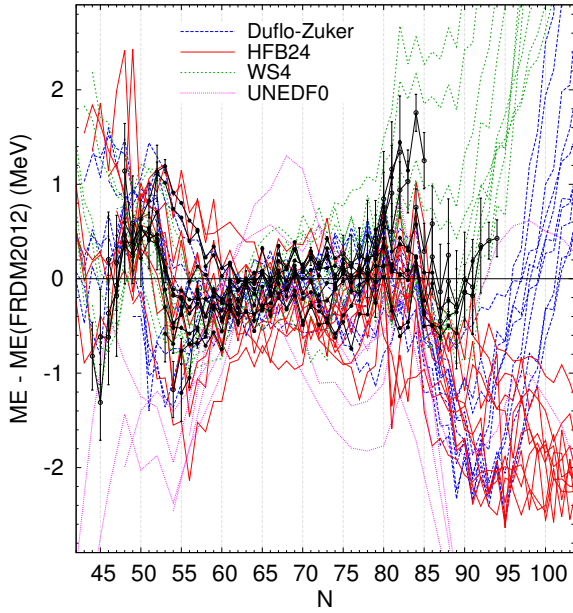


Figure 11: Comparison of experimental mass-excess values to different theoretical models for isotopic chains from Rh ( $Z=45$ ) to Cs ( $Z=55$ ) as a function of neutron number  $N$ . FRDM2012 has been used as a baseline. Black solid points are experimental values and hollow points are AME2012 extrapolated values.

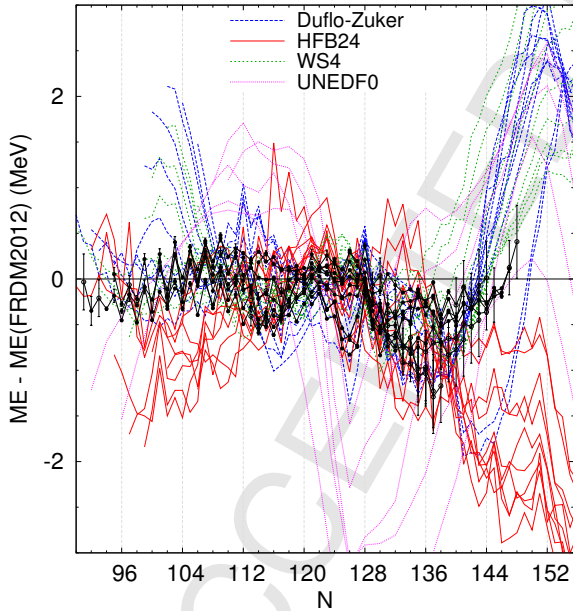


Figure 12: Comparison of experimental mass-excess values to different theoretical models for isotopic chains from Rh ( $Z=80$ ) to Th ( $Z=90$ ) as a function of neutron number  $N$ . FRDM2012 has been used as a baseline. Black solid points are experimental values and hollow points are AME2012 extrapolated values.

744 cussed above. It should also be noted that the mass  
745 differentials are usually better predicted by the models  
746 than the absolute mass values (see e.g. Section 3.2.5 for  
747 two-neutron shell gap energies). Thus, scatter e.g. in  
748 neutron-separation energies required for the astrophysical  
749 r-process modeling may not deviate as much as the  
750 mass values shown in Figs. 10, 11 and 12.

### 751 3.2. Two-nucleon binding energies and shell gaps

752 A novel mass measurement technique offered by ion  
753 traps provides an accurate microscope to study the fine  
754 structure of the nuclear mass surface away from the val-  
755 ley of stability. This is best viewed through the sys-  
756 tematic evaluation of various mass differentials as a  
757 function of proton and neutron number. Such differ-  
758 entials, as already mentioned in the introductory sec-  
759 tion of this review are, for example, to the first order  
760 the one- and two-nucleon separation energies and decay  
761  $Q$ -values and to the second order the shell gap energies  
762 and odd-even staggering of masses related to pairing ef-  
763 fects. With the ion-trap spectrometry these quantities  
764 are now typically available with accuracies of the or-  
765 der of 10 keV or better. This accuracy is comparable  
766 to that of excited states spectroscopy far from stability  
767 in the outskirts of the known nuclear landscape. Most  
768 of the new ion trap mass data since the last five years  
769 have been obtained for neutron-rich nuclei. Also, there  
770 is a high relevance of this data for nuclear astrophysics,  
771 where it is needed in modeling the synthesis of heavy  
772 elements via the rapid neutron capture processes occur-  
773 ring in high-temperature and density scenarios (see e.g.  
774 reviews [119, 120]). Therefore, in the following sec-  
775 tions we will focus on the systematic behavior of two-  
776 neutron separation energies in the light of the newest  
777 data published since the last atomic mass evaluation in  
778 2012. The two-neutron separation energy  $S_{2n}$  is ob-  
779 tained by using the following formula:

$$\begin{aligned} S_{2n} &= B(A, Z) - B(A - 2, Z) \\ &= (M(A - 2, Z) + 2M_n - M(A, Z))c^2, \quad (8) \end{aligned}$$

780 where  $B(A, Z)$  and  $M(A, Z)$  stand for the binding en-  
781 ergy and mass, respectively. This gives the energy re-  
782 quired to remove the last two neutrons from the nucleus  
783 to continuum. The overall trend for  $S_{2n}$  as a function  
784 of the increasing neutron number is its nearly mono-  
785 tonic decrease due to the filling of less bound, higher  
786 and higher-lying orbitals. As shown in Fig. 13, the  
787 above mentioned behavior is clearly seen in the  $S_{2n}$   
788 energies as a function of neutron number for neutron-  
789 rich isotopes from krypton to tin. For demonstrating the

790 progress in mass measurements in this region, we show  
 791 for comparison the knowledge on two-neutron separation  
 792 energies as in the 2003 atomic mass evaluation [50].  
 793 Very recently important new data has been obtained at  
 794 the ISOLTRAP, TITAN and JYFLTRAP facilities for  
 795 neutron-rich Kr, Rb, Cd and Sn isotopes. In addition,  
 796 since the atomic mass evaluation in 2003 over one hun-  
 797 dred new masses were measured with the JYFLTRAP  
 798 setup ranging from nickel to xenon, as reported in our  
 799 previous review article in 2012 [98].

800 In addition to a smooth behavior of  $S_{2n}$  shown in Fig.  
 801 13, there are kinks near  $N = 60$  in the isotopic chains  
 802 from yttrium to molybdenum outside of which a smooth  
 803 behavior is again observed. This behavior is known to  
 804 be due to a distinct shape change between  $N = 58$  and  
 805 60 at which strong prolate ground state deformation sets  
 806 in. The rapid onset is due to a shape transition and co-  
 807 existence of shapes around  $Z = 40$  and  $N = 60$ , see Ref.  
 808 [121] and references therein. While the ground states  
 809 of these nuclei below  $N \approx 60$  appear to be only weakly  
 810 deformed or nearly spherical, the heavier isotopes dis-  
 811 play mainly axially symmetric deformed shapes. The  
 812 shape changes and coexistence picture are well known  
 813 also from spectroscopic studies. This interpretation has  
 814 also been confirmed by a series of collinear laser spec-  
 815 troscopy experiments in the form of a sudden increase  
 816 of the mean-square charge radii around  $N = 60$ .

817 A recent theoretical study by Takahara et al. [122]  
 818 implied that the spin-orbit potential plays a decisive role  
 819 in the predominance of prolate deformation of ground  
 820 states. For neutron-rich nuclei above  $N = 60$ , neutrons  
 821 start to occupy deformed orbits deriving from the  $g_{7/2}$   
 822 having considerable overlap with the spin-orbit partner  
 823 proton levels deriving from the  $g_{9/2}$  single-particle level.  
 824 Interaction between the relevant neutron and proton or-  
 825 bits drives the nucleus to large deformations for nuclides  
 826 with  $Z = 37 - 44$  and  $N > 60$ . This interpretation is  
 827 supported by the new data obtained from the mass mea-  
 828 surements of neutron-rich Kr isotopes ( $Z = 36$ ). Here,  
 829 protons are mainly occupying orbitals below the  $g_{9/2}$  or-  
 830 bit, and hence this results in a nearly monotonically de-  
 831 creasing trend in two-neutron binding energies.

832 Concerning the evolution and persistence of the two-  
 833 neutron shell gap at  $N = 82$ , it is of interest to note  
 834 that the new measurement at ISOLTRAP has produced  
 835 accurate mass values for  $^{129,130,131}\text{Cd}$  isotopes. Derived  
 836 from that data one can observe that the  $S_{2n}$  values in-  
 837 dicate a smaller drop for Cd from  $N = 81$  to  $N = 83$   
 838 as compared with the neighbouring In and Sn isotope  
 839 chains. To confirm whether this trend is really happen-  
 840 ing it would be important to extend the accurate ion-trap  
 841 measurements to the nearby  $^{130,132}\text{In}$  and  $^{132}\text{Cd}$  isotopes.

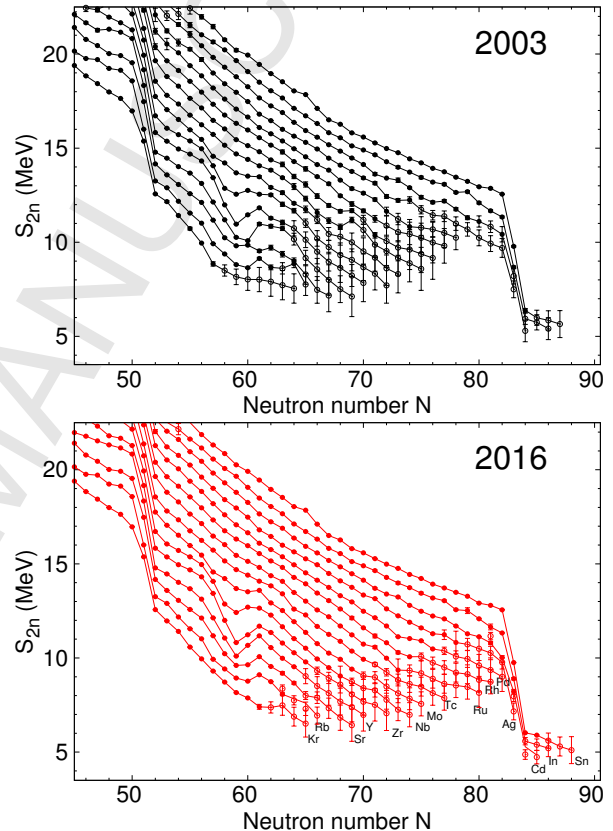


Figure 13: Two-neutron binding energy vs.  $N$  from Kr to Sn. Note that the experimental uncertainties, if not shown, are smaller than the data points.



842 In the following chapters, two-neutron separation energies are presented and discussed in three regions of  
 843 neutron-rich nuclei; near and above the spherical shell closures at  $N = 28, 82, 126$  and the deformed region  
 844 with  $N = 60$ . We compare the experimental data with DFT calculations employing two commonly used functionals  
 845 Sly4 [115, 116] and UNEDF0 [112], see chapter 3.1 for their description.  
 846  
 847  
 848  
 849

### 850 3.2.1. Neutron-rich Ca isotopes. A new shell closure?

851 Recent experiments employing the ISOLTRAP and TITAN have produced new accurate mass data up to the  
 852 neutron-rich  $^{54}\text{Ca}$  isotope with  $N = 34$ , see Ref. [69, 83]. The data show a distinct drop of about 5 MeV for  
 853  $S_{2n}$  between  $N = 28$  and  $N = 30$  as well as another drop of about 3 MeV from  $N = 32$  to 34. A similar trend was  
 854 observed for the neutron-rich K isotopes in a later study also with the ISOLTRAP mass spectrometer [58].  
 855  
 856  
 857  
 858

859 The drop at  $N = 34$  has been interpreted as a prominent new shell closure at  $N = 32$ . The observation  
 860 was explained to be due to the influence of three nucleon forces as calculated with a chiral effective field  
 861 theory. New measurements of the charge radii of the same Ca isotopes up to  $^{52}\text{Ca}$  by laser spectroscopy have  
 862 revealed a somewhat unexpected behavior of the charge radii, see Ref. [123]. Instead of the expected decrease  
 863 of the charge radius at the shell closure  $N = 32$ , a significant gradual increase from  $^{48}\text{Ca}$  towards heavier Ca  
 864 isotopes was observed. Adequate theoretical explanation for this is lacking, which sets a challenge for future  
 865 experiments as well as theories. Figure 14 shows the two-neutron separation energy for neutron-rich Ca  
 866 isotopes together with the theoretical values derived from the mass values of Ref. [111, 124]. The general agree-  
 867 ment is rather satisfactory, although the theoretical calculations seem rather insensitive to experimental shell  
 868 closures at  $N = 28$  and  $N = 32$ .  
 869  
 870  
 871  
 872  
 873  
 874  
 875  
 876  
 877

### 878 3.2.2. Neutron-rich Kr and Zr isotopes. Deformation around $N=60$

879 As shown in the previous discussion and in Fig. 13 the onset of large deformation is observed between  
 880  $N=58$  and 60 for Zr isotopes in the form of a kink in the two-neutron binding energy curve but at the same time  
 881 this feature seems to completely disappear for krypton isotopes at the corresponding neutron number. Figure  
 882 15 shows a comparison between DFT calculations and experimental data for Kr (a) and Zr (b) isotope chains.  
 883 The Sly4 functional seems to describe the data better, even overemphasizing behavior at the spherical closed  
 884 shells, whereas the UNEDF0 functional gives clearly a  
 885  
 886  
 887  
 888  
 889  
 890

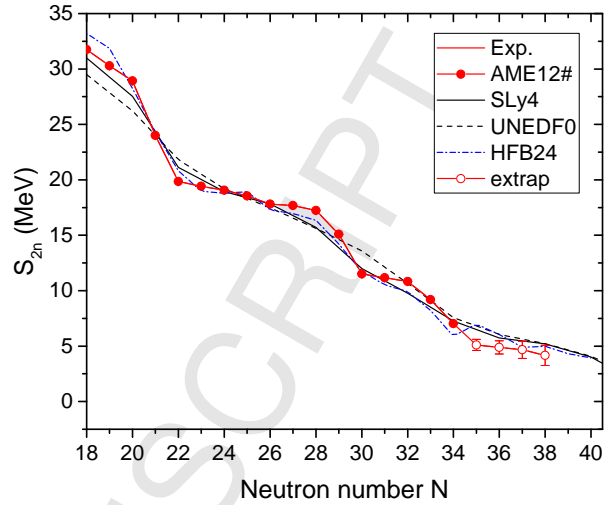


Figure 14: Two-neutron separation energies for neutron-rich calcium isotopes.

891 better overall description including the region of deformation (Zr) around  $N = 60$ .  
 892

### 893 3.2.3. Neutron-rich radium and francium isotopes

894 Heavy neutron-rich francium ( $Z = 87$ ) and radium ( $Z = 88$ ) isotopes were studied at ISOLTRAP providing  
 895 accurate mass data up to  $N=146$ , being one of the most neutron-rich data sets far from the valley of beta stability,  
 896 see Ref. [75]. Both Fr and Ra behave in a similar way for their two-neutron separation energies. Since the  
 897 DFT calculations are only available for the even-even nuclides we show in Fig. 16 the  $S_{2n}$  plots only for the  
 898 radium isotopes. It seems that the UNEDF0 functional gives a very nice agreement with the experimental data  
 899 in particular beyond  $N = 132$ . SLy4 seems to overpredict the values at and below  $N = 126$  and underpredict  
 900 above.  
 901  
 902  
 903  
 904  
 905  
 906

### 907 3.2.4. Evolution of the two-neutron shell closure at $N = 50$

908 For more quantitative insight into the question of the changes in mass values around shell closures, one can  
 909 investigate the two-nucleon binding energy differences for neutrons or protons. For this purpose, we have  
 910 plotted two-neutron separation energies in Fig. 17 for  $N = 46, 48, 50, 52$  and 54 isotones as a function of  
 911 the proton number. The energy difference between the  $N = 50$  and  $N = 52$  isotones corresponds to a two-  
 912 neutron shell gap across  $N = 50$ . When moving down in  $Z$  from the semi-doubly magic  $^{90}\text{Zr}$ , there is an obvi-  
 913 ous trend for lowering the value having a minimum at Ge ( $Z = 32$ ). This corresponds also to a minimum in  
 914  
 915  
 916  
 917  
 918  
 919  
 920

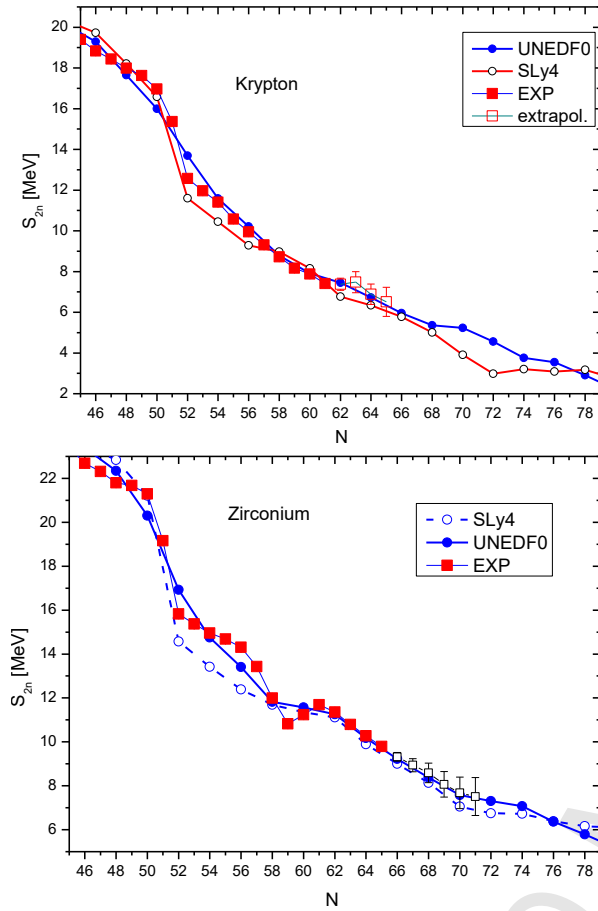


Figure 15: Two-neutron separation energies for neutron-rich krypton and zirconium isotopes.

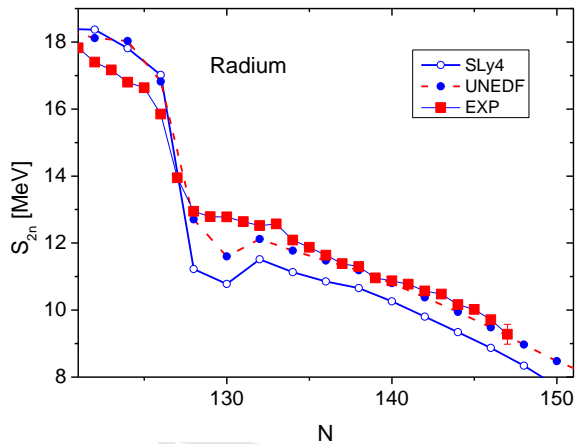


Figure 16: Two-neutron separation energies for neutron-rich radium isotopes.

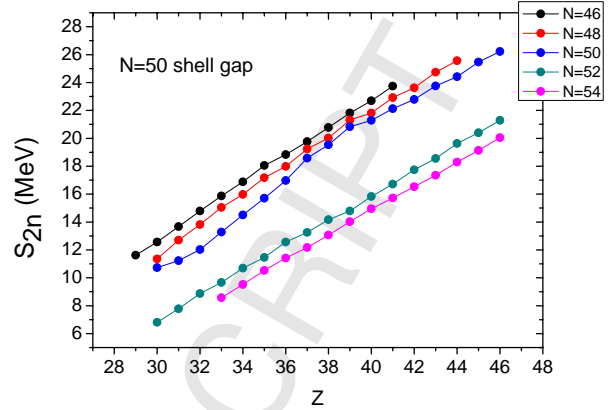


Figure 17: Experimental two-neutron separation energies as a function of proton number for  $N = 50$  shell gap. The uncertainties are smaller than the sizes of the data points.

921 the systematics of the first  $2^+$  energies of known even-  
 922  $A$   $N = 50$  isotones suggesting maximum impact from  
 923 core polarization effects. The isotone curves also indicate that the  $N = 50$  gap seems to increase towards  
 924 the doubly-magic Ni core ( $Z = 28$ ). Since our previous review a new and important additional data point  
 925 obtained from the measurement of the mass of  $^{82}\text{Zn}$  at  
 926 ISOLTRAP [70] could be included in the plot.  
 927  
 928

### 929 3.2.5. Two-neutron shell gaps and theoretical comparison

930  
 931 The question of how the known spherical shell closures persist when moving far away from the valley of  
 932 stability is a fundamental and important question for nuclear structure physics. Therefore, the comparisons of  
 933 the data with various theoretical approaches are needed. Figures 18 and 19 show the comparison of the exper-  
 934 imental values with three different types of theoretical models. These models are described and tested against  
 935 the total mass values in chapter 3.1. It is obvious that all models follow the general trend of the shell gaps for  
 936 all studied neutron shell closures in a reasonable way. The new finite range droplet model FRDM2012 seems  
 937 to reproduce the shell gaps in the studied region rather well. Also, the other similar microscopic-macroscopic  
 938 approach WS-4 follows the FRDM2012 values closely except for the  $N = 50$  but with some shifts in the neu-  
 939 tron number. The more universal HFB model HFB24 seems to reproduce the trends best, in particular near  
 940 the  $Z = 28, N = 50$  region. However, its prediction below  $Z = 28$  shows somewhat odd large drop which is  
 941 difficult to understand.  
 942  
 943  
 944  
 945  
 946  
 947  
 948  
 949  
 950  
 951

952 The values obtained with two density functionals  
 953 used in the mean-field calculations, Sly4 and UNEDF0

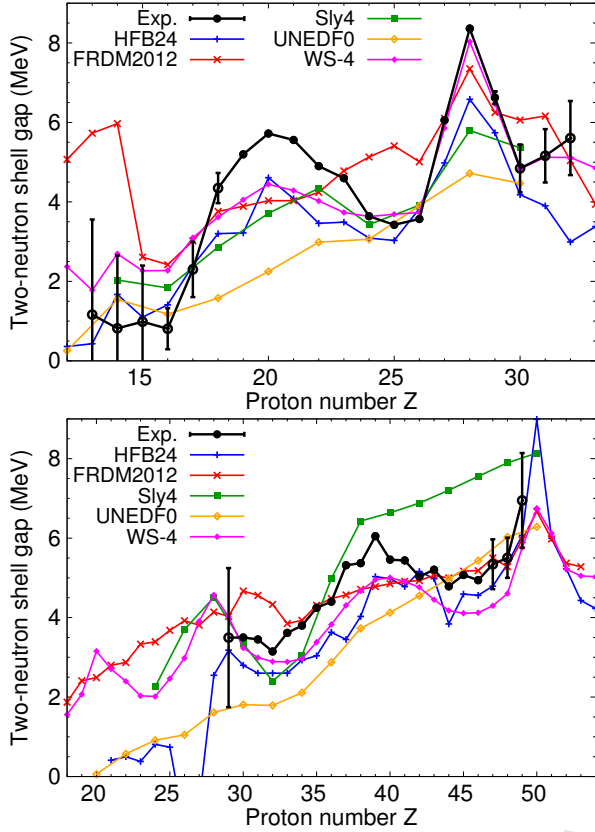


Figure 18: The  $N = 28$  (top panel) and  $N = 50$  (bottom panel) two-neutron shell gaps as a function of the proton numbers. See text for the explanation of the model calculations.

954 differ strongly from each other. The former one pro-  
 955 duces better the doubly-closed shell-gap values, but the  
 956 UNEDF0 functional is rather insensitive to those, and  
 957 rather exhibits a gradual reduction in its value outwards  
 958 from stability. In fact, it even seems to predict a gradual  
 959 disappearance of the shell gap towards the limits of nu-  
 960 clear binding. This is very interesting in the light of its  
 961 fairly good agreement with the two-neutron binding en-  
 962 ergies shown in Figs. 14, 15 and 16 in the neutron-rich  
 963 wings of the curves.

#### 964 4. Isobaric mass doublets and isospin multiplets

965 As described in section 2.3.1, measurements of mass  
 966 differences of mass doublets (those that have the same  
 967  $A/q$ ) form a special subset of Penning trap mass spec-  
 968 trometry. From experimental point of view, the mass  
 969 difference can be determined with extremely high preci-  
 970 sion: even on the order of  $10^{-10}$  in the frequency ratio,  
 971 allowing eV-level precision for  $Q$ -value determination

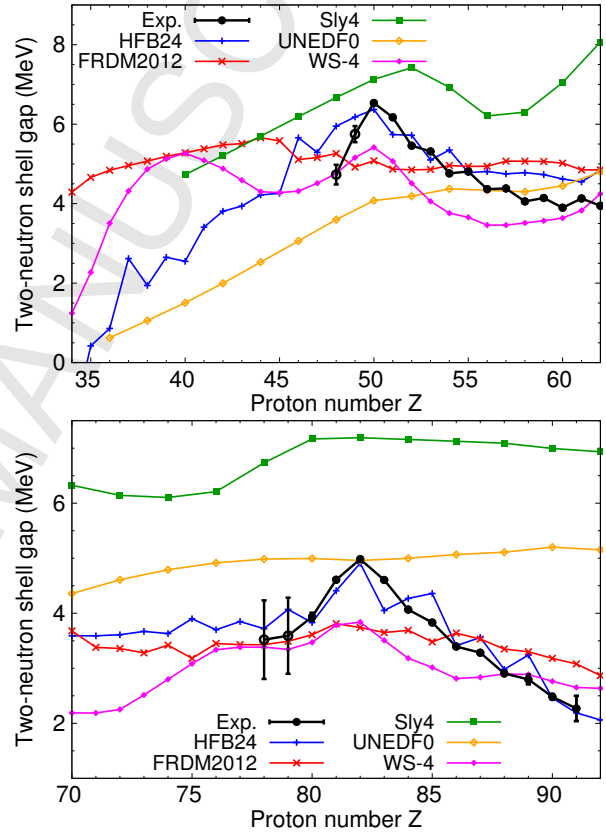


Figure 19: The  $N = 82$  (top panel) and  $N = 126$  (bottom panel) two-neutron shell gaps as a function of the proton numbers. See text for the explanation of the model calculations.

972 [27] with the PI-ICR technique or  $10^{-9}$  level with TOF-  
973 ICR technique.

#### 974 4.1. Superallowed and $T = 1/2$ mirror beta decays

975 The doublet technique has been extensively used for  
976 measuring the  $Q_{EC}$  values of  $T = 1$  superallowed and  
977  $T = 1/2$  mirror beta decays. In these cases the par-  
978 ent and daughter have always same mass number. Both  
979 mirror  $\beta$  decays and superallowed  $\beta$  decays contribute  
980 to the testing of the Standard Model of Particle Physics.  
981 Namely, the  $V_{ud}$  of the Cabibbo-Kobayashi-Maskawa  
982 (CKM) quark mixing matrix can be deduced. Here  
983 the superallowed beta decays, due to very simple de-  
984 cay matrix element, produce the most precise  $V_{ud}$  value  
985 [125]. In addition to half-life, branching ratio and  $Q$ -  
986 value needed for superallowed  $\beta$  decays, it is necessary  
987 to determine  $\beta - \nu$  angular correlations for mirror nuclei  
988 [126].

##### 989 4.1.1. Superallowed $\beta$ decays

990 As of today,  $Q$ -values of all the “well known” Su-  
991 perallowed  $\beta$  emitters spanning in 14 transitions in to-  
992 tal, have been measured to a high precision with Pen-  
993 ning traps (see Ref. [125] and references therein).  
994 JYFLTRAP has been the most contributing trap here  
995 and some cases like  $^{38}\text{Ca}$ , have been measured with  
996 many trap facilities. The  $Q$ -value of the final 14th,  $^{14}\text{O}$   
997 was measured in 2015 by LEBIT [127].

998 The most controversial findings of the  $Q$ -values was  
999 the disagreement of  $^{46}\text{V}$   $Q$ -value to the older reaction-  
1000 based results [128, 129] by CPT and JYFLTRAP  
1001 groups. Measurements of  $^{50}\text{Mn}$  and  $^{54}\text{Co}$  revealed sim-  
1002 ilar disagreements prompting for re-evaluation of the  
1003 isospin-symmetry breaking corrections [130].

##### 1004 4.1.2. Mirror decays

1005 Mirror decays might soon yield the next-best  $V_{ud}$   
1006 value after superallowed  $\beta$  emitters. Clearly the most  
1007 challenging quantity to measure is the  $\beta - \nu$  angular cor-  
1008 relation coefficient, which are currently being pursued  
1009 at many facilities.

1010 The  $Q$ -values are now actively being measured, and  
1011 several new  $Q$ -values have emerged recently, summa-  
1012 rized in Table 6. Some mirror nuclei have been already  
1013 measured earlier at JYFLTRAP, such as  $^{23}\text{Mg}$  [131],  $^{31}\text{S}$   
1014 [132], and heavier mirror nuclei  $^{53}\text{Co}$ ,  $^{55}\text{Ni}$ ,  $^{57}\text{Cu}$ , and  
1015  $^{59}\text{Zn}$  [133].

#### 1016 4.2. Isobaric Multiplet Mass Equation

1017 Assuming nuclear force is charge-independent, the  
1018 masses of the members of an isobaric multiplet should

Table 6:  $Q_{EC}$ -values of mirror nuclei published recently. Both the reported  $Q_{EC}$ -value and comparison from AME2012 derived values are given.

| Decay            | new $Q_{EC}$ (keV) | AME2012     | Ref. |
|------------------|--------------------|-------------|------|
| $^{21}\text{Na}$ | 3547.11(9)         | 3547.14(28) | [93] |
| $^{23}\text{Mg}$ | 4056.35(16)        | 4056.6(7)   | [94] |
| $^{25}\text{Al}$ | 4276.805(45)       | 4276.6(5)   | [95] |
| $^{29}\text{P}$  | 4942.18(37)        | 4942.6(6)   | [93] |
| $^{45}\text{V}$  | 7123.82(22)        | 7128(8)     | [96] |
| $^{49}\text{Mn}$ | 7712.42(24)        | 7695(10)    | [96] |

1019 show a quadratic behaviour:

$$1020 \quad M(A, T, T_Z) = a(A, T) + b(A, T)T_Z + c(A, T)T_Z^2 \quad (9)$$

1021 where  $T$  is the isospin,  $T_Z$  the isospin projection and  
1022  $M(A, T, T_Z)$  is the mass of the isobaric analogue state  
1023 (IAS) of the  $T_Z$  member in the  $T$  isobaric multiplet. The  
1024 Eq. (9) is known as the Isobaric Multiplet Mass Equa-  
1025 tion (IMME). The quadratic form works quite well for  
1026 a majority of isobaric multiplets, see e.g. recent reviews  
1027 and compilations of the IMME coefficients [134–136].  
1028 However, in a couple of cases, it deviates significantly  
1029 from the quadratic form. Penning-trap measurements  
1030 have revealed a breakdown of the quadratic IMME for  
1031 several multiplets. The TITAN mass measurements of  
1032  $^8\text{He}$  [137],  $^9\text{Li}$  [90],  $^9\text{Be}$  [90] and  $^{21}\text{Mg}$  [91] have re-  
1033 vealed breakdowns of the quadratic IMME for the  $T = 2$   
1034 quintet at  $A = 8$  [137, 138], as well as for the  $T = 3/2$   
1035 quartets at  $A = 9$  [90] and  $A = 21$  [91], respectively. Re-  
1036 cent measurement of  $^{31}\text{Cl}$  [92] at JYFLTRAP has shown  
1037 that the quadratic form cannot describe the  $T = 3/2$   
1038 quartet at  $A = 31$ . The  $T = 2$  quintet at  $A = 32$   
1039 has been probed via  $^{32}\text{Si}$  and  $^{32}\text{S}$  mass measurements at  
1040 LEBIT [139],  $^{32}\text{Ar}$  at ISOLTRAP [140], and indirectly  
1041 via the mass measurement of  $^{31}\text{S}$  [132] at JYFLTRAP  
1042 combined with the measured proton separation energy  
1043 of  $^{32}\text{Cl}$ , and it has been shown to be significantly deviate  
1044 from the quadratic form. The ISOLTRAP measurement  
1045 of  $^{35}\text{K}$  for the  $T = 3/2$  quartet at  $A = 35$  [141] has also  
1046 revealed a breakdown of the IMME. The breakdown of  
1047 the IMME has been explained, e.g. by isospin mixing  
1048 of the states and charge-dependent effects [90, 142].

1049 The precision achieved in Penning-trap measure-  
1050 ments today is so high that the the excitation energies  
1051 of the isobaric analog states of the other members of  
1052 multiplets than  $T_Z = \pm T$ , in particular of the  $T_Z = 1 - T$   
1053 member, have become the limiting factors for probing  
1054 the validity of the IMME. For example, the TITAN ex-  
1055 periment on  $^{20}\text{Mg}$  showed a breakdown of the IMME  
1056 [91], but it was later revalidated by a new measurement

of the IAS in  $^{20}\text{Na}$  via  $\beta^+$  decay of  $^{20}\text{Mg}$ . The break-downs for the  $T = 3/2$  quartets at  $A = 33$  [143] and  $A = 53$  [144], have also been revalidated by measurements of the IAS energies in  $^{33}\text{Cl}$  [145] and  $^{53}\text{Co}$  [146].

## 5. Trap-assisted spectroscopy

Although ion traps in nuclear physics are mostly used for direct measurements of nuclear masses they can also contribute to providing isotopically and sometimes even isomerically pure sources for measurements of radioactive decays. Routinely, the mass resolving power  $M/\Delta M$  of the order of  $10^5$  can be reached which allows clean separation of neighboring isobaric nuclides and thus decay spectroscopy of sources free from contaminant activities. Recently separation of a heavy ion isomeric beam with a multiple-reflection time-of-flight mass spectrometer has also been demonstrated as a potential device for trap-assisted spectroscopy [147].

With the Ramsey cleaning technique, as described in chapter 2.6 for JYFLTRAP, decay spectroscopy of a nucleus in its pure isomeric state with energy of the order of  $> 100$  keV has become possible. Ions of isotopically or isomerically purified radionuclides can either be extracted out of or stored in the trap for subsequent in-trap decay measurements. In the former case, ions are extracted out of the trap as a beam which is directed and deposited on a catcher foil or a movable tape for subsequent decay measurements using standard detector arrays for beta-, gamma-, neutron or charged particle detection. In the latter case, the ions can also be kept by the trapping potential inside the trap vacuum where their decays are observed. Such massless sources of short half-lived nuclei provide ideal conditions for high-resolution detection of emitted charged particles down to very low energies

### 5.1. In-trap spectroscopy

Measurement of particles and photons emitted in the decays of radioactive ions stored in a trap offers many interesting applications for fundamental physics as well as for nuclear structure physics. Such experiments can utilize, for example, Paul traps, Penning traps or electron beam ion traps (EBITs) or coupled combinations of them.

#### 5.1.1. Penning trap spectroscopy

Among the first applications of ion traps for in-trap spectroscopy has been discrete-energy conversion electron spectroscopy. As an example, the scheme of the JYFLTRAP setup used in feasibility studies for short-lived isomers is shown in Fig. 20 (from Ref. [148]).

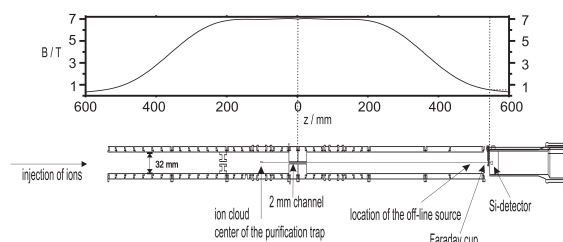


Figure 20: The electrode structure inside the magnetic solenoid of the JYFLTRAP spectrometer. This figure is from Ref. [148].

The studied nuclei in their isomeric states were produced in proton-induced fission of  $^{238}\text{U}$  at the IGISOL3 facility followed by their injection into the linear RFQ cooler buncher device. Ions were then extracted in short bunches and injected into a double Penning trap described in chapter 2. Inside the first trapping region the motion of ions was cooled with helium buffer gas and simultaneously applying successive magnetron ( $\nu_-$ ) and cyclotron ( $\nu_c$ ) excitations. As a result of this mass-selective process, only the ions obeying the cyclotron resonance condition were centered in the symmetry axis of the trap. In order to maintain the ions in a cloud of about 1 mm in diameter, successive RF pulses at  $\nu_c$  were applied for a repeated re-centering [148]. Conversion electrons emitted from the centered ions were transported through a 2 mm diameter channel to the Si-detector while the electrons emitted from the off-centered ions hit the center electrode of the trap. The measurements employed a high-resolution Si-detector having a  $10 \text{ mm}^2$  sensitive area and a thickness of  $500 \mu\text{m}$  and with a dead-layer thickness of  $250 \text{ \AA}$ .

A conversion electron spectrum recorded from the decays of short-lived  $^{117\text{m}}\text{Pd}$  isomer is shown in Fig. 21. The decay of this isomer is featured by electron peaks due to two converted transitions at 34.5 and 168.6 keV. The corresponding K conversion lines at 9 and 143 keV show a resolution of about 2 keV, which consists of the intrinsic resolution of the detector itself and broadening of the lines due to back-scattering effects. The intrinsic line widths of the measured transitions were estimated to be less than eV, due to natural line widths of the transitions as well as thermal effects in the electron emitting ion cloud. The overall detection efficiency for the transitions seen in Fig. 21 were estimated in Ref. [148] to be of the order of 30-40 %.

#### 5.1.2. Paul and Penning trap spectroscopy for beta-neutrino correlation measurements

The early applications of in-trap spectroscopy were devoted to studies of energy and angular correlations



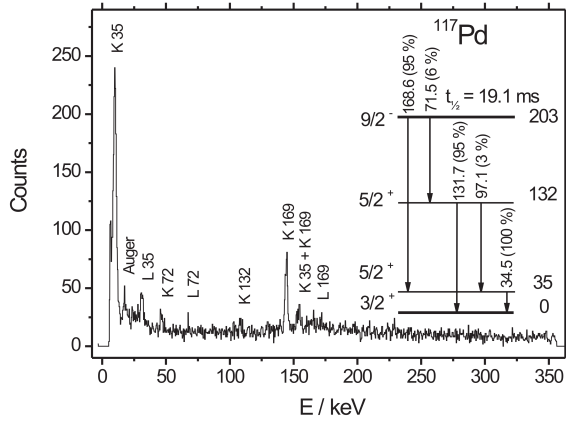


Figure 21: In-trap electron spectrum recorded for  $^{117m}\text{Pd}$ . This figure is from Ref. [148].

between beta particles and recoil nuclei with the aim to search for scalar and tensor currents in the weak interaction. Two examples of applying Paul trap in such experiments are described in refs. [149, 150]. The results of both approaches are consistent with a purely V-A interaction, and in the case of couplings, to right-handed neutrinos. The LPC trap is operational at GANIL and has a transparent electrode structure which allows high-efficiency and precise measurements of the  $\beta - \nu$  angular correlation parameter in nuclear  $\beta$  decays. The setup is installed at the low energy beam line, LIRAT, of the GANIL/SPIRAL facility. Measurements have been performed for three different nuclei  $^6\text{He}$ ,  $^{19}\text{Ne}$  and  $^{35}\text{Ar}$  that were ionized in an ECR ion source prior to their injection to the measurement trap. With the precise value of the angular correlation parameter, the experiment on the  $^{35}\text{Ar}$  mirror decay will also contribute to the more accurate extraction of the  $V_{ud}$  matrix element of the CKM matrix of the standard model.

At Argonne National Laboratory beta-neutrino correlations are studied in the beta decay of  $^8\text{Li}^+$  ions stored in the Beta-Decay Paul Trap (BPT) [151]. This trap is a linear Paul trap constructed with thin planar electrodes that provide an open geometry to allow for large solid-angle detector coverage. Prior to Paul trap the ions produced in  $^7\text{Li}(d,p)$  reactions were prepared for injection in the CPT Penning trap. The beta-recoil correlation measurement was based on the detection of  $\beta$  decay of  $^8\text{Li}$  and subsequent breakup of the  $^8\text{Be}$  daughter to two  $\alpha$ -particles.

In the Penning trap side, the WITCH (the Weak Interaction Trap for Charged Particles) trap is dedicated for  $\beta - \nu$  angular correlation measurements [152]. There, the

angular correlation coefficient is derived from the shape of the recoil energy spectrum by using retardation potential.

### 5.1.3. Paul trap spectroscopy for beta-delayed neutrons

The Beta-Decay Paul trap configuration as the one described above has also been applied in a feasibility study for beta-delayed neutron spectroscopy. Neutron energy was determined using the beta-recoil-ion coincidence time of flight, see ref. [21]. Neutron emission leads to high-energy recoils having short TOFs, with the lower-energy recoil imparted by the electron and antineutrino being a small perturbation to the measurement. The setup used in this study is shown in Fig. 22. The neutron precursor  $^{137}\text{I}$  was produced in fission from a 1 mCi  $^{252}\text{Cf}$  source and thermalized as singly charged ions in a large-volume gas catcher [153]. The  $A = 137$  singly-charged fission product ions were separated by the Canadian Penning Trap (CPT) prior to their injection into the open Paul trap structure. Recoil-ion TOF spectrum collected with a 30 ions/s  $^{137}\text{I}^+$  beam is shown in Fig. 22. The TOF spectrum of the  $^{136}\text{Xe}$  recoil ions from beta-delayed neutron emission, highlighted by the dotted box, is shown in the inset. The energy range covered extended from about 200 keV threshold energy up to 1.5 MeV. The study showed that this technique has a high potential for delayed-neutron energy measurements with high efficiency of the order of 1 %, neutron-energy thresholds of about 100 keV and a good energy resolution.

### 5.1.4. Electron Beam Ion Trap for gamma- and X-ray spectroscopy.

A novel concept for in-trap decay spectroscopy has been devised at ISAC of TRIUMF where electron-beam ion trap (EBIT) has been used for long-term storage of highly charged ions [154]. The setup has been developed with a special emphasis on precision spectroscopy of low branching ratios and is being developed in the context of measuring electron-capture branching ratios needed for determining the nuclear ground-state properties of the intermediate odd-odd nuclei in double-beta ( $\beta\beta$ ) decay. The EBIT is a central part of the TITAN ion trap system and can be fed with purified samples from the adjacent linear RFQ trap. Storage of radioactive ions in vacuum in an open-access EBIT allows observing their decay in a backing-free environment. Simultaneously, the high magnetic field of EBIT provided an efficient spatial separation between decay photons and decay positrons removing bremsstrahlung background. This unique feature is especially advantageous in cases of electron-capture (EC) decays, where



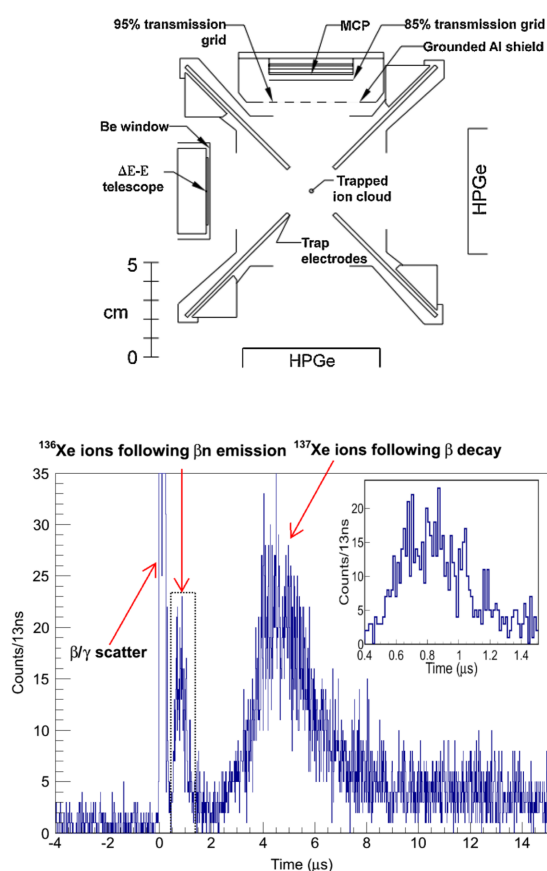


Figure 22: *Above*: A cut view of the Open Paul trap at ANL, *Below*: Time of Flight spectrum of  $^{137}\text{Xe}$  ions triggered by the beta detector. These figures are from Ref. [21].

1227 the measurements of low-intensity and low-energy X-  
 1228 rays are required. The approach has been successfully  
 1229 demonstrated by a measurement of the decays of highly  
 1230 charged radioactive ions of  $^{124}\text{In}$  and  $^{124}\text{Cs}$  [155].

## 1231 5.2. Post-trap decay spectroscopy

1232 Decay spectroscopy for nuclear structure physics at  
 1233 ISOL facilities has long been a backbone in studies of  
 1234 exotic nuclei far from stability. However, when mov-  
 1235 ing further from the valley of stable nuclei, increas-  
 1236 ing complexity of decay patterns and low production  
 1237 rates of these nuclei have led to even more stringent re-  
 1238 quirements for experimental methods. On top of this  
 1239 development there have been many innovations on se-  
 1240 lective ionization methods applicable to produce ini-  
 1241 tially purified beams. However, with the introduction of  
 1242 novel universal production methods, such as in-flight or  
 1243 IGISOL methods, requirements for fast purification of  
 1244 isomers and isotopes for decay spectroscopy have be-  
 1245 come necessary. In addition, the ion manipulation by  
 1246 ion traps can significantly improve the emittance, re-  
 1247 duce the energy spread and modify the time structure  
 1248 of the ion beams used for decay spectroscopy.

### 1249 5.2.1. Conventional decay spectroscopy of trap- 1250 purified isotope sources

1251 Ion trap systems coupled to ISOL or in-flight gas  
 1252 catcher based production facilities can offer powerful  
 1253 means for spectroscopy applications. In this context  
 1254 we introduce two programs, one at ISOLDE and one  
 1255 at IGISOL, where the method is already in full use. The  
 1256 ISOLTRAP facility at ISOLDE in combination with  
 1257 the recently installed decay-spectroscopy setup [156]  
 1258 will make it possible to combine high-precision mass  
 1259 measurements with nuclear-decay spectroscopy. This  
 1260 combination allows the assignment of masses with the  
 1261 corresponding decaying states, particularly important  
 1262 in cases where isomeric state(s) are involved. A re-  
 1263 cent experiment utilizing this approach revealed identity  
 1264 (spin/parity/mass) for the ground and isomeric states of  
 1265 even neutron-deficient  $^{190,194}\text{Tl}$  isotopes [157].

1266 An active decay spectroscopy program using the  
 1267 JYFLTRAP setup has addressed mainly the nuclear  
 1268 structure studies of neutron-rich nuclei produced in fis-  
 1269 sion. Additionally, a few half-life and branching-ratio  
 1270 measurement campaigns for the superallowed beta de-  
 1271 cays have been carried out, see e.g. [158–160]. In the  
 1272 next section, we mainly focus on decays of medium-  
 1273 mass neutron-rich nuclei. These nuclides are typically  
 1274 produced in fast proton-induced fission of  $^{238}\text{U}$ . Short-  
 1275 lived fission fragments thermalized in helium gas as

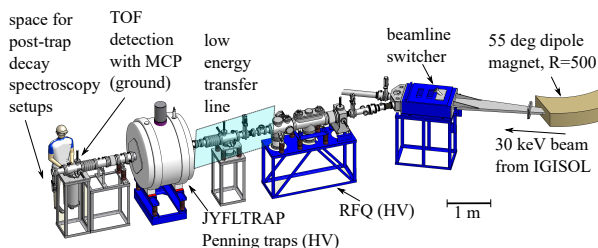


Figure 23: JYFLTRAP setup at IGISOL3. The beam from the IGISOL gas cell is separated with an ordinary dipole magnet (right) before injecting the mass-selected beam to into the RFQ. See text for more explanation.

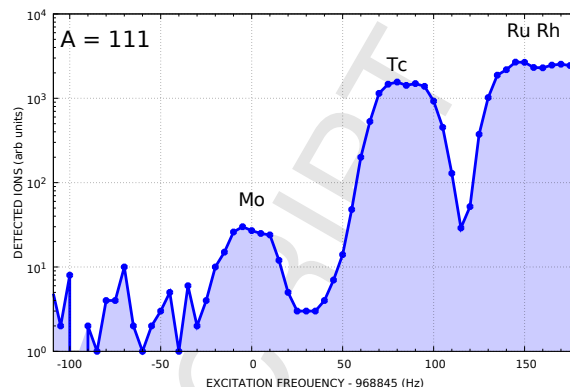


Figure 24: Mass spectrum of  $A = 111$  isobars.

ions are reaccelerated and separated by the IGISOL system with a mass resolving power of  $M/\Delta M \sim 500$ . This resolving power is good enough to separate nuclei of one mass number only from all other nuclear species produced in fission. Thus, separated radioactive beam consist of a complete chain of nuclei within the same isobar produced directly in fission. In the past, these multi-component isobaric beams were successfully used to study many exotic, neutron-rich nuclei of refractory elements unavailable at other ISOL facilities. However, a serious problem with isobaric contaminants made it very difficult to extend these studies weakly produced nuclides further from stability. Therefore, the double Penning trap system JYFLTRAP was developed and constructed to provide high enough mass resolving power for the production of pure isotopic as well as even isomeric beams for nuclear spectroscopy. The layout of the JYFLTRAP at IGISOL3 [24] setup is shown in Fig. 23.

Ions after the mass separation at IGISOL are injected into a buffer-gas filled RFQ trap where they are rapidly ( $\sim$ ms) cooled and subsequently stored in a potential well produced by the combination of the electric RF and DC potential. Ions are then extracted in the form of short, typically a few  $\mu$ s long bunches and transported into the double Penning trap system for purification. The necessary steps for cleaning are described in chapter 2.5. In the simplest approach, mass selective buffer-gas cooling is applied in the first trap, after which the ions are ejected through a narrow channel separating the purification and the precision traps, and out from the trap system to the spectroscopy setup. Another approach, if necessary, would be to use the higher resolution precision trap for additional purification. This technique has been used for example to resolve the ground and isomeric states of  $^{100}\text{Nb}$  to study their beta decay schemes to  $^{100}\text{Mo}$  [161].

### 5.2.2. Nuclear structure studies

The focus of the decay spectroscopy program at IGISOL has for some years been in studies of the evolution of coexisting shapes in neutron-rich nuclei around  $A=100-120$ . This mass region located between the closed doubly magic core nuclei  $^{78}\text{Ni}$  and  $^{132}\text{Sn}$  is very rich consisting of different structures, including those with prolate, oblate and triaxial shapes. Experimental tracking of the systematics of these structures provides important testing ground for theoretical calculations, which are eventually needed in predicting the properties of even more neutron-rich nuclides involved, for example, in understanding the r-process synthesis of heavy elements. As an example of such a study we describe here the decay spectroscopic study of a neutron-rich isotope  $^{111}\text{Mo}$  which employed isotopically purified sources of  $^{111}\text{Mo}$  nuclei [162]. The mass spectrum of the  $A = 111$  isobars as measured by the purification trap of the JYFLTRAP setup is shown in Fig. 24. As shown in this figure, a monoisotopic beam of  $^{111}\text{Mo}$  could be delivered for decay spectroscopy when the filtering frequency of the trap was set to 968845 Hz. A typical rate of about 20 ions/s of  $^{111}\text{Mo}$  was observed with the MCP detector positioned after the trap. This rate allowed for a complete X-ray spectroscopy for constructing the low-lying level structure for the daughter nucleus  $^{111}\text{Tc}$ . Due to a short half-life of about 200 ms the trap purification cycle of 120 ms was used. The daughter nucleus  $^{111}\text{Tc}$  has also a relatively short half-life of about 350 ms. Therefore, its beta-delayed gamma-transitions are also observed as daughter products in the gamma-ray spectrum corresponding to the  $^{111}\text{Mo}$  setting of the trap, see Fig. 25.

The level scheme of  $^{111}\text{Tc}$  constructed from this experiment revealed excited structures fed in the beta decay up to slightly below 600 keV in excitation energy.

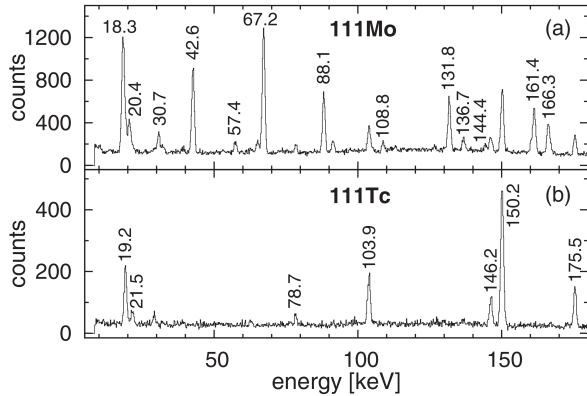


Figure 25: Beta-gated gamma-ray spectra corresponding to the trap cyclotron resonance frequencies for  $^{111}\text{Mo}$  and  $^{111}\text{Tc}$ .

Earlier unobserved, new excited levels in  $^{111}\text{Tc}$  populated in the  $\beta$ -decay of  $^{111}\text{Mo}$  provided the first indication for a low-lying oblate deformation in the mass  $A \approx 110$  region. This solution coupled to the QPRM calculations offers an explanation for the two lowest-energy states with  $I = (1/2, 3/2)^+$  at 30.7 keV and  $I = 5/2^+$  at 42.6 keV to present the first clear indication of a tri-axial oblate shape in the  $A \approx 110$  neutron-rich nuclei. Additionally, a wide range of levels with different spins indicate the existence of at least two  $\beta$ -decaying states in  $^{111}\text{Mo}$  which could not be separated with the available resolving power of  $M/\Delta M \sim 30,000$ . One should note, however, that the beta-decay energy window or the  $Q_\beta$ -value of  $^{111}\text{Mo}$  is considerably larger, e.g. 9085(5) keV as determined by the JYFLTRAP mass measurement. Therefore, although important for producing relevant information on the low-lying level structure of  $^{111}\text{Tc}$  the described spectroscopy experiment could cover only marginally gross beta-decay properties of  $^{111}\text{Mo}$ .

### 5.2.3. Total Absorption Gamma-ray Spectroscopy

To correct for the deficit related to observing weak branches to high-lying states, another approach based on the total absorption spectroscopy has to be applied in combination with trap-produced isotopes. So far, in addition to nuclear structure studies, this technique in connection with the trap-purified isotope sources has been applied for the measurements of interest for the decay heat of the nuclear reactors and for the determination of the electron antineutrino spectrum from thermal reactors of relevance for the neutrino oscillation experiments [163]. In the former case,  $\beta$ -feeding probabilities for three important contributors to the decay heat in nuclear reactors, namely  $^{102,104,105}\text{Tc}$ , have been measured, resulting significant improvements and solving a large

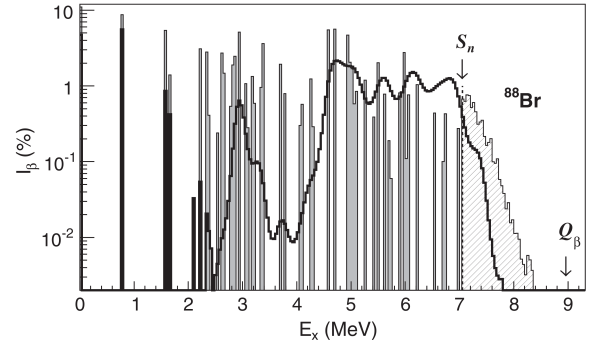


Figure 26: Beta decay strength distribution for  $^{88}\text{Br}$ , from Ref. [165].

part of the discrepancy in the decay-heat data of  $^{239}\text{Pu}$  in the 300–3000 s cooling interval. In the latter case, the decay of  $^{92}\text{Rb}$ , which makes the dominant contribution to the reactor antineutrino spectrum in the 5–8 MeV range, was investigated, see ref. [164]. In these experiments, previously unobserved beta feeding was seen in the 4.5–5.5 MeV region and the ground-state to ground-state feeding was found to be 87.5(25) %, which is 7.7 % smaller than the previously used value. The overall impact of the new result from this experiment on the reactor antineutrino spectra is discussed in more detail in Ref. [164]. In another recent study, total absorption spectroscopy was used to investigate the  $\beta$ -decay feeding to states below and above the neutron separation energy followed by  $\gamma$ -ray emission in  $^{87,88}\text{Br}$  and  $^{94}\text{Rb}$ . An unexpected large  $\gamma$ -emission intensity was observed in all three cases extending well above the excitation energy region where neutron emission is no longer hindered by the angular momentum barrier, see ref. [165]. This is exemplified by the measured beta intensity distribution for  $^{88}\text{Br}$  in Fig. 26, where a significant amount of feeding to neutron unbound states can be seen to lead to gamma-emission.

### 5.2.4. Delayed neutron spectroscopy at JYFLTRAP

Beta-delayed neutron and multi-neutron emission become very important ingredients in the decay processes far away from the valley of stability. They also have a significant impact on the elemental and isotopic abundance distributions of the r-process nuclear synthesis. Thus, the total neutron emission probabilities, often denoted as  $P_n$ , are critical for r-process calculations (see, e.g. Ref. [119]). An example of the importance of the role of delayed neutron emission in the beta decay of highly neutron-rich nuclides is demonstrated in Fig. 27 below. Beta-delayed neutron emission probability in the case of niobium isotopes becomes observable already at

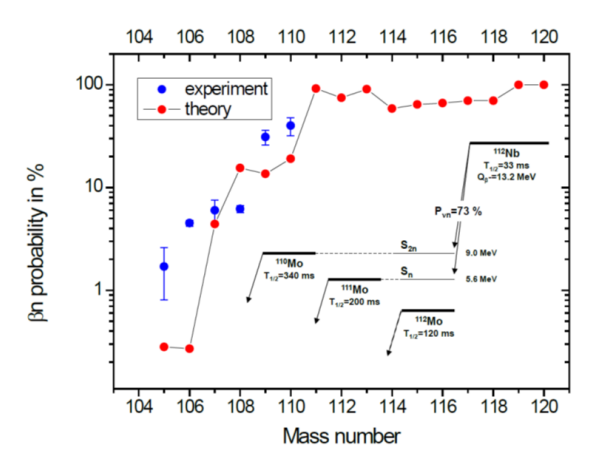


Figure 27: Beta-delayed neutron emission probability for a chain of Nb isotopes. Theoretical values are based on theoretical calculation employing the QRPA calculation and the finite range droplet model, from Ref. [168].

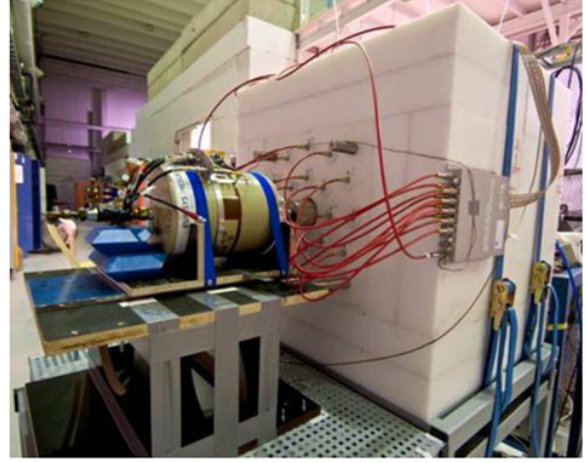


Figure 28: The neutron long counter system behind the JYFLTRAP setup. The setup includes also a HPGe detector for simultaneous gamma-ray spectroscopy.

1419 and beyond  $^{106}\text{Nb}_{65}$  and reaches rapidly nearly a 100 %  
 1420 probability for more neutron-rich Nb isotopes [166].  
 1421 As a consequence, beta-decay schemes become highly  
 1422 complex and experimental conditions demanding. One  
 1423 of the key requirements will then be set by the availabili-  
 1424 ty of isobarically and isotopically pure sources. One  
 1425 approach to reach such conditions is provided by the  
 1426 Penning-trap purified radioactive sources [167].

1427 On the other hand, the beta-decay feeding to individ-  
 1428 ual nuclear states and their de-excitation by gamma-ray  
 1429 and (multiple) neutron emission need to be known for  
 1430 nuclear structure studies. This necessitates the mea-  
 1431 surement of neutron energy, which can be done by using  
 1432 either secondary nuclear reactions or a time-of-flight  
 1433 method. These measurements are challenging due to  
 1434 the high complexity of required detection systems, such  
 1435 as large arrays of either  $^3\text{He}$ -based counters or scintil-  
 1436 lator detection systems, respectively. The total num-  
 1437 ber of neutrons can best be measured using a neutron  
 1438 long counter technique where neutrons are first thermal-  
 1439 ized and then detected, for example, by an array of  $^3\text{He}$   
 1440 counters embedded in a thermalisation medium. The  $P_n$   
 1441 value can then be extracted from the ratio of the mea-  
 1442 sured neutrons to the number of  $\beta$ -particles emitted from  
 1443 the source. The experimental uncertainty is highly depen-  
 1444 dent on the isotopic purity of the source which can  
 1445 be provided by the trap-assisted approach. A detec-  
 1446 tion system under development for the use at the future  
 1447 FAIR facility was recently commissioned with Penning-  
 1448 trap purified delayed neutron activities, see Fig. 28.  
 1449 In this setup, neutrons were detected with the BELEN

1450  $4\pi$  neutron counter, described in ref. [167]. The em-  
 1451 ployed detector configuration consisted of 20  $^3\text{He}$  pro-  
 1452 portional counter tubes at a pressure of about 20 atm.  
 1453 The tubes were embedded in a high density polyethy-  
 1454 lene block with overall dimensions 90 cm  $\times$  90 cm  $\times$   
 1455 80 cm, which acts as both neutron moderator and neu-  
 1456 tron background shielding. The detection efficiency  $\varepsilon_n$   
 1457 for the setup, as deduced from Monte Carlo (MC) sim-  
 1458 ulations, was close to 50% for neutron energies up to  
 1459 1 MeV. Well-known neutron-rich neutron emitters  $^{88}\text{Br}$ ,  
 1460  $^{94,95}\text{Rb}$  and  $^{138}\text{I}$  used in the commissioning experi-  
 1461 ment were produced in fission, separated by the IGISOL fa-  
 1462 cility and prepared as isotopically pure sources with the  
 1463 JYFLTRAP setup. Fig. 29 shows the growth and decay  
 1464 curves for the beta- and neutron-activities for the trap-  
 1465 purified  $^{94}\text{Rb}$  activity ( $T_{1/2} = 2.7$  s). The neutron time  
 1466 spectrum could be fitted very nicely using a single half-  
 1467 life component combined with a constant background.

Following this commissioning experiment, some ear-  
 1468 lier measured delayed neutron emitters east of the  $N=50$   
 1469 neutron shell were studied by this setup, see Ref. [169].  
 1470 The measured preliminary  $P_n$  values for four isotopes  
 1471 ( $^{85}\text{Ge}_{53}$ ,  $^{85}\text{As}_{52}$ ,  $^{86}\text{As}_{53}$  and  $^{91}\text{Br}_{56}$ ) agreed perfectly  
 1472 with the earlier measured data whereas the theoret-  
 1473 ical values based on QRPA- and shell-model based ap-  
 1474 proaches showed remarkable difference between theory  
 1475 and experiment, see Ref. [169] for more detailed infor-  
 1476 mation.



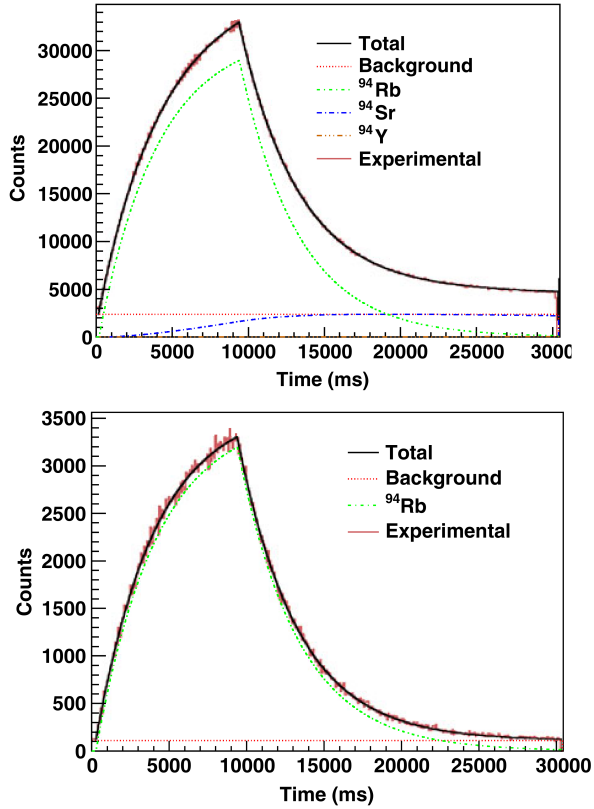


Figure 29: Growth-in and decay curves for trap-purified source of  $^{94}\text{Rb}$  as measured with the beta-counter only (top) and beta-gated neutron long counter (bottom). This figure is from Ref. [166].

### 5.3. Double Beta decay studies of relevance for neutrino physics

Neutrinos are one of the least understood fundamental particles. For half a century physicists thought that neutrinos, like photons, had no mass. But recent data from the neutrino oscillation experiments at SuperKamiokande, SNO, and KamLAND overturned this view and confirmed that the neutrinos are massive particles. However, oscillation experiments can yield only the differences in the squares of the neutrino masses, therefore, no absolute mass scale can be determined. In addition, another question remains concerning the fundamental character of neutrinos, whether they are Dirac or Majorana particles. Neutrinoless double beta decay is a process which can address both issues raised above. This decay process is forbidden according to the Standard Model of Particle Physics since it violates the lepton-number conservation and is only allowed if neutrinos are massive Majorana particles. The detection of this mode of double beta decay could result in the missing information on the neutrino mass scale and possibly also its mass hierarchy. In this context, an interesting application for the accurate mass measurements, available by the Penning trap technique, is to measure the decay energy values of all potentially interesting double beta-decaying nuclei. The accurate decay energy measurements are crucial for any experiment by searching for discrete sum energy peak of two emitted electrons (positrons) related to a neutrinoless double beta decay. Penning-trap experiments have recently provided new accurate  $Q$ -values for all currently relevant double-beta decay experiments and measured several additional and potentially interesting cases. These included not only  $0\nu\beta^-\beta^-$  or  $2\nu\beta^-\beta^-$  decaying isotopes but also  $0\nu ECEC$  and  $2\nu ECEC$  decaying nuclides. A decisive summary of the current experimental status of these  $Q$ -value measurements performed using Penning trap mass spectrometry is given in Refs. [22, 34]. In addition to the accurate  $Q$ -values needed for searching the signal from the neutrino experiments, also the relevant nuclear matrix elements for the transitions involved in the decay have to be known. This information, needed for the extracting the effective mass of the Majorana neutrino, will have to be obtained from theory. The half-life for  $0\nu\beta\beta$ , when mediated by the virtual exchange of light but massive Majorana neutrinos (the simplest interpretation), is given by:

$$\frac{1}{T_{1/2}^{0\nu}} = G_{0\nu} g_A^4 |M^{0\nu}|^2 \langle m_{\beta\beta} \rangle^2 \quad (10)$$

where  $G_{0\nu}$  is the energy-dependent phase space factor,  $M^{0\nu}$  is the nuclear matrix element (NME) and

1528  $m_{\beta\beta}$  is the effective neutrino mass. The NME has to  
 1529 be obtained from theory and has currently significant  
 1530 uncertainties. It can be calculated based on differ-  
 1531 ent modern methods of nuclear structure, such as Nu-  
 1532 clear Shell Model, Quasi-Random Phase Approxima-  
 1533 tion, Interaction Boson Model or Projected Hartree-  
 1534 Fock-Bogoliubov approach.

1535 The  $\beta\beta$  decay process, with neutrinos or without, can  
 1536 proceed via two-step virtual transitions through states in  
 1537 the intermediate nucleus. The  $0\nu\beta\beta$  decay would pro-  
 1538 ceed via intermediate states of all spins and parities,  
 1539 whereas the  $2\nu\beta\beta$  decay is restricted to Gamow-Teller  
 1540 (GT) transitions through states in the intermediate nu-  
 1541 cleus with  $J^\pi = 1^+$ . Therefore, experiments testing  
 1542 different theories for these matrix elements would be  
 1543 important. Three such systems, where linking transi-  
 1544 tions via the intermediate nucleus are available, have  
 1545 now been studied using the Penning trap setup at the  
 1546 IGISOL facility. These are the mass 96, 100 and 116  
 1547 multiplets related to possible candidates of  $^{96}\text{Zr}$ ,  $^{100}\text{Mo}$   
 1548 and  $^{116}\text{Cd}$  for the search experiments of the neutrino-  
 1549 less decay, see refs. [51, 170, 171] respectively. In the  
 1550 following we would like to focus on the most recent of  
 1551 these, the cases of  $^{116}\text{Cd}$  and  $^{96}\text{Mo}$ .

1552  **$^{116}\text{In}$  case.** Fig. 30 shows a simplified energy scheme  
 1553 of relevance for the double- $\beta$  decay of  $^{116}\text{Cd}$ . In this  
 1554 figure, the energy scale for  $^{116}\text{In}$  is magnified. The  
 1555 electron-capture decay branch of the  $^{116}\text{In}$   $1^+$  ground  
 1556 state mediated by the Gamow-Teller decay to the ground  
 1557 state of  $^{116}\text{Cd}$  was determined using a Penning-trap puri-  
 1558 fied  $^{116}\text{In}$  isotopic source and a high-resolution X-ray  
 1559 detector. Due to a small decay energy  $462.81 \pm 0.27$  keV  
 1560 the corresponding branch is very small and therefore its  
 1561 determination required ultra-pure source of  $^{116}\text{In}$ .

1562 In another experiment, the atomic mass difference  
 1563 between  $^{116}\text{Cd}$  and  $^{116}\text{Sn}$  was determined by a Pen-  
 1564 ning trap technique to be  $2813.50(13)$  keV [172]. This  
 1565 value differed by as much as 4.5 keV from the earlier  
 1566 value and was 30 times more precise. The ratio for the  
 1567 EC branch of  $[2.46 \pm 0.44(\text{stat.}) \pm 0.39(\text{syst.})] \times 10^{-4}$   
 1568 was obtained. This value represents the first measure-  
 1569 ment of EC on  $^{116}\text{In}$  with a statistical significance over  
 1570 five standard deviations in agreement with the previous  
 1571 data, see Ref. [170]. The final value extracted from  
 1572 this experiment for the GT transition strength of  $^{116}\text{In}$   
 1573 to  $^{116}\text{Cd}$  ground state turned out as  $B(\text{GT}) = 0.402 \pm$   
 1574  $0.072(\text{stat.}) \pm 0.064(\text{syst.})$ . Combining the obtained ma-  
 1575 trix element with the corresponding one for  $^{116}\text{In}$   $\beta^-$   
 1576 decay one obtains the  $2\nu\beta\beta$ -decay matrix element for  
 1577 the virtual transition through the ground state of  $^{116}\text{In}$  as  
 1578  $0.168 \pm 0.015(\text{stat.}) \pm 0.13(\text{syst.})\text{MeV}^{-1}$ . This value ex-  
 1579 ceed only slightly the total value of  $0.129 \pm 0.005\text{MeV}^{-1}$

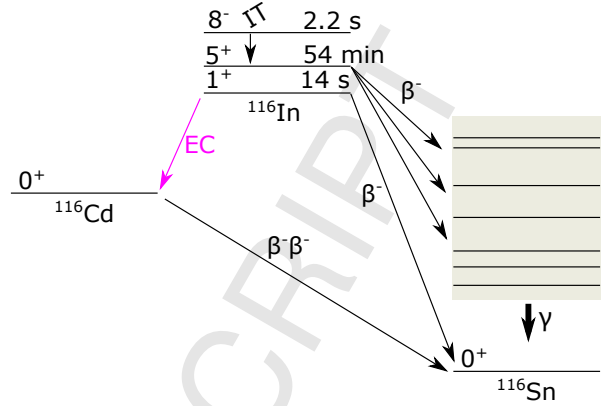


Figure 30: The A=116 system of relevance for the double beta decay of  $^{116}\text{Cd}$ .

1581 derived using the directly measured  $2\nu\beta\beta$  decay rate of  
 1582  $^{116}\text{Cd}$ . This shows that the intermediate ground state  
 1583 makes a significant contribution to the  $^{116}\text{Cd}$   $2\nu\beta\beta$  de-  
 1584 cay.

1585 **The  $^{96}\text{Zr}$  case.** The mass differences of the iso-  
 1586 baric multiplet  $^{96}\text{Zr}$ - $^{96}\text{Nb}$ - $^{96}\text{Mo}$  were recently measured  
 1587 with about 100 eV accuracy by the JYFLTRAP mass  
 1588 spectrometer employing a technique where the mea-  
 1589 surements were performed by switching between the  
 1590 ion species in the pairs ( $^{96}\text{Zr}$ ,  $^{96}\text{Nb}$ ), ( $^{96}\text{Nb}$ ,  $^{96}\text{Mo}$ ), and  
 1591 ( $^{96}\text{Zr}$ ,  $^{96}\text{Mo}$ ) [51]. This eliminated to a high degree any  
 1592 mass-dependent systematic uncertainties. By provid-  
 1593 ing the new highly accurate values for the single- and  
 1594 double-beta decay energies this measurement sheds new  
 1595 light on the corresponding transition strengths, respec-  
 1596 tively. If the single beta decay of  $^{96}\text{Zr}$  to  $^{96}\text{Nb}$  were  
 1597 directly observed, a comparison of the measured and  
 1598 theoretical single  $\beta$ -decay rate would allow a direct test  
 1599 of the nuclear-matrix-element calculations for  $\beta\beta$  de-  
 1600 cay, as these follow the same theoretical description.  
 1601 However, this case involves four-fold forbidden transi-  
 1602 tions resulting in additional complications for the calcu-  
 1603 lations. However, the  $0\nu\beta\beta$  decay would proceed via in-  
 1604 termediate states of all spins and parities, and therefore  
 1605 the case of  $^{96}\text{Nb}$  would be particularly interesting case  
 1606 for testing the theory for matrix element calculations.

1607 The  $\beta\beta$  decay of  $^{96}\text{Zr}$  to  $^{96}\text{Mo}$  features a large de-  
 1608 cay  $Q$ -value of  $3356.097(86)$  keV, which makes it an  
 1609 ideal candidate for the search experiments for neutrino-  
 1610 less double-beta decay. The partial half-life for the  
 1611  $2\nu$  variant of the  $\beta\beta$  decay to the  $^{96}\text{Mo}$  ground state is  
 1612 known from the experiments by the NEMO-3 Collabora-  
 1613 tion with the value of  $T_{1/2} = (2.3 \pm 0.2) \times 10^{19}$  y [51].  
 1614 On the other hand, a geochemical measurement has re-  
 1615 sulted in a total half-life of  $T_{1/2} = (0.94 \pm 0.32) \times 10^{19}$  y.

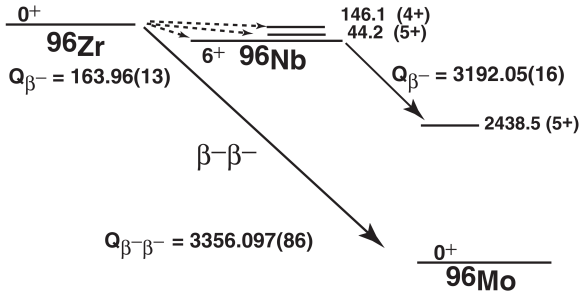


Figure 31: The  $A=96$  system of relevance for the double beta decay of  $^{96}\text{Zr}$ . This figure is from Ref. [51].

However,  $^{96}\text{Zr}$  is also unstable against single  $\beta$  decay and the corresponding half-life can be derived to be  $T_{1/2} = (1.6 \pm 0.9) \times 10^{19} \text{y}$ . The mass difference, e.g. the  $Q$ -value for single beta decay of  $^{96}\text{Zr}$  is 163.96(13) keV. The theoretical single  $\beta$ -decay rate has been recalculated using a shell-model approach and assuming a quenched axial-vector coupling constant of  $g_A \approx 1$ . The resulting half-life,  $11 \times 10^{19} \text{y}$  [51], is a factor of two smaller than the value from earlier QRPA calculations, and significantly higher as the experimental value deduced above. However, this indicates that  $^{96}\text{Zr}$  single  $\beta$ -decay lifetime is needed and is within reach of an experimental verification.

## 6. Conclusion and outlook

Ion traps are versatile instruments offering possibilities to explore several interesting physics questions. Precise ground- and isomeric-state ion-trap mass measurements have been important for many aspects of nuclear structure, such as evolution of the shell gaps far from stability, onset of deformation, the role of pairing, three-nucleon forces, and charge symmetry in nuclei. The accuracy of the Penning-trap mass measurements has made it possible to observe subtle changes in nuclear pairing energies and deviations from the quadratic form of the isobaric multiplet mass equation. Precise mass measurements have also provided a fruitful basis to develop theory, for example the role of three-nucleon forces in nuclei.

Modeling of nucleosynthesis in stars requires rather accurate knowledge of nuclear binding energies which play a central role for example in the calculations for the astrophysical  $r$  process proceeding along neutron-rich nuclei. Penning-trap measurements have contributed significantly to the mass data needed for nuclear astrophysics modeling. For example, most of the nuclei above  $^{56}\text{Ni}$  involved in the rapid proton capture process

occurring in type I X-ray bursts [173] were either experimentally unknown or based on beta-decay endpoint energies prone to accumulated uncertainties and missed decay branches to excited states at higher energies in daughter nuclei before Penning-trap measurements. For the astrophysical  $r$  process, to answer the question of its astrophysical site(s), more mass measurements in combination with the development of theoretical mass models are needed. New techniques, such as PI-ICR, and MR-TOR devices currently being developed or commissioned at many facilities, will help in this task.

Precise  $Q$ -value measurements performed with Penning traps have played a central role in the studies of superallowed beta decays needed to test the CVC hypothesis and the unitarity of the CKM matrix. Many mirror-beta decay  $Q_{EC}$  values have also been measured with unprecedented accuracy using Penning traps, and are being actively studied at different facilities. Penning-trap measurements have contributed to neutrino physics studies by determining the  $Q$  values for all currently relevant double-beta decay experiments, and finding several additional, potentially interesting cases. The determination of the neutrino mass and solving the neutrino hierarchy problem are one of the biggest open questions in modern physics, setting challenges for future ion-trap experiments.

Ion traps have been exploited in many kinds of decay studies observing decay from trapped ions for example for beta-neutrino angular correlation experiments or for conversion electron spectroscopy. Penning traps and MR-TOF devices have also shown their strength in the beam purification for contaminant-free spectroscopy studies after the trap. The possibility to provide even isomerically pure beams has yielded new possibilities for studies of isomers, but also applications, such as the production of isomerically pure radioxenon  $^{133m}\text{Xe}$  and  $^{133g}\text{Xe}$  calibration samples for monitoring the nuclear weapon test ban treaty [174].

Ion traps are pivotal for many experiments driven both by fundamental physics questions and by applications. As a consequence, new ion traps are being planned or constructed for present and future radioactive facilities to continue the quest towards measurements of more exotic, unknown nuclei. Novel ion-trapping techniques are being pursued to reach highest accuracies in future ion-trap measurements. To conclude, ion traps have established a firm position in modern nuclear physics experiments.



## Acknowledgements

The authors would like to thank prof. Ari Jokinen for fruitful discussions. This work has been supported by the Academy of Finland under the Finnish Centre of Excellence Programme 2012-2017 (Nuclear and Accelerator Based Physics Research at JYFL). AK acknowledges the support from the Academy of Finland under project No. 275389.

- [1] S. Rainville, J. K. Thompson, D. E. Pritchard, An Ion Balance for Ultra-High-Precision Atomic Mass Measurements, *Science* 303 (5656) (2004) 334, doi:10.1126/science.1092320, URL <http://www.sciencemag.org/cgi/content/abstract/303/5656/334>.
- [2] R. S. Van Dyck, Jr., S. L. Zafonte, S. Van Liew, D. B. Pinegar, P. B. Schwinberg, Ultraprecise Atomic Mass Measurement of the alpha Particle and  $^4\text{He}$ , *Phys. Rev. Lett.* 92 (22) (2004) 220802, URL <http://link.aps.org/doi/10.1103/PhysRevLett.92.220802>.
- [3] E. G. Myers, A. Wagner, H. Kracke, B. A. Wesson, Atomic Masses of Tritium and Helium-3, *Phys. Rev. Lett.* 114 (1), doi:10.1103/physrevlett.114.013003, URL <http://dx.doi.org/10.1103/PhysRevLett.114.013003>.
- [4] A. Kellerbauer, T. Kim, R. Moore, P. Varfalvy, Buffer gas cooling of ion beams, *Nucl. Instrum. Methods Phys. Res., Sect. A* 469 (2) (2001) 276–285, doi:10.1016/S0168-9002(01)00286-8, URL [http://dx.doi.org/10.1016/S0168-9002\(01\)00286-8](http://dx.doi.org/10.1016/S0168-9002(01)00286-8).
- [5] H. Dehmelt, Experiments with an isolated subatomic particle at rest, *Rev. Mod. Phys.* 62 (3) (1990) 525, URL <http://link.aps.org/abstract/RMP/v62/p525>.
- [6] A. Nieminen, P. Campbell, J. Billowes, D. H. Forest, J. A. R. Griffith, J. Huikari, A. Jokinen, I. D. Moore, R. Moore, G. Tungate, J. Äystö, On-Line Ion Cooling and Bunching for Collinear Laser Spectroscopy, *Phys. Rev. Lett.* 88 (9) (2002) 094801, URL <http://link.aps.org/abstract/PRL/v88/e094801>.
- [7] T. Sun, S. Schwarz, G. Bollen, D. Lawton, R. Ringle, P. Schury, Commissioning of the ion beam buncher and cooler for LEBIT, *Eur. Phys. J. A* 25 (S1) (2005) 61–62, doi:10.1140/epjad/i2005-06-126-9, URL <http://dx.doi.org/10.1140/epjad/i2005-06-126-9>.
- [8] A. Nieminen, J. Huikari, A. Jokinen, J. Äystö, P. Campbell, E. C. A. Cochrane, Beam cooler for low-energy radioactive ions, *Nucl. Instrum. Methods Phys. Res., Sect. A* 469 (2) (2001) 244, URL <http://www.sciencedirect.com/science/article/B6TJM-43PGJKX-D/2/d5a1a85b9a62763e751fb5a1fcb3716>.
- [9] F. Herfurth, J. Dilling, A. Kellerbauer, G. Bollen, S. Henry, H. J. Kluge, E. Lamour, D. Lunney, R. B. Moore, C. Scheidenberger, S. Schwarz, G. Sikler, J. Szerypo, A linear radiofrequency ion trap for accumulation, bunching, and emittance improvement of radioactive ion beams, *Nucl. Instrum. Methods Phys. Res., Sect. A* 469 (2) (2001) 254, ISSN 0168-9002, URL <http://www.sciencedirect.com/science/article/B6TJM-43PGJKX-D/2/d5a1a85b9a62763e751fb5a1fcb3716>.
- [10] G. Savard, S. Baker, C. Davids, A. Levand, E. Moore, R. Pardo, R. Vondrasek, B. Zabransky, G. Zinkann, Radioactive beams from gas catchers: The CARIBU facility, *Nucl. Instrum. Methods Phys. Res., Sect. B* 266 (19–20) (2008) 4086–4091, doi:10.1016/j.nimb.2008.05.091, URL <http://dx.doi.org/10.1016/j.nimb.2008.05.091>.
- [11] R. Boussaid, G. Ban, J. F. Cam, C. Vandamme, Simulations of high intensity ion beam RFQ cooler for DESIR/SPIRAL 2: SHIRaC, *J. Inst.* 9 (07) (2014) P07009, doi:10.1088/1748-0221/9/07/p07009, URL <http://dx.doi.org/10.1088/1748-0221/9/07/p07009>.
- [12] S. Kaufman, High-resolution laser spectroscopy in fast beams, *Opt. Commun.* 17 (3) (1976) 309–312, doi:10.1016/0030-4018(76)90267-4, URL [http://dx.doi.org/10.1016/0030-4018\(76\)90267-4](http://dx.doi.org/10.1016/0030-4018(76)90267-4).
- [13] K. R. Anton, S. L. Kaufman, W. Klempt, G. Moruzzi, R. Neugart, E. W. Otten, B. Schinzler, Collinear Laser Spectroscopy on Fast Atomic Beams, *Phys. Rev. Lett.* 40 (10) (1978) 642–645, doi:10.1103/physrevlett.40.642, URL <http://dx.doi.org/10.1103/PhysRevLett.40.642>.
- [14] R. Wolf, F. Wienholtz, D. Atanasov, D. Beck, K. Blaum, C. Borgmann, F. Herfurth, M. Kowalska, S. Kreim, Y. A. Litvinov, D. Lunney, V. Manea, D. Neidherr, M. Rosenbusch, L. Schweikhard, J. Stanja, K. Zuber, ISOLTRAP’s multi-reflection time-of-flight mass separator/spectrometer, *Int. J. Mass Spectrom.* 349–350 (2013) 123–133, doi:10.1016/j.ijms.2013.03.020, URL <http://dx.doi.org/10.1016/j.ijms.2013.03.020>.
- [15] W. R. Plaß, T. Dickel, C. Scheidenberger, Multiple-reflection time-of-flight mass spectrometry, *Int. J. Mass Spectrom.* doi:10.1016/j.ijms.2013.06.005, URL <http://dx.doi.org/10.1016/j.ijms.2013.06.005>.
- [16] P. Schury, M. Wada, Y. Ito, S. Naimi, T. Sonoda, H. Mita, A. Takamine, K. Okada, H. Wollnik, S. Chon, H. Haba, D. Kaji, H. Koura, H. Miyatake, K. Morimoto, K. Morita, A. Ozawa, A multi-reflection time-of-flight mass spectrograph for short-lived and super-heavy nuclei, *Nucl. Instrum. Methods Phys. Res., Sect. B* 317 (0) (2013) 537–543, ISSN 0168-583X, URL <http://www.sciencedirect.com/science/article/pii/S0168583X13000>.
- [17] W. Paul, Electromagnetic traps for charged and neutral particles, *Rev. Mod. Phys.* 62 (3) (1990) 531–540, doi:10.1103/revmodphys.62.531, URL <http://dx.doi.org/10.1103/RevModPhys.62.531>.
- [18] G. Ban, D. Durand, X. Fléchar, E. Liénard, O. Naviliat-Cuncic, Precision measurements in nuclear  $\beta$ -decay with LPCTrap, *Annalen der Physik* (2013) DOI: 10.1002/andp.201300043ISSN 1521-3889, doi:10.1002/andp.201300043, URL <http://dx.doi.org/10.1002/andp.201300043>.
- [19] X. Fléchar, E. Liénard, A. Méry, D. Rodríguez, G. Ban, D. Durand, F. Duval, M. Herbane, M. Labalme, F. Mager, O. Naviliat-Cuncic, J. C. Thomas, P. Velten, Paul Trapping of Radioactive  $^6\text{He}^+$  Ions and Direct Observation of Their  $\beta$  Decay, *Phys. Rev. Lett.* 101 (21), doi:10.1103/physrevlett.101.212504, URL <http://dx.doi.org/10.1103/PhysRevLett.101.212504>.
- [20] J. DiSciaccia, M. Marshall, K. Marable, G. Gabrielse, Resolving an Individual One-Proton Spin Flip to Determine a Proton Spin State, *Phys. Rev. Lett.* 110 (14) (2013) 140406–, URL <http://link.aps.org/doi/10.1103/PhysRevLett.110.140406>.
- [21] R. M. Yee, N. D. Scielzo, P. F. Bertone, F. Buchinger, S. Caldwell, J. A. Clark, C. M. Deibel, J. Fallis, J. P. Greene, S. Gulick, D. Lascar, A. F. Levand, G. Li, E. B. Norman, M. Pedretti, G. Savard, R. E. Segel, K. S. Sharma, M. G. Sternberg, J. Van Schelt, B. J. Zabransky,  $\beta$ -Delayed Neutron Spectroscopy Using Trapped Radioactive Ions, *Phys. Rev. Lett.* 110 (9) (2013) 092501–, URL <http://link.aps.org/doi/10.1103/PhysRevLett.110.092501>.
- [22] K. Blaum, J. Dilling, W. Nörtershäuser, Precision atomic physics techniques for nuclear physics with radioactive beams, *Phys. Scr.* 2013 (T152) (2013) 014017, ISSN 1402-4896, doi:10.1088/0031-8949/2013/T152/014017, URL <http://stacks.iop.org/1402-4896/2013/i=T152/a=014017>.

- [23] S. Streubel, T. Eronen, M. Höcker, J. Ketter, M. Schuh, J. Van Dyck, R.S., K. Blaum, Toward a more accurate Q value measurement of tritium: status of THE-Trap, *Appl. Phys. B* 114 (1-2) (2014) 137–145, ISSN 0946-2171, doi:10.1007/s00340-013-5669-x, URL <http://dx.doi.org/10.1007/s00340-013-5669-x>.
- [24] T. Eronen, V. Kolhinen, V. V. Elomaa, D. Gorelov, U. Hager, J. Hakala, A. Jokinen, A. Kankainen, P. Karvonen, S. Kopecky, I. D. Moore, H. Penttilä, S. Rahaman, S. Rinta-Antila, J. Rissanen, A. Saastamoinen, J. Szerypo, C. Weber, J. Äystö, JYFLTRAP: a Penning trap for precision mass spectroscopy and isobaric purification, *Eur. Phys. J. A* 48 (4) (2012) 46, doi: 10.1140/epja/i2012-12046-1.
- [25] M. Kretzschmar, Single particle motion in a Penning trap: description in the classical canonical formalism, *Phys. Scr.* 46 (6) (1992) 544, doi:10.1088/0031-8949/46/6/011, URL <http://stacks.iop.org/1402-4896/46/i=6/a=011>.
- [26] G. Gabrielse, The true cyclotron frequency for particles and ions in a Penning trap, *Int. J. Mass Spectrom.* 279 (2-3) (2009) 107, ISSN 1387-3806, URL <http://www.sciencedirect.com/science/article/B6VND-4TT9GRKry/2/ba-Penning-42prf-495bim35d-173180>.
- [27] S. Eliseev, K. Blaum, M. Block, S. Chenmarev, H. Dorrer, C. E. Düllmann, C. Enss, P. E. Filianin, L. Gastaldo, M. Goncharov, et al., Direct Measurement of the Mass Difference of  $^{163}\text{Ho}$   $^{163}\text{Dy}$  Solves the Q-Value Puzzle for the Neutrino Mass Determination, *Phys. Rev. Lett.* 115 (6), ISSN 1079-7114, doi:10.1103/physrevlett.115.062501, URL <http://dx.doi.org/10.1103/PhysRevLett.115.062501>.
- [28] K. Gulyuz, J. Ariche, G. Bollen, S. Bustabad, M. Eibach, C. Izzo, S. J. Novario, M. Redshaw, R. Ringle, R. Sandler, S. Schwarz, A. A. Valverde, Determination of the direct double- $\beta$ -decay Q value of  $^{96}\text{Zr}$  and atomic masses of  $^{90-92,94,96}\text{Zr}$  and  $^{92,94-98,100}\text{Mo}$ , *Phys. Rev. C* 91 (5), doi:10.1103/physrevc.91.055501, URL <http://dx.doi.org/10.1103/PhysRevC.91.055501>.
- [29] K. Blaum, G. Bollen, F. Herfurth, A. Kellerbauer, H.-J. Kluge, M. Kuckein, E. Sauvan, C. Scheidenberger, L. Schweikhard, Carbon clusters for absolute mass measurements at ISOLTRAP, *Eur. Phys. J. A* 15 (1-2) (2002) 245–248, ISSN 1434-6001, doi:10.1140/epja/i2001-10262-4, URL <http://dx.doi.org/10.1140/epja/i2001-10262-4>.
- [30] G. Bollen, R. B. Moore, G. Savard, H. Stolzenberg, The accuracy of heavy-ion mass measurements using time of flight-ion cyclotron resonance in a Penning trap, *J. Appl. Phys.* 68 (9) (1990) 4355–4374, doi:10.1063/1.346185, URL <http://dx.doi.org/10.1063/1.346185>.
- [31] J. Ketter, T. Eronen, M. Höcker, S. Streubel, K. Blaum, First-order perturbative calculation of the frequency-shifts caused by static cylindrically-symmetric electric and magnetic imperfections of a Penning trap, *Int. J. Mass Spectrom.* 358 (2014) 1–16, ISSN 1387-3806, URL <http://www.sciencedirect.com/science/article/pii/S1387380614000872>.
- [32] C. Roux, K. Blaum, M. Block, C. Droese, S. Eliseev, M. Goncharov, F. Herfurth, E. M. Ramirez, D. A. Nesterenko, Y. N. Novikov, L. Schweikhard, Data analysis of Q-value measurements for double-electron capture with SHIPTRAP, *Eur. Phys. J. D* 67 (7) (2013) 1–9, ISSN 1434-6060, doi:10.1140/epjd/e2013-40110-x, URL <http://dx.doi.org/10.1140/epjd/e2013-40110-x>.
- [33] T. Eronen, J. C. Hardy, High-precision  $Q_{EC}$ -value measurements for superallowed decays, *Eur. Phys. J. A* 48 (4) (2012) 48, doi:10.1140/epja/i2012-12048-y, URL <http://dx.doi.org/10.1140/epja/i2012-12048-y>.
- [34] S. A. Eliseev, Y. N. Novikov, K. Blaum, Search for resonant enhancement of neutrinoless double-electron capture by high-precision Penning-trap mass spectrometry, *J. Phys. G: Nucl. Part. Phys.* 39 (12) (2012) 124003, URL <http://stacks.iop.org/0954-3899/39/i=12/a=124003>.
- [35] G. Gräff, H. Kalinowsky, J. Traut, A direct determination of the proton electron mass ratio, *Z. Phys. A* 297 (1) (1980) 35–39, doi:10.1007/BF01414243, URL <http://dx.doi.org/10.1007/BF01414243>.
- [36] M. König, G. Bollen, H.-J. Kluge, T. Otto, J. Szerypo, Quadrupole excitation of stored ion motion at the true cyclotron frequency, *Int. J. Mass Spectrom. Ion Process.* 142 (1–2) (1995) 95, doi:10.1016/0168-1176(95)04146-C, URL <http://www.sciencedirect.com/science/article/pii/016811769504146C>.
- [37] R. Ringle, G. Bollen, A. Prinke, J. Savory, P. Schury, S. Schwarz, T. Sun, A "Lorentz" steerer for ion injection into a Penning trap, *Int. J. Mass Spectrom.* 263 (1) (2007) 38, URL <http://www.sciencedirect.com/science/article/B6VND-4MS3JBM-1/1>.
- [38] S. George, K. Blaum, F. Herfurth, A. Herlert, M. Kretzschmar, S. Nagy, S. Schwarz, L. Schweikhard, C. Yazidjian, The Ramsey method in high-precision mass spectrometry, *Int. J. Mass Spectrom.* 264 (2-3) (2007) 110, ISSN 1387-3806, URL <http://www.sciencedirect.com/science/article/B6VND-4NF7Y9X-2/2>.
- [39] H.-J. Kluge, Penning trap mass spectrometry of radionuclides, *Int. J. Mass Spectrom.* 349–350 (0) (2013) 26–37, ISSN 1387-3806, URL <http://www.sciencedirect.com/science/article/pii/S1387380613001180>.
- [40] R. Ringle, G. Bollen, P. Schury, S. Schwarz, T. Sun, Octupolar excitation of ion motion in a Penning trap—A study performed at LEBIT, *Int. J. Mass Spectrom.* 262 (1-2) (2007) 33, URL <http://www.sciencedirect.com/science/article/B6VND-4MC0TRN-2/1>.
- [41] S. Eliseev, M. Block, A. Chaudhuri, F. Herfurth, H.-J. Kluge, A. Martin, C. Rauth, G. Vorobjev, Octupolar excitation of ions stored in a Penning trap mass spectrometer—A study performed at SHIPTRAP, *Int. J. Mass Spectrom.* 262 (1-2) (2007) 45, URL <http://www.sciencedirect.com/science/article/B6VND-4M9415X-1/1>.
- [42] S. Eliseev, C. Roux, K. Blaum, M. Block, C. Droese, F. Herfurth, M. Kretzschmar, M. I. Krivoruchenko, E. Minaya Ramirez, Y. N. Novikov, L. Schweikhard, V. M. Shabaev, F. Simkovic, I. I. Tupitsyn, K. Zuber, N. A. Zubova, Octupolar-Excitation Penning-Trap Mass Spectrometry for Q-Value Measurement of Double-Electron Capture in  $^{164}\text{Er}$ , *Phys. Rev. Lett.* 107 (15) (2011) 152501, URL <http://link.aps.org/doi/10.1103/PhysRevLett.107.152501>.
- [43] A. Lapiere, M. Brodeur, T. Brunner, S. Etenauer, A. Gallant, V. Simon, M. Good, M. Froese, J. C. López-Urrutia, P. Delheij, S. Epp, R. Ringle, S. Schwarz, J. Ullrich, J. Dilling, The TITAN EBIT charge breeder for mass measurements on highly charged short-lived isotopes—First online operation, *Nuclear Instruments and Methods in Research Section A: Accelerators, Spectrometers, Detectors and Associated Equipment* 624 (1) (2010) 54–64, doi:10.1016/j.nima.2010.09.030, URL <http://dx.doi.org/10.1016/j.nima.2010.09.030>.
- [44] S. Eliseev, K. Blaum, M. Block, C. Droese, M. Goncharov, E. Minaya Ramirez, D. A. Nesterenko, Y. N. Novikov, L. Schweikhard, Phase-Imaging Ion-Cyclotron-Resonance Measurements for Short-Lived Nuclides, *Phys. Rev. Lett.* 110 (8) (2013) 082501, URL <http://link.aps.org/doi/10.1103/PhysRevLett.110.082501>.
- [45] S. Eliseev, K. Blaum, M. Block, A. Dörr, C. Droese, T. Eronen, M. Goncharov, M. Höcker, J. Ketter, E. Ramirez, D. Nesterenko, Y. Novikov, L. Schweikhard, A phase-imaging technique for cyclotron-frequency measure-

- ments, Appl. Phys. B: Lasers Opt. 114 (1-2) (2014) 107, ISSN 0946-2171, doi:10.1007/s00340-013-5621-0, URL <http://dx.doi.org/10.1007/s00340-013-5621-0>.
- [46] G. Savard, S. Becker, G. Bollen, H. J. Kluge, R. B. Moore, T. Otto, L. Schweikhard, H. Stolzenberg, U. Wiess, A new cooling technique for heavy ions in a Penning trap, Phys. Lett. A 158 (5) (1991) 247, ISSN 0375-9601, URL <http://www.sciencedirect.com/science/article/B6T3W-46T4MHS17P/2/c4a0251d2g0608b0b049f2jmb20f7e01.002>.
- [47] J. V. Roosbroeck, C. Guenaut, G. Audi, D. Beck, K. Blaum, G. Bollen, J. Cederkall, P. Delahaye, H. D. Witte, D. Fedorov, V. Fedoseyev, S. Franchoo, H. Fynbo, M. Gorska, F. Herfurth, K. Heyde, M. Huysse, A. Kellerbauer, H.-J. Kluge, U. Köster, K. Kruglov, D. Lunney, A. D. Maesschalck, V. Mishin, W. Müller, S. Nagy, S. Schwarz, L. Schweikhard, N. Smirnova, K. V. de Vel, P. V. Duppen, A. V. Dyck, W. Walters, L. Weissmann, C. Yazidjian, Unambiguous identification of three  $\beta$ -decaying isomers in  $^{70}\text{Cu}$ , Phys. Rev. Lett. 92 (2004) 112501.
- [48] A. Kwiatkowski, G. Bollen, M. Redshaw, R. Ringle, S. Schwarz, Isobaric beam purification for high precision Penning trap mass spectrometry of radioactive isotope beams with SWIFT, Int. J. Mass Spectrom. 379 (2015) 9–15, doi:10.1016/j.ijms.2014.09.016, URL <http://dx.doi.org/10.1016/j.ijms.2014.09.016>.
- [49] T. Eronen, V.-V. Elomaa, U. Hager, J. Hakala, A. Jokinen, A. Kankainen, S. Rahaman, J. Rissanen, C. Weber, J. Äystö, Preparing isomerically pure beams of short-lived nuclei at JYFLTRAP, Nucl. Instrum. Methods Phys. Res., Sect. B 266 (19-20) (2008) 4527, ISSN 0168-583X, URL <http://dx.doi.org/10.1016/j.nimb.2008.05.076>.
- [50] G. Audi, A. Wapstra, C. Thibault, The Ame2003 atomic mass evaluation: (II). Tables, graphs and references, Nucl. Phys. A 729 (1) (2003) 337 – 676, ISSN 0375-9474, doi:10.1016/j.nuclphysa.2003.11.003, URL <http://www.sciencedirect.com/science/article/pii/S0375947403008309>.
- [51] M. Alanssari, D. Frekers, T. Eronen, L. Canete, J. Dilling, M. Haaranen, J. Hakala, M. Holl, M. Jeřšovský, A. Jokinen, A. Kankainen, J. Koponen, A. J. Mayer, I. D. Moore, D. A. Nesterenko, I. Pohjalainen, P. Povinec, J. Reinikainen, S. Rinta-Antila, P. C. Srivastava, J. Suhonen, R. I. Thompson, A. Voss, M. E. Wieser, Single and Double Beta-Decay  $Q$  Values among the Triplet  $^{96}\text{Zr}$ ,  $^{96}\text{Nb}$ , and  $^{96}\text{Mo}$ , Phys. Rev. Lett. 116 (7), doi:10.1103/PhysRevLett.116.072501, URL <http://dx.doi.org/10.1103/PhysRevLett.116.072501>.
- [52] G. Bollen, H.-J. Kluge, M. König, T. Otto, G. Savard, H. Stolzenberg, R. B. Moore, G. Rouleau, G. Audi, I. Collaboration, Resolution of nuclear ground and isomeric states by a Penning trap mass spectrometer, Phys. Rev. C 46 (6) (1992) R2140, URL <http://link.aps.org/abstract/PRC/v46/pR2140>.
- [53] A. Kankainen, J. Hakala, T. Eronen, D. Gorelov, A. Jokinen, V. S. Kolhinen, I. D. Moore, H. Penttilä, S. Rinta-Antila, J. Rissanen, A. Saastamoinen, V. Sonnenschein, J. Äystö, Isomeric states close to doubly magic  $^{132}\text{Sn}$  studied with the double Penning trap JYFLTRAP, Phys. Rev. C 87 (2013) 024307, doi:10.1103/PhysRevC.87.024307, URL <http://link.aps.org/doi/10.1103/PhysRevC.87.024307>.
- [54] M. Rosenbusch, K. Blaum, C. Borgmann, S. Kreim, M. Kretschmar, D. Lunney, L. Schweikhard, F. Wienholtz, R. Wolf, Buffer-gas-free mass-selective ion centering in Penning traps by simultaneous dipolar excitation of magnetron motion and quadrupolar excitation for interconversion between magnetron and cyclotron motion, Int. J. Mass Spectrom. 325-327 (2012) 51–57, doi:10.1016/j.ijms.2012.06.008, URL <http://dx.doi.org/10.1016/j.ijms.2012.06.008>.
- [55] M. Rosenbusch, C. Böhm, C. Borgmann, M. Breitenfeldt, A. Herlert, M. Kowalska, S. Kreim, G. Marx, S. Naimi, D. Neidherr, R. Schneider, L. Schweikhard, A study of octupolar excitation for mass-selective centering in Penning traps, Int. J. Mass Spectrom. 314 (2012) 6–12, doi:10.1016/j.ijms.2012.01.002, URL <http://dx.doi.org/10.1016/j.ijms.2012.01.002>.
- [56] H. Wollnik, M. Przewloka, Time-of-flight mass spectrometers with multiply reflected ion trajectories, Int. J. Mass Spectrom. Ion Process. 96 (3) (1990) 267–274, doi:10.1016/0168-1176(90)85127-n, URL [http://dx.doi.org/10.1016/0168-1176\(90\)85127-n](http://dx.doi.org/10.1016/0168-1176(90)85127-n).
- [57] T. Dickel, W. Plaß, A. Becker, U. Czok, H. Geissel, E. Haettner, C. Jesch, W. Kinsel, M. Petrick, C. Scheidenberger, A. Simon, M. Yavor, A high-performance multiple-reflection time-of-flight mass spectrometer and isobar separator for the research with exotic nuclei, Nucl. Instrum. Methods Phys. Res., Sect. A 777 (2015) 172–188, doi:10.1016/j.nima.2014.12.094, URL <http://dx.doi.org/10.1016/j.nima.2014.12.094>.
- [58] M. Rosenbusch, P. Ascher, D. Atanasov, C. Barbieri, D. Beck, K. Blaum, C. Borgmann, M. Breitenfeldt, R. B. Cakirli, A. Cipollone, S. George, F. Herfurth, M. Kowalska, S. Kreim, D. Lunney, V. Manea, P. Navrátil, D. Neidherr, L. Schweikhard, V. Somà, J. Stanja, F. Wienholtz, R. N. Wolf, K. Zuber, Probing the  $N = 32$  Shell Closure below the Magic Proton Number  $Z = 20$ : Mass Measurements of the Exotic Isotopes  $^{52,53}\text{K}$ , Phys. Rev. Lett. 114 (2015) 202501, doi:10.1103/PhysRevLett.114.202501, URL <http://link.aps.org/doi/10.1103/PhysRevLett.114.202501>.
- [59] S. Kreim, M. Hempel, D. Lunney, J. Schaffner-Bielich, Nuclear masses and neutron stars, Int. J. Mass Spectrom. 349-350 (0) (2013) 63–68, ISSN 1387-3806, URL <http://www.sciencedirect.com/science/article/pii/S1387380613000375>.
- [60] J. Clark, G. Savard, Precision masses for studies of the astrophysical r process, Int. J. Mass Spectrom. 349-350 (0) (2013) 81–86, ISSN 1387-3806, URL <http://www.sciencedirect.com/science/article/pii/S1387380613000375>.
- [61] M. Block, D. Ackermann, K. Blaum, A. Chaudhuri, Z. Di, S. Eliseev, R. Ferrer, D. Habs, F. Herfurth, F. P. Heßberger, S. Hofmann, H.-J. Kluge, G. Maero, A. Martin, G. Marx, M. Mazzocco, M. Mukherjee, J. B. Neumayr, W. R. Plaß, W. Quint, S. Rahaman, C. Rauth, D. Rodríguez, C. Scheidenberger, L. Schweikhard, P. G. Thirolf, G. Vorobjev, C. Weber, Towards direct mass measurements of nobelium at SHIP-TRAP, Eur. Phys. J. D 45 (1) (2007) 39, ISSN 1434-6060, URL <http://dx.doi.org/10.1140/epjd/e2007-00189-2>.
- [62] E. M. Ramirez, D. Ackermann, K. Blaum, M. Block, C. Droese, C. E. Düllmann, M. Dworschak, M. Eibach, S. Eliseev, E. Haettner, F. Herfurth, F. P. Heßberger, S. Hofmann, J. Ketelaer, G. Marx, M. Mazzocco, D. Nesterenko, Y. N. Novikov, W. R. Plaß, D. Rodríguez, C. Scheidenberger, L. Schweikhard, P. G. Thirolf, C. Weber, Direct Mapping of Nuclear Shell Effects in the Heaviest Elements, Science 337 (6099) (2012) 1207–1210, ISSN 0036-8075, doi:10.1126/science.1225636, URL <http://science.sciencemag.org/content/337/6099/1207>.
- [63] M. Block, D. Ackermann, K. Blaum, C. Droese, M. Dworschak, S. Eliseev, T. Fleckenstein, E. Haettner, F. Herfurth, F. P. Heßberger, S. Hofmann, J. Ketelaer, J. Ketter, H.-J. Kluge, G. Marx, M. Mazzocco, Y. N. Novikov, W. R. Plaß, A. Popeko, S. Rahaman, D. Rodríguez, C. Scheidenberger, L. Schweikhard, P. G. Thirolf, G. K. Vorobyev, C. Weber, Direct mass measurements above uranium bridge the gap to the

- island of stability, *Nature* 463 (7282) (2010) 785, ISSN 0028-0836, URL <http://dx.doi.org/10.1038/nature08774>.
- [64] M. Block, Direct mass measurements of the heaviest elements with Penning traps, *Int. J. Mass Spectrom.* 349–350 (2013) 94 – 101, ISSN 1387-3806, doi:<http://dx.doi.org/10.1016/j.ijms.2013.02.013>, URL <http://www.sciencedirect.com/science/article/pii/S1387380613000742>.
- [65] A. Kwiatkowski, T. Macdonald, C. Andreou, J. Bale, T. Brunner, A. Chaudhuri, U. Chowdhury, S. Ettenauer, A. Gallant, A. Grossheim, A. Lennarz, E. Mane, M. Pearson, B. Schultz, M. Simon, V. Simon, J. Dilling, Precision mass measurements at TITAN with radioactive ions, *Nucl. Instrum. Methods Phys. Res., Sect. B* 317 (2013) 517, ISSN 0168-583X, URL <http://www.sciencedirect.com/science/article/pii/S0168583X13001064>.
- [66] R. Ringle, S. Schwarz, G. Bollen, Penning trap mass spectrometry of rare isotopes produced via projectile fragmentation at the LEBIT facility, *International Journal of Mass Spectrometry* 349–350 (0) (2013) 87–93, ISSN 1387-3806, URL <http://www.sciencedirect.com/science/article/pii/S1387380613001070>.
- [67] J. Ketelaer, J. Krämer, D. Beck, K. Blaum, M. Block, K. Eberhardt, G. Eitel, R. Ferrer, C. Geppert, S. George, F. Herfurth, J. Ketter, S. Nagy, D. Neidherr, R. Neugart, W. Nörtershäuser, J. Repp, C. Smorra, N. Trautmann, C. Weber, TRIGA-SPEC: A setup for mass spectrometry and laser spectroscopy at the research reactor {TRIGA} Mainz, *Nuclear Instruments and Methods in Physics Research Section A: Accelerators, Spectrometers, Detectors and Associated Equipment* 594 (2) (2008) 162 – 177, ISSN 0168-9002, doi:<http://dx.doi.org/10.1016/j.nima.2008.06.023>, URL <http://www.sciencedirect.com/science/article/pii/S0168900208003693>.
- [68] M. Wang, G. Audi, A. Wapstra, F. Kondev, M. MacCormick, X. Xu, B. Pfeiffer, The Ame2012 atomic mass evaluation, *Chinese Physics C* 36 (12) (2012) 1603, URL <http://stacks.iop.org/1674-1137/36/i=12/a=003>.
- [69] F. Wienholtz, D. Beck, K. Blaum, C. Borgmann, M. Breitenfeldt, R. B. Cakirli, S. George, F. Herfurth, J. D. Holt, M. Kowalska, S. Kreim, D. Lunney, V. Manea, J. Menendez, D. Neidherr, M. Rosenbusch, L. Schweikhard, A. Schwenk, J. Simonis, J. Stanja, R. N. Wolf, K. Zuber, Masses of exotic calcium isotopes pin down nuclear forces, *Nature* 498 (2013) 346–349, doi:[10.1038/nature12226](https://doi.org/10.1038/nature12226), URL <http://dx.doi.org/10.1038/nature12226>.
- [70] R. N. Wolf, D. Beck, K. Blaum, C. Böhm, C. Borgmann, M. Breitenfeldt, N. Chamel, S. Goriely, F. Herfurth, M. Kowalska, S. Kreim, D. Lunney, V. Manea, E. Minaya Ramirez, S. Naimi, D. Neidherr, M. Rosenbusch, L. Schweikhard, J. Stanja, F. Wienholtz, K. Zuber, Plumbing Neutron Stars to New Depths with the Binding Energy of the Exotic Nuclide  $^{82}\text{Zn}$ , *Phys. Rev. Lett.* 110 (4) (2013) 041101, doi:[10.1103/PhysRevLett.110.041101](https://doi.org/10.1103/PhysRevLett.110.041101), URL <http://link.aps.org/doi/10.1103/PhysRevLett.110.041101>.
- [71] V. Manea, D. Atanasov, D. Beck, K. Blaum, C. Borgmann, R. B. Cakirli, T. Eronen, S. George, F. Herfurth, A. Herlert, M. Kowalska, S. Kreim, Y. A. Litvinov, D. Lunney, D. Neidherr, M. Rosenbusch, L. Schweikhard, F. Wienholtz, R. N. Wolf, K. Zuber, Collective degrees of freedom of neutron-rich  $A \approx 100$  nuclei and the first mass measurement of the short-lived nuclide  $^{100}\text{Rb}$ , *Phys. Rev. C* 88 (2013) 054322, doi:[10.1103/PhysRevC.88.054322](https://doi.org/10.1103/PhysRevC.88.054322), URL <http://link.aps.org/doi/10.1103/PhysRevC.88.054322>.
- [72] D. Atanasov, P. Ascher, K. Blaum, R. B. Cakirli, T. E. Cocolios, S. George, S. Goriely, F. Herfurth, H.-T. Janka, O. Just, M. Kowalska, S. Kreim, D. Kisler, Y. A. Litvinov, D. Lunney, V. Manea, D. Neidherr, M. Rosenbusch, L. Schweikhard, A. Welker, F. Wienholtz, R. N. Wolf, K. Zuber, Precision Mass Measurements of  $^{129}\text{I}$  and  $^{131}\text{I}$  and Their Impact on Stellar Nucleosynthesis via the Rapid Neutron Capture Process, *Phys. Rev. Lett.* 115 (2015) 232501, doi:[10.1103/PhysRevLett.115.232501](https://doi.org/10.1103/PhysRevLett.115.232501), URL <http://link.aps.org/doi/10.1103/PhysRevLett.115.232501>.
- [73] D. Lascar, G. Savard, J. A. Clark, P. F. Bertone, S. Caldwell, A. Chaudhuri, A. F. Levand, G. Li, G. E. Morgan, R. Orford, R. E. Segel, K. S. Sharma, M. G. Sternberg, First Results from the CARIBU Facility: Mass Measurements on the r-Process Path, *Phys. Rev. Lett.* 111 (6) (2013) 061102, URL <http://link.aps.org/doi/10.1103/PhysRevLett.111.061102>.
- [74] J. Stanja, C. Borgmann, J. Agramunt, A. Algora, D. Beck, C. Böhm, M. Breitenfeldt, T. E. Cocolios, L. M. Fraile, F. Herfurth, A. Herlert, M. Kowalska, S. Kreim, D. Lunney, V. Manea, E. Minaya Ramirez, S. Naimi, D. Neidherr, M. Rosenbusch, L. Schweikhard, G. Simpson, F. Wienholtz, R. N. Wolf, K. Zuber, Mass spectrometry and decay spectroscopy of isomers across the  $Z = 82$  shell closure, *Phys. Rev. C* 88 (2013) 054304, doi:[10.1103/PhysRevC.88.054304](https://doi.org/10.1103/PhysRevC.88.054304), URL <http://link.aps.org/doi/10.1103/PhysRevC.88.054304>.
- [75] S. Kreim, D. Beck, K. Blaum, C. Borgmann, M. Breitenfeldt, T. E. Cocolios, A. Gottberg, F. Herfurth, M. Kowalska, Y. A. Litvinov, D. Lunney, V. Manea, T. M. Mendonca, S. Naimi, D. Neidherr, M. Rosenbusch, L. Schweikhard, T. Stora, F. Wienholtz, R. N. Wolf, K. Zuber, Competition between pairing correlations and deformation from the odd-even mass staggering of francium and radium isotopes, *Phys. Rev. C* 90 (2014) 024301, doi:[10.1103/PhysRevC.90.024301](https://doi.org/10.1103/PhysRevC.90.024301), URL <http://link.aps.org/doi/10.1103/PhysRevC.90.024301>.
- [76] J. Hakala, J. Dobaczewski, D. Gorelov, T. Eronen, A. Jokinen, A. Kankainen, V. S. Kolhinen, M. Kortelainen, I. D. Moore, H. Penttilä, S. Rinta-Antila, J. Rissanen, A. Saastamoinen, V. Sonnenschein, J. Äystö, Precision Mass Measurements beyond  $^{132}\text{Sn}$ : Anomalous Behavior of Odd-Even Staggering of Binding Energies, *Phys. Rev. Lett.* 109 (2012) 032501, doi:[10.1103/PhysRevLett.109.032501](https://doi.org/10.1103/PhysRevLett.109.032501), URL <http://link.aps.org/doi/10.1103/PhysRevLett.109.032501>.
- [77] J. Erler, N. Birge, M. Kortelainen, W. Nazarewicz, E. Olsen, A. M. Perhac, M. Stoitsov, The limits of the nuclear landscape, *Nature* 486 (2012) 509–512, doi:[10.1038/nature11188](https://doi.org/10.1038/nature11188), URL <http://dx.doi.org/10.1038/nature11188>.
- [78] T. Ohnishi, T. Kubo, . Kusaka, A. Yoshida, K. Yoshida, M. Ohtake, N. Fukuda, H. Takeda, D. Kameda, K. Tanaka, N. Inabe, Y. Yanagisawa, Y. Gono, H. Watanabe, H. Otsu, H. Baba, T. Ichihara, Y. Yamaguchi, M. Takechi, S. Nishimura, H. Ueno, A. Yoshimi, H. Sakurai, T. Motobayashi, T. Nakao, Y. Mizoi, M. Matsushita, K. Ieki, N. Kobayashi, K. Tanaka, Y. Kawada, N. Tanaka, S. Deguchi, Y. Satou, Y. Kondo, T. Nakamura, K. Yoshinaga, C. Ishii, H. Yoshii, Y. Miyashita, N. Uematsu, Y. Shiraki, T. Sumikama, J. Chiba, E. Ideguchi, A. Saito, T. Yamaguchi, I. Hachiuma, T. Suzuki, T. Moriguchi, A. Ozawa, T. Ohtsubo, M. A. Famiano, H. Geissel, A. S. Nettleton, O. B. Tarasov, D. P. Bazin, B. M. Sherrill, S. L. Manikonda, J. A. Nolen, Identification of 45 New Neutron-Rich Isotopes Produced by In-Flight Fission of a  $^{238}\text{U}$  Beam at 345 MeV/nucleon, *J. Phys. Soc. Jpn* 79 (7) (2010) 073201, doi:[10.1143/JPSJ.79.073201](https://doi.org/10.1143/JPSJ.79.073201), URL <http://jpsj.ipap.jp/link?JPSJ/79/073201/>.
- [79] G. Lorusso, S. Nishimura, Z. Y. Xu, A. Jungclaus, Y. Shimizu, G. S. Simpson, P.-A. Söderström, H. Watanabe, F. Browne, P. Doornenbal, G. Gey, H. S. Jung, B. Meyer, T. Sumikama, J. Taprogge, Z. Vajta, J. Wu, H. Baba, G. Benzoni, K. Y. Chae, F. C. L. Crespi, N. Fukuda, R. Gernhäuser, N. Inabe, T. Isobe,

- 2215 T. Kajino, D. Kameda, G. D. Kim, Y.-K. Kim, I. Kojouharov, 2280  
 2216 F. G. Kondev, T. Kubo, N. Kurz, Y. K. Kwon, G. J. Lane, 2281  
 2217 Z. Li, A. Montaner-Pizá, K. Moschner, F. Naqvi, M. Niikura, 2282  
 2218 H. Nishibata, A. Odahara, R. Orlandi, Z. Patel, Z. Podolyák, 2283  
 2219 H. Sakurai, H. Schaffner, P. Schury, S. Shibagaki, K. Steiger, 2284  
 2220 H. Suzuki, H. Takeda, A. Wendt, A. Yagi, K. Yoshinaga, 2285  
 2221  $\beta$ -Decay Half-Lives of 110 Neutron-Rich Nuclei across the 2286  
 2222  $N = 82$  Shell Gap: Implications for the Mechanism and Uni- 2287  
 2223 versality of the Astrophysical  $r$  Process, Phys. Rev. Lett. 114 2288  
 2224 (2015) 192501, doi:10.1103/PhysRevLett.114.192501, URL 2289  
 2225 <http://link.aps.org/doi/10.1103/PhysRevLett.114.192501>. 2290
- [80] J. Van Schelt, D. Lascar, G. Savard, J. A. Clark, S. Cald- 2291  
 2227 well, A. Chaudhuri, J. Fallis, J. P. Greene, A. F. Levand, 2292  
 2228 G. Li, K. S. Sharma, M. G. Sternberg, T. Sun, B. J. Zabrans- 2293  
 2229 sky, Mass measurements near the  $r$ -process path using the 2294  
 2230 Canadian Penning Trap mass spectrometer, Phys. Rev. C 2295  
 2231 85 (2012) 045805, doi:10.1103/PhysRevC.85.045805, URL 2296  
 2232 <http://link.aps.org/doi/10.1103/PhysRevC.85.045805>. 2297
- [81] M. Mumpower, R. Surman, G. McLaughlin, A. Apra- 2298  
 2234 hamian, The impact of individual nuclear properties on 2299  
 2235  $r$ -process nucleosynthesis, Progress in Particle and Nu- 2300  
 2236 clear Physics 86 (2016) 86 – 126, ISSN 0146-6410, 2301  
 2237 doi:<http://dx.doi.org/10.1016/j.ppnp.2015.09.001>, URL 2302  
 2238 <http://www.sciencedirect.com/science/article/pii/S0146641015000827>. 2303
- [82] A. T. Gallant, J. C. Bale, T. Brunner, U. Chowdhury, S. Ette- 2304  
 2240 nauer, A. Lennarz, D. Robertson, V. V. Simon, A. Chaudhuri, 2305  
 2241 J. D. Holt, A. A. Kwiatkowski, E. Mané, J. Menéndez, 2306  
 2242 B. E. Schultz, M. C. Simon, C. Andreoiu, P. Delheij, M. R. 2307  
 2243 Pearson, H. Savajols, A. Schwenk, J. Dilling, New Precision 2308  
 2244 Mass Measurements of Neutron-Rich Calcium and Potassium 2309  
 2245 Isotopes and Three-Nucleon Forces, Phys. Rev. Lett. 109 2310  
 2246 (2012) 032506, doi:10.1103/PhysRevLett.109.032506, URL 2311  
 2247 <http://link.aps.org/doi/10.1103/PhysRevLett.109.032506>. 2312
- [83] A. Lapiere, M. Brodeur, T. Brunner, S. Ettenauer, P. Fin- 2313  
 2248 lay, A. T. Gallant, V. V. Simon, P. Delheij, D. Lunney, 2314  
 2249 R. Ringle, H. Savajols, J. Dilling, Penning-trap mass 2315  
 2250 measurements of the neutron-rich K and Ca isotopes: 2316  
 2251 Resurgence of the  $N = 28$  shell strength, Phys. Rev. C 2317  
 2252 85 (2012) 024317, doi:10.1103/PhysRevC.85.024317, URL 2318  
 2253 <http://link.aps.org/doi/10.1103/PhysRevC.85.024317>. 2319
- [84] C. Böhm, C. Borgmann, G. Audi, D. Beck, K. Blaum, 2320  
 2256 M. Breitenfeldt, R. B. Cakirli, T. E. Cocolios, S. Eliseev, 2321  
 2257 S. George, F. Herfurth, A. Herlert, M. Kowalska, S. Kreim, 2322  
 2258 D. Lunney, V. Manea, E. Minaya Ramirez, S. Naimi, 2323  
 2259 D. Neidherr, M. Rosenbusch, L. Schweikhard, J. Stanja, 2324  
 2260 M. Wang, R. N. Wolf, K. Zuber, Evolution of nuclear 2325  
 2261 ground-state properties of neutron-deficient isotopes around 2326  
 2262  $Z = 82$  from precision mass measurements, Phys. Rev. C 2327  
 2263 90 (2014) 044307, doi:10.1103/PhysRevC.90.044307, URL 2328  
 2264 <http://link.aps.org/doi/10.1103/PhysRevC.90.044307>. 2329
- [85] V. V. Simon, T. Brunner, U. Chowdhury, B. Eber- 2330  
 2266 hardt, S. Ettenauer, A. T. Gallant, E. Mané, M. C. Si- 2331  
 2267 mon, P. Delheij, M. R. Pearson, G. Audi, G. Gwinner, 2332  
 2268 D. Lunney, H. Schatz, J. Dilling, Penning-trap mass 2333  
 2269 spectrometry of highly charged, neutron-rich Rb and 2334  
 2270 Sr isotopes in the vicinity of  $A \approx 100$ , Phys. Rev. C 2335  
 2271 85 (2012) 064308, doi:10.1103/PhysRevC.85.064308, URL 2336  
 2272 <http://link.aps.org/doi/10.1103/PhysRevC.85.064308>. 2337
- [86] U. Hager, T. Eronen, J. Hakala, A. Jokinen, V. S. Kolhinen, 2338  
 2274 S. Kopecky, I. Moore, A. Nieminen, M. Oinonen, S. Rinta- 2339  
 2275 Antila, J. Szerypo, J. Äystö, First Precision Mass Measure- 2340  
 2276 ments of Refractory Fission Fragments, Phys. Rev. Lett. 96 2341  
 2277 (2006) 042504, doi:10.1103/PhysRevLett.96.042504, URL 2342  
 2278 <http://link.aps.org/doi/10.1103/PhysRevLett.96.042504>. 2343
- [87] S. Rahaman, U. Hager, V. V. Elomaa, T. Eronen, 2344  
 2279 J. Hakala, A. Jokinen, A. Kankainen, P. Karvonen, 2345  
 2280 I. D. Moore, H. Penttilä, S. Rinta-Antila, J. Rissanen, 2346  
 2281 A. Saastamoinen, T. Sonoda, J. Äystö, Precise atomic 2347  
 2282 masses of neutron-rich Br and Rb nuclei close to the 2348  
 2283  $r$ -process path, Eur. Phys. J. A 32 (1) (2007) 87– 2349  
 2284 96, ISSN 1434-601X, doi:10.1140/epja/i2006-10297-y, URL 2350  
 2285 <http://dx.doi.org/10.1140/epja/i2006-10297-y>. 2351
- [88] S. Naimi, G. Audi, D. Beck, K. Blaum, C. Böhm, 2352  
 2286 C. Borgmann, M. Breitenfeldt, S. George, F. Herfurth, 2353  
 2287 A. Herlert, A. Kellerbauer, M. Kowalska, D. Lunney, E. Mi- 2354  
 2288 naya Ramirez, D. Neidherr, M. Rosenbusch, L. Schweikhard, 2355  
 2289 R. N. Wolf, K. Zuber, Surveying the  $N = 40$  island 2356  
 2290 of inversion with new manganese masses, Phys. Rev. C 2357  
 2291 86 (2012) 014325, doi:10.1103/PhysRevC.86.014325, URL 2358  
 2292 <http://link.aps.org/doi/10.1103/PhysRevC.86.014325>. 2359
- [89] A. Chaudhuri, C. Andreoiu, T. Brunner, U. Chowdhury, 2360  
 2293 S. Ettenauer, A. T. Gallant, G. Gwinner, A. A. Kwiatkowski, 2361  
 2294 A. Lennarz, D. Lunney, T. D. Macdonald, B. E. Schultz, 2362  
 2295 M. C. Simon, V. V. Simon, J. Dilling, Evidence for the 2363  
 2296 extinction of the  $N = 20$  neutron-shell closure for 2364  
 2297  $^{32}\text{Mg}$  from direct mass measurements, Phys. Rev. C 88 2365  
 2298 (2013) 054317, doi:10.1103/PhysRevC.88.054317, URL 2366  
 2299 <http://link.aps.org/doi/10.1103/PhysRevC.88.054317>. 2367
- [90] B. A. Brown, D. Lunney, J. Dilling, Elucidation of the Anoma- 2368  
 2300 lous  $A = 9$  Isospin Quartet Behavior, Phys. Rev. Lett. 108 2369  
 2301 (2012) 212501, doi:10.1103/PhysRevLett.108.212501, URL 2370  
 2302 <http://link.aps.org/doi/10.1103/PhysRevLett.108.212501>. 2371
- [91] A. T. Gallant, M. Brodeur, C. Andreoiu, A. Bader, A. Chaud- 2372  
 2303 huri, U. Chowdhury, A. Grossheim, R. Klawitter, A. A. 2373  
 2304 Kwiatkowski, K. G. Leach, A. Lennarz, T. D. Macdon- 2374  
 2305 ald, B. E. Schultz, J. Lassen, H. Heggen, S. Raeder, 2375  
 2306 A. Teigelhöfer, B. A. Brown, A. Magilligan, J. D. Holt, 2376  
 2307 J. Menéndez, J. Simonis, A. Schwenk, J. Dilling, Break- 2377  
 2308 down of the Isobaric Multiplet Mass Equation for the 2378  
 2309  $A = 20$  and 21 Multiplets, Phys. Rev. Lett. 113 (2014) 2379  
 2310 082501, doi:10.1103/PhysRevLett.113.082501, URL 2380  
 2311 <http://link.aps.org/doi/10.1103/PhysRevLett.113.082501>. 2381
- [92] A. Kankainen, L. Canete, T. Eronen, D. Gorelov, J. Hakala, 2382  
 2312 A. Jokinen, J. Koponen, I. Moore, D. Nesterenko, 2383  
 2313 J. Reinikainen, S. Rinta-Antila, A. Voss, J. Äystö, Mass 2384  
 2314 of astrophysically relevant  $^{31}\text{Cl}$  and the breakdown of the 2385  
 2315 isobaric multiplet mass equation, Phys. Rev. C Rapid. Comm. 2386  
 2316 Accepted for publication. 2387
- [93] M. Eibach, G. Bollen, M. Brodeur, K. Cooper, K. Gulyuz, 2388  
 2317 C. Izzo, D. J. Morrissey, M. Redshaw, R. Ringle, R. San- 2389  
 2318 dler, S. Schwarz, C. S. Sumithrarachchi, A. A. Valverde, 2390  
 2319 A. C. Villari, Determination of the  $Q_{EC}$  values of the 2391  
 2320  $T = 1/2$  mirror nuclei  $^{21}\text{Na}$  and  $^{29}\text{P}$  at LEBIT, Phys. Rev. C 2392  
 2321 92 (2015) 045502, doi:10.1103/PhysRevC.92.045502, URL 2393  
 2322 <http://link.aps.org/doi/10.1103/PhysRevC.92.045502>. 2394
- [94] B. E. Schultz, M. Brodeur, C. Andreoiu, A. Bader, A. Chaud- 2395  
 2323 huri, U. Chowdhury, A. T. Gallant, A. Grossheim, R. Klawitter, 2396  
 2324 A. A. Kwiatkowski, K. G. Leach, A. Lennarz, T. D. Macdon- 2397  
 2325 ald, J. Lassen, H. Heggen, S. Raeder, A. Teigelhöfer, J. Dilling, 2398  
 2326 Precision  $Q_{EC}$ -value measurement of  $^{23}\text{Mg}$  for testing the 2399  
 2327 Cabibbo-Kobayashi-Maskawa matrix unitarity, Phys. Rev. C 2400  
 2328 90 (2014) 012501, doi:10.1103/PhysRevC.90.012501, URL 2401  
 2329 <http://link.aps.org/doi/10.1103/PhysRevC.90.012501>. 2402
- [95] L. Canete, A. Kankainen, T. Eronen, D. Gorelov, J. Hakala, 2403  
 2330 A. Jokinen, V. Kolhinen, J. Koponen, I. Moore, J. Reinikainen, 2404  
 2331 S. Rinta-Antila, High-precision mass measurements of  $^{25}\text{Al}$  2405  
 2332 and  $^{30}\text{P}$  at JYFLTRAP, Eur. Phys. J. A Accepted for publica- 2406  
 2333 tion. 2407
- [96] A. Kankainen, T. Eronen, D. Gorelov, J. Hakala, A. Jokinen, 2408

- 2345 V. S. Kolhinen, M. Reponen, J. Rissanen, A. Saastamoinen, 2410  
 2346 V. Sonnenschein, J. Äystö, Coulomb displacement energies 2411  
 2347 as a probe for nucleon pairing in the  $f_{7/2}$  shell, Phys. Rev. C 2412  
 2348 89 (2014) 051302, doi:10.1103/PhysRevC.89.051302, URL 2413  
 2349 <http://link.aps.org/doi/10.1103/PhysRevC.89.051302>, 2414
- [97] K. Gulyuz, J. Ariche, G. Bollen, S. Bustabad, M. Eibach, 2415  
 2350 C. Izzo, S. J. Novario, M. Redshaw, R. Ringle, R. Sandler, 2416  
 2351 S. Schwarz, A. A. Valverde, Determination of 2417  
 2352 the direct double- $\beta$ -decay  $Q$  value of  $^{96}\text{Zr}$  and atomic 2418  
 2353 masses of  $^{90-92,94,96}\text{Zr}$  and  $^{92,94-98,100}\text{Mo}$ , Phys. Rev. C 2419  
 2354 91 (2015) 055501, doi:10.1103/PhysRevC.91.055501, URL 2420  
 2355 <http://link.aps.org/doi/10.1103/PhysRevC.91.055501>, 2421
- [98] A. Kankainen, J. Äystö, A. Jokinen, High-accuracy mass 2422  
 2356 spectrometry of fission products with Penning traps, J. 2423  
 2357 Phys. G: Nucl. Part. Phys. 39 (9) (2012) 093101, URL 2424  
 2358 <http://stacks.iop.org/0954-3889/39/i=9/a=093101>, 2425
- [99] M. Alanssari, D. Frekers, T. Eronen, L. Canete, J. Dilling, 2426  
 2361 M. Haaranen, J. Hakala, M. Holl, M. Jeřkovič, A. Jokinen, 2427  
 2362 A. Kankainen, J. Koponen, A. J. Mayer, I. D. 2428  
 2363 Moore, D. A. Nesterenko, I. Pohjalainen, P. Povinec, 2429  
 2364 J. Reinikainen, S. Rinta-Antila, P. C. Srivastava, J. Suhonen, 2430  
 2365 R. I. Thompson, A. Voss, M. E. Wieser, Single 2431  
 2366 and Double Beta-Decay  $Q$  Values among the Triplet 2432  
 2367  $^{96}\text{Zr}$ ,  $^{96}\text{Nb}$ , and  $^{96}\text{Mo}$ , Phys. Rev. Lett. 116 (2016) 2433  
 2368 072501, doi:10.1103/PhysRevLett.116.072501, URL 2434  
 2370 <http://link.aps.org/doi/10.1103/PhysRevLett.116.072501>, 2435
- [100] C. Smorra, T. R. Rodríguez, T. Beyer, K. Blaum, 2436  
 2371 M. Block, C. E. Düllmann, K. Eberhardt, M. Eibach, 2437  
 2372 S. Eliseev, K. Langanke, G. Martínez-Pinedo, S. Nagy, 2438  
 2373 W. Nörtershäuser, D. Renisch, V. M. Shabaev, I. I. 2439  
 2374 Tupitsyn, N. A. Zubova,  $Q$  value and half-life of 2440  
 2375 double-electron capture in  $^{184}\text{Os}$ , Phys. Rev. C 86 2441  
 2376 (2012) 044604, doi:10.1103/PhysRevC.86.044604, URL 2442  
 2377 <http://link.aps.org/doi/10.1103/PhysRevC.86.044604>, 2443
- [101] U. Chowdhury, K. G. Leach, C. Andreoiu, A. Bader, 2444  
 2379 M. Brodeur, A. Chaudhuri, A. T. Gallant, A. Grossheim, 2445  
 2380 G. Gwinner, R. Klawitter, A. A. Kwiatkowski, 2446  
 2381 A. Lennarz, T. D. Macdonald, J. Parkes, B. E. 2447  
 2382 Schultz, J. Dilling, First direct mass measurement of 2448  
 2383 the neutron-deficient nucleus  $^{24}\text{Al}$ , Phys. Rev. C 92 2449  
 2384 (2015) 045803, doi:10.1103/PhysRevC.92.045803, URL 2450  
 2385 <http://link.aps.org/doi/10.1103/PhysRevC.92.045803>, 2451
- [102] A. A. Kwiatkowski, T. Brunner, J. D. Holt, A. Chaudhuri, 2452  
 2387 U. Chowdhury, M. Eibach, J. Engel, A. T. Gallant, 2453  
 2388 A. Grossheim, M. Horoi, A. Lennarz, T. D. Macdonald, 2454  
 2389 M. R. Pearson, B. E. Schultz, M. C. Simon, 2455  
 2390 R. A. Senkov, V. V. Simon, K. Zuber, J. Dilling, New 2456  
 2391 determination of double- $\beta$ -decay properties in  $^{48}\text{Ca}$ : 2457  
 2392 High-precision  $Q_{\beta\beta}$ -value measurement and improved 2458  
 2393 nuclear matrix element calculations, Phys. Rev. C 89 2459  
 2394 (2014) 045502, doi:10.1103/PhysRevC.89.045502, URL 2460  
 2395 <http://link.aps.org/doi/10.1103/PhysRevC.89.045502>, 2461
- [103] S. Malbrunot-Ettenauer, T. Brunner, U. Chowdhury, A. T. Gallant, 2462  
 2397 V. V. Simon, M. Brodeur, A. Chaudhuri, E. Mané, M. C. 2463  
 2398 Simon, C. Andreoiu, G. Audi, J. R. Crespo López-Urrutia, 2464  
 2399 P. Delheij, G. Gwinner, A. Lapierre, D. Lunney, M. R. Pearson, 2465  
 2400 R. Ringle, J. Ullrich, J. Dilling, Penning trap mass measurements 2466  
 2401 utilizing highly charged ions as a path to benchmark 2467  
 2402 isospin-symmetry breaking corrections in  $^{74}\text{Rb}$ , Phys. Rev. C 2468  
 2403 91 (2015) 045504, doi:10.1103/PhysRevC.91.045504, URL 2469  
 2404 <http://link.aps.org/doi/10.1103/PhysRevC.91.045504>, 2470
- [104] A. A. Valverde, G. Bollen, K. Cooper, M. Eibach, K. Gulyuz, 2471  
 2406 C. Izzo, D. J. Morrissey, R. Ringle, R. Sandler, 2472  
 2407 S. Schwarz, C. S. Sumithrarachchi, A. C. C. Villari, 2473  
 2408 Penning trap mass measurement of  $^{72}\text{Br}$ , Phys. Rev. C 2474  
 2409 91 (2015) 037301, doi:10.1103/PhysRevC.91.037301, URL  
 2410 <http://link.aps.org/doi/10.1103/PhysRevC.91.037301>.
- [105] F. Schneider, T. Beyer, K. Blaum, M. Block, S. Chenmarev, 2475  
 2411 H. Dorrer, C. Düllmann, K. Eberhardt, M. Eibach, 2476  
 2412 S. Eliseev, J. Grund, U. Köster, S. Nagy, Y. Novikov, 2477  
 2413 D. Renisch, A. Türler, K. Wendt, Preparatory studies for a high-precision Penning-trap measurement of the 2478  
 2414  $^{163}\text{Ho}$  electron capture  $Q$ -value, Eur. Phys. J. A 51 (7) 2479  
 2415 89, ISSN 1434-6001, doi:10.1140/epja/i2015-15089-8, URL 2480  
 2416 <http://dx.doi.org/10.1140/epja/i2015-15089-8>.
- [106] C. Droese, D. Ackermann, L.-L. Andersson, K. Blaum, 2481  
 2417 M. Block, M. Dworschak, M. Eibach, S. Eliseev, U. Forsberg, 2482  
 2418 E. Haettner, F. Herfurth, F. Hessberger, S. Hofmann, 2483  
 2419 J. Ketelaer, G. Marx, E. Minaya Ramirez, D. Nesterenko, 2484  
 2420 Y. Novikov, W. Plass, D. Rodriguez, D. Rudolph, C. Scheidenberger, 2485  
 2421 L. Schweikhard, S. Stolze, P. Thirolf, C. Weber, High-precision mass 2486  
 2422 measurements of  $^{203-207}\text{Rn}$  and  $^{213}\text{Ra}$  with SHIPTRAP, Eur. Phys. J. A 49 (1) 2487  
 2423 13, ISSN 1434-6001, doi:10.1140/epja/i2013-13013-0, URL 2488  
 2424 <http://dx.doi.org/10.1140/epja/i2013-13013-0>.
- [107] M. Eibach, T. Beyer, K. Blaum, M. Block, C. E. Düllmann, 2489  
 2425 K. Eberhardt, J. Grund, S. Nagy, H. Nitsche, W. Nörtershäuser, 2490  
 2426 D. Renisch, K. P. Rykaczewski, F. Schneider, C. Smorra, J. Vieten, 2491  
 2427 M. Wang, K. Wendt, Direct high-precision mass measurements on 2492  
 2428  $^{241,243}\text{Am}$ ,  $^{244}\text{Pu}$ , and  $^{249}\text{Cf}$ , Phys. Rev. C 89 (2014) 064318, doi:10.1103/PhysRevC.89.064318, URL 2493  
 2429 <http://link.aps.org/doi/10.1103/PhysRevC.89.064318>.
- [108] P. Möller, A. Sierk, T. Ichikawa, H. Sagawa, Nuclear ground-state masses and deformations: FRDM(2012), At. Data and Nucl. Data Tables 109–110 (2016) 1 – 204, ISSN 0092-640X, doi:http://dx.doi.org/10.1016/j.adt.2015.10.002, URL <http://www.sciencedirect.com/science/article/pii/S0092640X16000000>
- [109] J. Duflo, A. Zuker, Microscopic mass formulas, Phys. Rev. C 52 (1995) R23–R27, doi:10.1103/PhysRevC.52.R23, URL <http://link.aps.org/doi/10.1103/PhysRevC.52.R23>.
- [110] N. Wang, M. Liu, X. Wu, J. Meng, Surface diffuseness correction in global mass formula, Phys. Lett. B 734 (2014) 215 – 219, ISSN 0370-2693, doi: <http://dx.doi.org/10.1016/j.physletb.2014.05.049>, URL <http://www.sciencedirect.com/science/article/pii/S0370269314000000>
- [111] S. Goriely, N. Chamel, J. M. Pearson, Further explorations of Skyrme-Hartree-Fock-Bogoliubov mass formulas. XIII. The 2012 atomic mass evaluation and the symmetry coefficient, Phys. Rev. C 88 (2013) 024308, doi:10.1103/PhysRevC.88.024308, URL <http://link.aps.org/doi/10.1103/PhysRevC.88.024308>.
- [112] M. Kortelainen, T. Lesinski, J. Moré, W. Nazarewicz, J. Sarich, N. Schunck, M. V. Stoitsov, S. Wild, Nuclear energy density optimization, Phys. Rev. C 82 (2010) 024313, doi:10.1103/PhysRevC.82.024313, URL <http://link.aps.org/doi/10.1103/PhysRevC.82.024313>.
- [113] P. Möller, J. Nix, W. Myers, W. Swiatecki, Nuclear Ground-State Masses and Deformations, At. Data Nucl. Data Tables 59 (2) (1995) 185 – 381, ISSN 0092-640X, doi:10.1006/adnd.1995.1002, URL <http://www.sciencedirect.com/science/article/pii/S0092640X85710000>
- [114] J. Mendoza-Temis, J. G. Hirsch, A. P. Zuker, The anatomy of the simplest Duflo–Zuker mass formula, Nucl. Phys. A 843 (1–4) (2010) 14 – 36, ISSN 0375-9474, doi: <http://dx.doi.org/10.1016/j.nuclphysa.2010.05.055>, URL <http://www.sciencedirect.com/science/article/pii/S0375947410000000>
- [115] M. V. Stoitsov, J. Dobaczewski, W. Nazarewicz, S. Pitel, D. J. Dean, Systematic study of deformed nuclei at the drip lines and beyond, Phys. Rev. C 68 (2003) 054312, doi:10.1103/PhysRevC.68.054312, URL



- 2475 <http://link.aps.org/doi/10.1103/PhysRevC.68.054324>  
 2476 [116] M. Stoitsov, J. Dobaczewski, W. Nazarewicz, P. Borycki, 2541  
 2477 Large-scale self-consistent nuclear mass calculations, 2542  
 2478 Int. J. Mass Spectrom. 251 (2 - 3) (2006) 243 – 251, 2543  
 2479 ISSN 1387-3806, doi:10.1016/j.ijms.2006.01.040, URL 2544  
 2480 <http://www.sciencedirect.com/science/article/pii/S1387380606000344>  
 2481 [117] Y. Gao, J. Dobaczewski, M. Kortelainen, J. Toiva- 2546  
 2482 nen, D. Tarpanov, Propagation of uncertainties in the 2547  
 2483 Skyrme energy-density-functional model, Phys. Rev. C 2548  
 2484 87 (2013) 034324, doi:10.1103/PhysRevC.87.034324, URL 2549  
 2485 <http://link.aps.org/doi/10.1103/PhysRevC.87.034324>  
 2486 [118] M. Kortelainen, Propagation of uncertainties in the 2551  
 2487 nuclear DFT models, Journal of Physics G: Nuclear 2552  
 2488 and Particle Physics 42 (3) (2015) 034021, URL 2553  
 2489 <http://stacks.iop.org/0954-3899/42/i=3/a=034021>, 2554  
 2490 [119] M. Mumpower, R. Surman, G. McLaughlin, A. Apra- 2555  
 2491 hamian, The impact of individual nuclear properties on 2556  
 2492 r-process nucleosynthesis, Progress in Particle and Nu- 2557  
 2493 clear Physics 86 (2016) 86 – 126, ISSN 0146-6410, 2558  
 2494 doi:<http://dx.doi.org/10.1016/j.pnpnp.2015.09.001>, URL 2559  
 2495 <http://www.sciencedirect.com/science/article/pii/S0146641015000899>  
 2496 [120] B. H. Sun, Y. A. Litvinov, I. Tanihata, Y. H. Zhang, Toward 2561  
 2497 precision mass measurements of neutron-rich nuclei relevant 2562  
 2498 to r-process nucleosynthesis, Frontiers of Physics 10 (4) (2015) 2563  
 2499 1–25, ISSN 2095-0470, doi:10.1007/s11467-015-0503-z, URL 2564  
 2500 <http://dx.doi.org/10.1007/s11467-015-0503-z>, 2565  
 2501 [121] K. Heyde, J. L. Wood, Shape coexistence in 2566  
 2502 atomic nuclei, Rev. Mod. Phys. 83 (4) (2011) 2567  
 2503 1467–1521, doi:10.1103/revmodphys.83.1467, URL 2568  
 2504 <http://dx.doi.org/10.1103/RevModPhys.83.1467>, 2569  
 2505 [122] S. Takahara, N. Onishi, Y. R. Shimizu, N. Tajima, 2570  
 2506 The role of spin-orbit potential in nuclear prolate- 2571  
 2507 shape dominance, Phys. Lett. B 702 (5) (2011) 2572  
 2508 429–432, doi:10.1016/j.physletb.2011.07.030, URL 2573  
 2509 <http://dx.doi.org/10.1016/j.physletb.2011.07.030>, 2574  
 2510 [123] R. F. G. Ruiz, M. L. Bissell, K. Blaum, A. Ekström, 2575  
 2511 N. Frömmgen, G. Hagen, M. Hammen, K. Hebeler, J. D. 2576  
 2512 Holt, G. R. Jansen, M. Kowalska, K. Kreim, W. Nazarewicz, 2577  
 2513 R. Neugart, G. Neyens, W. Nörtershäuser, T. Papenbrock, 2578  
 2514 J. Papuga, A. Schwenk, J. Simonis, K. A. Wendt, D. T. 2579  
 2515 Yordanov, Unexpectedly large charge radii of neutron-rich 2580  
 2516 calcium isotopes, Nat Phys doi:10.1038/nphys3645, URL 2581  
 2517 <http://dx.doi.org/10.1038/nphys3645>, 2582  
 2518 [124] URL <http://massexplorer.frib.msu.edu/>, ??? 2583  
 2519 [125] J. C. Hardy, I. S. Towner, Superallowed  $0^+ \rightarrow 0$  2584  
 2520  $^+$  nuclear  $\beta$  decays: 2014 critical survey, with pre- 2585  
 2521 cise results for  $V_{ud}$  and CKM unitarity, Phys. Rev. 2586  
 2522 C 91 (2), doi:10.1103/physrevc.91.025501, URL 2587  
 2523 <http://dx.doi.org/10.1103/PhysRevC.91.025501>, 2588  
 2524 [126] N. Severijns, O. Naviliat-Cuncic, Structure and sym- 2589  
 2525 metries of the weak interaction in nuclear beta de- 2590  
 2526 cay, Phys. Scr. T152 (T152) (2013) 014018, URL 2591  
 2527 <http://stacks.iop.org/1402-4896/2013/i=T152/a=014018>, [137]  
 2528 A. A. Valverde, G. Bollen, M. Brodeur, R. A. Bryce, 2593  
 2529 K. Cooper, M. Eibach, K. Gulyuz, C. Izzo, D. J. Mor- 2594  
 2530 rissey, M. Redshaw, R. Ringle, R. Sandler, S. Schwarz, 2595  
 2531 C. S. Sumthrarachchi, A. C. C. Villari, First Di- 2596  
 2532 rect Determination of the Superallowed  $\beta$ -Decay 2597  
 2533  $Q_{EC}$  Value for  $^{14}\text{O}$ , Phys. Rev. Lett. 114 (2015) 2598  
 2534 232502, doi:10.1103/PhysRevLett.114.232502, URL 2599  
 2535 <http://link.aps.org/doi/10.1103/PhysRevLett.114.232502>, [138]  
 2536 G. Savard, F. Buchinger, J. A. Clark, J. E. Crawford, S. Gulick, 2601  
 2537 J. C. Hardy, A. A. Hecht, J. K. P. Lee, A. F. Levand, N. D. 2602  
 2538 Scielzo, H. Sharma, K. S. Sharma, I. Tanihata, A. C. C. Villari, 2603  
 2539 Y. Wang, Q Value of the Superallowed Decay of  $^{46}\text{V}$  and Its 2604  
 Influence on  $V_{ud}$  and the Unitarity of the Cabibbo-Kobayashi-  
 Maskawa Matrix, Phys. Rev. Lett. 95 (10) (2005) 102501, URL  
<http://link.aps.org/abstract/PRL/v95/e102501>.  
 [129] T. Eronen, V. Elomaa, U. Hager, J. Hakala, A. Joki-  
 nen, A. Kankainen, I. Moore, H. Penttilä, S. Rahaman,  
 A. Saastamoinen, A. Saastamoinen, T. Sonoda, J. Äystö, J. C.  
 Hardy, V. S. Kolhinen,  $Q$  Values of the Superallowed  $\beta$   
 Emitters  $^{26}\text{Al}^m$ ,  $^{42}\text{Sc}$ , and  $^{46}\text{V}$  and Their Impact on  
 $V_{ud}$  and the Unitarity of the Cabibbo-Kobayashi-Maskawa  
 Matrix, Phys. Rev. Lett. 97 (23) (2006) 232501, URL  
<http://link.aps.org/abstract/PRL/v97/e232501>.  
 [130] I. S. Towner, J. C. Hardy, Improved calculation of the  
 isospin-symmetry-breaking corrections to superallowed Fermi  
 beta decay, Phys. Rev. C 77 (2) (2008) 025501, URL  
<http://link.aps.org/abstract/PRC/v77/e025501>.  
 [131] A. Saastamoinen, T. Eronen, A. Jokinen, V. V. Elomaa,  
 J. Hakala, A. Kankainen, I. D. Moore, S. Rahaman, J. Risa-  
 sanen, C. Weber, J. Äystö, L. Trache, Mass of  $^{23}\text{Al}$  for  
 testing the isobaric multiplet mass equation, Phys. Rev. C  
 80 (2009) 044330, doi:10.1103/PhysRevC.80.044330, URL  
<http://link.aps.org/doi/10.1103/PhysRevC.80.044330>.  
 [132] A. Kankainen, T. Eronen, D. Gorelov, J. Hakala, A. Joki-  
 nen, V. S. Kolhinen, M. Reponen, J. Rissanen, A. Saas-  
 tamoinen, V. Sonnenschein, J. Äystö, High-precision  
 mass measurement of  $^{31}\text{S}$  with the double Penning trap  
 JYFLTRAP improves the mass value for  $^{32}\text{Cl}$ , Phys. Rev. C  
 82 (2010) 052501, doi:10.1103/PhysRevC.82.052501, URL  
<http://link.aps.org/doi/10.1103/PhysRevC.82.052501>.  
 [133] A. Kankainen, V.-V. Elomaa, T. Eronen, D. Gorelov,  
 J. Hakala, A. Jokinen, T. Kessler, V. S. Kolhinen, I. D.  
 Moore, S. Rahaman, M. Reponen, J. Rissanen, A. Saas-  
 tamoinen, C. Weber, J. Äystö, Mass measurements in the  
 vicinity of the doubly magic waiting point  $^{56}\text{Ni}$ , Phys. Rev. C  
 82 (2010) 034311, doi:10.1103/PhysRevC.82.034311, URL  
<http://link.aps.org/doi/10.1103/PhysRevC.82.034311>.  
 [134] M. MacCormick, G. Audi, Evaluated experimental isobaric  
 analogue states from to and associated {IMME} coeffi-  
 cients, Nucl. Phys. A 925 (2014) 61 – 95, ISSN 0375-9474,  
 doi:<http://dx.doi.org/10.1016/j.nuclphysa.2014.01.007>, URL  
<http://www.sciencedirect.com/science/article/pii/S0375947414000000>  
 [135] M. MacCormick, G. Audi, Corrigendum to “Evaluated ex-  
 perimental isobaric analogue states from to and associated  
 {IMME} coefficients” [Nucl. Phys. A 925 (2014) 61–95],  
 Nucl. Phys. A 925 (2014) 296 – 297, ISSN 0375-9474,  
 doi:<http://dx.doi.org/10.1016/j.nuclphysa.2014.05.010>, URL  
<http://www.sciencedirect.com/science/article/pii/S0375947414000000>  
 [136] Y. H. Lam, B. Blank, N. A. Smirnova, J. B. Bueb,  
 M. S. Antony, The isobaric multiplet mass equa-  
 tion for revisited, At. Data and Nucl. Data Tables 99 (6)  
 (2013) 680 – 703, ISSN 0092-640X, doi:<http://dx.doi.org/10.1016/j.adt.2012.11.002>, URL  
<http://www.sciencedirect.com/science/article/pii/S0092640X13000000>  
 M. Brodeur, T. Brunner, C. Champagne, S. Etenauer, M. J.  
 Smith, A. Lapiere, R. Ringle, V. L. Ryjkov, S. Bacca,  
 P. Delheij, G. W. F. Drake, D. Lunney, A. Schwenk,  
 J. Dilling, First Direct Mass Measurement of the Two-  
 Neutron Halo Nucleus  $^6\text{He}$  and Improved Mass for the  
 Four-Neutron Halo  $^8\text{He}$ , Phys. Rev. Lett. 108 (2012)  
 052504, doi:10.1103/PhysRevLett.108.052504, URL  
<http://link.aps.org/doi/10.1103/PhysRevLett.108.052504>.  
 R. J. Charity, J. M. Elson, J. Manfredi, R. Shane, L. G.  
 Sobotka, Z. Chajecski, D. Coupland, H. Iwasaki, M. Kil-  
 burn, J. Lee, W. G. Lynch, A. Sanetullaev, M. B. Tsang,  
 J. Winkelbauer, M. Youngs, S. T. Marley, D. V. Shetty,  
 A. H. Wuosmaa, T. K. Ghosh, M. E. Howard, Isobaric

- 2605 multiplet mass equation for  $A = 7$  and  $8$ , Phys. Rev. C 2670  
 2606 84 (2011) 051308, doi:10.1103/PhysRevC.84.051308, URL 2671  
 2607 <http://link.aps.org/doi/10.1103/PhysRevC.84.051308>, 2672  
 2608 [139] A. A. Kwiatkowski, B. R. Barquest, G. Bollen, C. M. Camp- 2673  
 2609 bell, D. L. Lincoln, D. J. Morrissey, G. K. Pang, A. M. 2674  
 2610 Prinke, J. Savory, S. Schwarz, C. M. Folden, D. Melconian, 2675  
 2611 S. K. L. Sjøe, M. Block, Precision test of the isobaric multiplet 2676  
 2612 mass equation for the  $A = 32$ ,  $T = 2$  quintet, Phys. Rev. C 2677  
 2613 80 (2009) 051302, doi:10.1103/PhysRevC.80.051302, URL 2678  
 2614 <http://link.aps.org/doi/10.1103/PhysRevC.80.051302>, 2679  
 2615 [140] K. Blaum, G. Audi, D. Beck, G. Bollen, F. Herfurth, 2680  
 2616 A. Kellerbauer, H.-J. Kluge, E. Sauvan, S. Schwarz, Masses 2681  
 2617 of  $^{32}\text{Ar}$  and  $^{33}\text{Ar}$  for Fundamental Tests, Phys. Rev. Lett. 91 2682  
 2618 (2003) 260801, doi:10.1103/PhysRevLett.91.260801, URL 2683  
 2619 <http://link.aps.org/doi/10.1103/PhysRevLett.91.260801>. 2684  
 2620 [141] C. Yazidjian, G. Audi, D. Beck, K. Blaum, S. George, 2685  
 2621 C. Guénaut, F. Herfurth, A. Herlert, A. Kellerbauer, H.-J. 2686  
 2622 Kluge, D. Lunney, L. Schweikhard, Evidence for a break- 2687  
 2623 down of the isobaric multiplet mass equation: A study 2688  
 2624 of the  $A = 35$ ,  $T = 3/2$  isospin quartet, Phys. Rev. C 2689  
 2625 76 (2007) 024308, doi:10.1103/PhysRevC.76.024308, URL 2690  
 2626 <http://link.aps.org/doi/10.1103/PhysRevC.76.024308>. 2691  
 2627 [142] A. Signoracci, B. A. Brown, Effects of isospin mix- 2692  
 2628 ing in the  $A = 32$  quintet, Phys. Rev. C 84 (2011) 2693  
 2629 031301, doi:10.1103/PhysRevC.84.031301, URL 2694  
 2630 <http://link.aps.org/doi/10.1103/PhysRevC.84.031301>. 2695  
 2631 [143] F. Herfurth, J. Dilling, A. Kellerbauer, G. Audi, D. Beck, 2696  
 2632 G. Bollen, H.-J. Kluge, D. Lunney, R. B. Moore, C. Schei- 2697  
 2633 denberger, S. Schwarz, G. Sikler, J. Szerypo, I. Col- 2698  
 2634 laboration, Breakdown of the Isobaric Multiplet Mass 2699  
 2635 Equation at  $A = 33$ ,  $T = 3/2$ , Phys. Rev. Lett. 87 2700  
 2636 (2001) 142501, doi:10.1103/PhysRevLett.87.142501, URL 2701  
 2637 <http://link.aps.org/doi/10.1103/PhysRevLett.87.142501>. 2702  
 2638 [144] Y. H. Zhang, H. S. Xu, Y. A. Litvinov, X. L. Tu, X. L. Yan, 2703  
 2639 S. Typel, K. Blaum, M. Wang, X. H. Zhou, Y. Sun, B. A. 2704  
 2640 Brown, Y. J. Yuan, J. W. Xia, J. C. Yang, G. Audi, X. C. Chen, 2705  
 2641 G. B. Jia, Z. G. Hu, X. W. Ma, R. S. Mao, B. Mei, P. Shuai, 2706  
 2642 Z. Y. Sun, S. T. Wang, G. Q. Xiao, X. Xu, T. Yamaguchi, Y. Ya- 2707  
 2643 maguchi, Y. D. Zang, H. W. Zhao, T. C. Zhao, W. Zhang, W. L. 2708  
 2644 Zhan, Mass Measurements of the Neutron-Deficient  $^{41}\text{Ti}$ , 2709  
 2645  $^{45}\text{Cr}$ ,  $^{49}\text{Fe}$ , and  $^{53}\text{Ni}$  Nuclides: First Test of the Isobaric Mul- 2710  
 2646 tiplet Mass Equation in  $f_p$ -Shell Nuclei, Phys. Rev. Lett. 109 2711  
 2647 (2012) 102501, doi:10.1103/PhysRevLett.109.102501, URL 2712  
 2648 <http://link.aps.org/doi/10.1103/PhysRevLett.109.102501>. 2713  
 2649 [145] M. C. Pyle, A. García, E. Tatar, J. Cox, B. K. Nayak, S. Tri- 2714  
 2650 ambak, B. Laughman, A. Komives, L. O. Lamm, J. E. Rolon, 2715  
 2651 T. Finnessy, L. D. Knutson, P. A. Voytas, Revalidation of 2716  
 2652 the Isobaric Multiplet Mass Equation, Phys. Rev. Lett. 88 2717  
 2653 (2002) 122501, doi:10.1103/PhysRevLett.88.122501, URL 2718  
 2654 <http://link.aps.org/doi/10.1103/PhysRevLett.88.122501>. 2719  
 2655 [146] J. Su, W. Liu, N. Zhang, Y. Shen, Y. Lam, N. Smirnova, 2720  
 2656 M. MacCormick, J. Wang, L. Jing, Z. Li, Y. Wang, B. Guo, 2721  
 2657 S. Yan, Y. Li, S. Zeng, G. Lian, X. Du, L. Gan, X. Bai, 2722  
 2658 Z. Gao, Y. Zhang, X. Zhou, X. Tang, J. He, Y. Yang, S. Jin, 2723  
 2659 P. Ma, J. Ma, M. Huang, Z. Bai, Y. Zhou, W. Ma, J. Hu, 2724  
 2660 S. Xu, S. Ma, S. Chen, L. Zhang, B. Ding, Z. Li, G. Audi, 2725  
 2661 Revalidation of the isobaric multiplet mass equation at  $A = 53$ , 2726  
 2662  $T = 3/2$ , Phys. Lett. B 756 (2016) 323 – 327, ISSN 0370-2693, 2727  
 2663 doi:<http://dx.doi.org/10.1016/j.physletb.2016.03.024>, URL 2728  
 2664 <http://www.sciencedirect.com/science/article/pii/S0370269316001954>. 2729  
 2665 [147] T. Dickel, W. Plaß, S. A. S. Andres, J. Ebert, H. Geissel, 2730  
 2666 E. Haettner, C. Hornung, I. Miskun, S. Pietri, S. Pu- 2731  
 2667 rushothaman, M. Reiter, A.-K. Rink, C. Scheidenberger, 2732  
 2668 H. Weick, P. Dendooven, M. Diwisch, F. Greiner, F. Heiße, 2733  
 2669 R. Knöbel, W. Lippert, I. Moore, I. Pohjalainen, A. Prochazka, 2734  
 M. Ranjan, M. Takechi, J. Winfield, X. Xu, First spatial  
 separation of a heavy ion isomeric beam with a multiple-  
 reflection time-of-flight mass spectrometer, Phys. Lett. B 744  
 (2015) 137–141, doi:10.1016/j.physletb.2015.03.047, URL  
<http://dx.doi.org/10.1016/j.physletb.2015.03.047>.  
 [148] J. Rissanen, V.-V. Elomaa, T. Eronen, J. Hakala, A. Jokinen,  
 S. Rahaman, S. Rinta-Antila, J. Äystö, Conversion  
 electron spectroscopy of isobarically purified trapped radio-  
 active ions, Eur. Phys. J. A 34 (2) (2007) 113, URL  
<http://dx.doi.org/10.1140/epja/i2007-10495-1>.  
 [149] E. Liénard, G. Ban, C. Couratin, P. Delahaye, D. Dur-  
 rand, X. Fabian, B. Fabre, X. Fléchar, P. Finlay,  
 F. Mauger, A. Méry, O. Naviliat-Cuncic, B. Pons, T. Porobic,  
 G. Quémener, N. Severijns, J. C. Thomas, P. Velten, Precision  
 measurements with LPCTrap at GANIL, Hyperfine Interact.  
 236 (1-3) (2015) 1–7, doi:10.1007/s10751-015-1198-9, URL  
<http://dx.doi.org/10.1007/s10751-015-1198-9>.  
 [150] M. G. Sternberg, R. Segel, N. D. Scielzo, G. Savard, J. A.  
 Clark, P. F. Bertone, F. Buchinger, M. Burkey, S. Caldwell,  
 A. Chaudhuri, J. E. Crawford, C. M. Deibel, J. Greene,  
 S. Gulick, D. Lascar, A. F. Levand, G. Li, A. P. Galván,  
 K. S. Sharma, J. V. Schelt, R. M. Yee, B. J. Zabransky,  
 Limit on Tensor Currents from  $^8\text{Li}$   $\beta$  Decay, Phys.  
 Rev. Lett. 115 (18), doi:10.1103/physrevlett.115.182501, URL  
<http://dx.doi.org/10.1103/PhysRevLett.115.182501>.  
 [151] N. Scielzo, G. Li, M. Sternberg, G. Savard, P. Bertone,  
 F. Buchinger, S. Caldwell, J. Clark, J. Crawford, C. Deibel,  
 J. Fallis, J. Greene, S. Gulick, A. Hecht, D. Lascar, J. Lee,  
 A. Levand, M. Pedretti, R. Segel, H. Sharma, K. Sharma,  
 I. Tanihata, J. Van Schelt, R. Yee, B. Zabransky, The  
 Paul trap: A radiofrequency-quadrupole ion trap for  
 precision studies, Nucl. Instrum. Methods Phys. Res.,  
 Sect. A 681 (0) (2012) 94–100, ISSN 0168-9002, URL  
<http://www.sciencedirect.com/science/article/pii/S0168900212000>.  
 [152] M. Beck, S. Coeck, V. Kozlov, M. Breitenfeldt, P. Dela-  
 haye, P. Friedag, F. Glück, M. Herbane, A. Herlert, I. Kraev,  
 J. Mader, M. Tandeci, S. Van Gorp, F. Wauters, C. Wein-  
 heimer, F. Wenander, N. Severijns, First detection and energy  
 measurement of recoil ions following beta decay in a Penning  
 trap with the WITCH experiment, Eur. Phys. J. A 47 (3) (2011)  
 1–9, ISSN 1434-6001, doi:10.1140/epja/i2011-11045-0, URL  
<http://dx.doi.org/10.1140/epja/i2011-11045-0>.  
 [153] G. Savard, J. Clark, C. Boudreau, F. Buchinger, J. Craw-  
 ford, H. Geissel, J. Greene, S. Gulick, A. Heinz, J. Lee,  
 A. Levand, M. Maier, G. Munzenberg, C. Scheidenberger,  
 D. Seweryniak, K. Sharma, G. Sprouse, J. Vaz, J. Wang,  
 B. Zabransky, Z. Zhou, Development and operation of gas  
 catchers to thermalize fusion-evaporation and fragmentation  
 products, Nucl. Instrum. Methods Phys. Res., Sect. B 204  
 (2003) 582–586, doi:10.1016/s0168-583x(02)02134-1, URL  
[http://dx.doi.org/10.1016/s0168-583x\(02\)02134-1](http://dx.doi.org/10.1016/s0168-583x(02)02134-1).  
 [154] T. Brunner, A. Lapiere, C. Andreoiu, M. Brodeur, P. Del-  
 heji, S. Ettenauer, D. Frekers, A. T. Gallant, R. Gern-  
 hauser, A. Grossheim, R. Krücken, A. Lennarz, D. Lun-  
 ney, D. Mücher, R. Ringle, M. C. Simon, V. V. Si-  
 mon, S. K. L. Sjøe, K. Zuber, J. Dilling, Trapped-ion  
 decay spectroscopy towards the determination of ground-  
 state components of double-beta decay matrix elements, Eur.  
 Phys. J. A 49 (11), doi:10.1140/epja/i2013-13142-4, URL  
<http://dx.doi.org/10.1140/epja/i2013-13142-4>.  
 [155] A. Lennarz, A. Grossheim, K. G. Leach, M. Alanssari,  
 T. Brunner, A. Chaudhuri, U. Chowdhury, J. R. C. López-  
 Urrutia, A. T. Gallant, M. Holl, A. A. Kwiatkowski,  
 J. Lassen, T. D. Macdonald, B. E. Schultz, S. Seeraji,  
 M. C. Simon, C. Andreoiu, J. Dilling, D. Frekers, In-

- Trap Spectroscopy of Charge-Bred Radioactive Ions, *Phys. Rev. Lett.* 113 (8), doi:10.1103/physrevlett.113.082502, URL <http://dx.doi.org/10.1103/PhysRevLett.113.082502>
- [156] M. Kowalska, S. Naimi, J. Agramunt, A. Algora, D. Beck, B. Blank, K. Blaum, C. Böhm, C. Borgmann, M. Breitenfeldt, L. Fraile, S. George, F. Herfurth, A. Herlert, S. Kreim, D. Lunney, E. Minaya-Ramirez, D. Neidherr, M. Rosenbusch, B. Rubio, L. Schweikhard, J. Stanja, K. Zuber, Trap-assisted decay spectroscopy with ISOLTRAP, *Nucl. Instrum. Methods Phys. Res., Sect. A* 689 (2012) 102–107, doi:10.1016/j.nima.2012.04.059, URL <http://dx.doi.org/10.1016/j.nima.2012.04.059>.
- [157] J. Stanja, C. Borgmann, J. Agramunt, A. Algora, D. Beck, K. Blaum, C. Böhm, M. Breitenfeldt, T. E. Cocolios, L. M. Fraile, F. Herfurth, A. Herlert, M. Kowalska, S. Kreim, D. Lunney, V. Manea, E. Minaya Ramirez, S. Naimi, D. Neidherr, M. Rosenbusch, L. Schweikhard, G. Simpson, F. Wienholtz, R. N. Wolf, K. Zuber, Mass spectrometry and decay spectroscopy of isomers across the  $Z = 82$  shell closure, *Phys. Rev. C* 88 (2013) 054304, doi:10.1103/PhysRevC.88.054304, URL <http://link.aps.org/doi/10.1103/PhysRevC.88.054304>.
- [158] I. Matea, J. Souin, J. Äystö, B. Blank, P. Delahaye, V. V. Elomaa, T. Eronen, J. Giovinazzo, U. Hager, J. Hakala, J. Huikari, A. Jokinen, A. Kankainen, I. D. Moore, J. L. Pedroza, S. Rahaman, J. Rissanen, J. Ronkainen, A. Saastamoinen, T. Sonoda, C. Weber, Precise half-life measurement of the  $^{26}\text{Si}$  ground state, *The European Physical Journal A* 37 (2) (2008) 151–158, ISSN 1434-601X, doi:10.1140/epja/i2008-10623-5, URL <http://dx.doi.org/10.1140/epja/i2008-10623-5>.
- [159] A. Bey, B. Blank, G. Canchel, C. Dossat, J. Giovinazzo, I. Matea, V. V. Elomaa, T. Eronen, U. Hager, J. Hakala, A. Jokinen, A. Kankainen, I. Moore, H. Penttilä, S. Rinta-Antila, A. Saastamoinen, T. Sonoda, J. Äystö, N. Adimi, G. de France, J. C. Thomas, G. Voltolini, T. Chaventré, Beta-decay branching ratios of  $^{62}\text{Ga}$ , *The European Physical Journal A* 36 (2) (2008) 121–126, ISSN 1434-601X, doi:10.1140/epja/i2008-10578-5, URL <http://dx.doi.org/10.1140/epja/i2008-10578-5>.
- [160] J. Souin, T. Eronen, P. Ascher, L. Audirac, J. Äystö, B. Blank, V. V. Elomaa, J. Giovinazzo, J. Hakala, A. Jokinen, V. S. Kolhinen, P. Karvonen, I. D. Moore, S. Rahaman, J. Rissanen, A. Saastamoinen, J. C. Thomas, Precision half-life and  $Q$  -value measurement of the super-allowed beta emitter  $^{30}\text{S}$ , *The European Physical Journal A* 47 (3) (2011) 1–7, ISSN 1434-601X, doi:10.1140/epja/i2011-11040-5, URL <http://dx.doi.org/10.1140/epja/i2011-11040-5>.
- [161] C. R. Triguero, A. M. Bruce, T. Eronen, I. D. Moore, M. Bowry, A. M. D. Bacelar, A. Y. Deo, V.-V. Elomaa, D. Gorelov, J. Hakala, A. Jokinen, A. Kankainen, P. Karvonen, V. S. Kolhinen, J. Kurpeta, T. Malkiewicz, P. J. R. Mason, H. Penttilä, M. Reponen, S. Rinta-Antila, J. Rissanen, A. Saastamoinen, G. S. Simpson, J. Äystö, Trap-assisted separation of nuclear states for gamma-ray spectroscopy: the example of  $^{100}\text{Nb}$ , *Journal of Physics G: Nuclear and Particle Physics* 39 (1) (2012) 015101, URL <http://stacks.iop.org/0954-3899/39/i=1/a=015101>.
- [162] J. Kurpeta, W. Urban, A. Plochocki, J. Rissanen, J. A. Pinston, V. V. Elomaa, T. Eronen, J. Hakala, A. Jokinen, A. Kankainen, P. Karvonen, I. D. Moore, H. Penttilä, A. Saastamoinen, C. Weber, J. Äystö, Signatures of oblate deformation in the  $^{111}\text{Tc}$  nucleus, *Phys. Rev. C* 84 (4) (2011) 044304, doi:10.1103/PhysRevC.84.044304.
- [163] D. Jordan, A. Algora, J. L. Tain, B. Rubio, J. Agramunt, A. B. Perez-Cerdan, F. Molina, L. Caballero, E. Nacher, A. Krasznahorkay, M. D. Hunyadi, J. Gulyas, A. Vitez, M. Csatos, L. Csige, J. Äystö, H. Penttilä, I. D. Moore, T. Eronen, A. Jokinen, A. Nieminen, J. Hakala, P. Karvonen, A. Kankainen, A. Saastamoinen, J. Rissanen, T. Kessler, C. Weber, J. Ronkainen, S. Rahaman, V. Elomaa, U. Hager, S. Rinta-Antila, T. Sonoda, K. Burkard, W. Hüller, L. Batist, W. Gelletly, A. L. Nichols, T. Yoshida, A. A. Sonzogni, K. Peräjärvi, A. Petrovici, K. W. Schmid, A. Faessler, Total absorption study of the  $\beta$  decay of  $^{102,104,105}\text{Tc}$ , *Phys. Rev. C* 87 (4) (2013) 044318, URL <http://link.aps.org/doi/10.1103/PhysRevC.87.044318>.
- [164] A.-A. Zakari-Issoufou, M. Fallot, A. Porta, A. Algora, J. L. Tain, E. Valencia, S. Rice, V. M. Bui, S. Cormon, M. Estienne, J. Agramunt, J. Äystö, M. Bowry, J. A. Briz, R. Caballero-Folch, D. Cano-Ott, A. Cucoanes, V.-V. Elomaa, T. Eronen, E. Estévez, G. F. Farrelly, A. R. Garcia, W. Gelletly, M. B. Gomez-Hornillos, V. Gorlychev, J. Hakala, A. Jokinen, M. D. Jordan, A. Kankainen, P. Karvonen, V. S. Kolhinen, F. G. Kondev, T. Martínez, E. Mendoza, F. Molina, I. Moore, A. B. Perez-Cerdán, Z. Podolyák, H. Penttilä, P. H. Regan, M. Reponen, J. Rissanen, B. Rubio, T. Shiba, A. A. Sonzogni, C. Weber, Total Absorption Spectroscopy Study of  $^{92}\text{Rb}$  Decay: A Major Contributor to Reactor Antineutrino Spectrum Shape, *Phys. Rev. Lett.* 115 (2015) 102503, doi:10.1103/PhysRevLett.115.102503, URL <http://link.aps.org/doi/10.1103/PhysRevLett.115.102503>.
- [165] J. L. Tain, E. Valencia, A. Algora, J. Agramunt, B. Rubio, S. Rice, W. Gelletly, P. Regan, A.-A. Zakari-Issoufou, M. Fallot, A. Porta, J. Rissanen, T. Eronen, J. Äystö, L. Batist, M. Bowry, V. M. Bui, R. Caballero-Folch, D. Cano-Ott, V.-V. Elomaa, E. Estevez, G. F. Farrelly, A. R. Garcia, B. Gomez-Hornillos, V. Gorlychev, J. Hakala, M. D. Jordan, A. Jokinen, V. S. Kolhinen, F. G. Kondev, T. Martínez, E. Mendoza, I. Moore, H. Penttilä, Z. Podolyák, M. Reponen, V. Sonnenschein, A. A. Sonzogni, Enhanced  $\gamma$ -Ray Emission from Neutron Unbound States Populated in  $\beta$  Decay, *Phys. Rev. Lett.* 115 (6), doi:10.1103/physrevlett.115.062502, URL <http://dx.doi.org/10.1103/PhysRevLett.115.062502>.
- [166] M. B. Gómez-Hornillos, J. Rissanen, J. L. Tain, A. Algora, K. L. Kratz, G. Lhersonneau, B. Pfeiffer, J. Agramunt, D. Cano-Ott, V. Gorlychev, R. Caballero-Folch, T. Martínez, L. Achouri, F. Calvino, G. Cortés, T. Eronen, A. García, M. Parlog, Z. Podolyak, C. Pretel, E. Valencia,  $\beta$ -delayed neutron emission studies, *Hyperfine Interact* 223 (1-3) (2014) 185–194, doi:10.1007/s10751-012-0617-4, URL <http://dx.doi.org/10.1007/s10751-012-0617-4>.
- [167] M. B. Gomez-Hornillos, J. Rissanen, J. L. Tain, A. Algora, D. Cano-Ott, J. Agramunt, V. Gorlychev, R. Caballero, T. Martinez, L. Achouri, J. Äystö, G. Cortes, V. V. Elomaa, T. Eronen, A. Garcia, J. Hakala, A. Jokinen, P. Karvonen, V. S. Kolhinen, I. Moore, M. Parlog, H. Penttilä, Z. Podolyak, C. Pretel, M. Reponen, V. Sonnenschein, E. Valencia, First Measurements with the BETA deLayEd Neutron Detector (BELEN-20) at JYFLTRAP, *J. Phys.: Conf. Ser.* 312 (5) (2011) 052008, ISSN 1742-6596, URL <http://stacks.iop.org/1742-6596/312/i=5/a=052008>.
- [168] P. Möller, J. Nix, K.-L. Kratz, NUCLEAR PROPERTIES FOR ASTROPHYSICAL AND RADIOACTIVE-ION-BEAM APPLICATIONS, *At. Data Nucl. Data Tables* 66 (2) (1997) 131–343, doi:10.1006/adnd.1997.0746, URL <http://dx.doi.org/10.1006/adnd.1997.0746>.
- [169] J. Agramunt, A. Garcia, A. Algora, J. Äystö, R. Caballero-Folch, F. Calvino, D. Cano-Ott, G. Cortes, C. Domingo-Pardo, T. Eronen, W. Gelletly, M. Gomez-Hornillos, J. Hakala, A. Jokinen, D. Jordan, A. Kankainen, V. Kol-

- 2865 hinen, T. Martinez, P. Mason, I. Moore, H. Penttilä,  
2866 Z. Podolyak, M. Reponen, A. Riego, J. Rissanen, B. Ru-  
2867 bio, A. Saastamoinen, J. Tain, E. Valencia, New Beta-delayed  
2868 Neutron Measurements in the Light-mass Fission Group,  
2869 Nuclear Data Sheets 120 (2014) 74 – 77, ISSN 0090-  
2870 3752, doi:<http://dx.doi.org/10.1016/j.nds.2014.07.010>, URL  
2871 <http://www.sciencedirect.com/science/article/pii/S0090375214004621>.
- [170] 2872 S. K. L. Sjue, D. Melconian, A. Garcia, I. Ahmad, A. Al-  
2873 gora, J. Äystö, V.-V. Elomaa, T. Eronen, J. Hakala, S. Hoedl,  
2874 A. Kankainen, T. Kessler, I. D. Moore, F. Naab, H. Pent-  
2875 tilä, S. Rahaman, A. Saastamoinen, H. E. Swanson, C. We-  
2876 ber, S. Triambak, K. Deryckx, Electron-capture branch  
2877 of  $^{100}\text{Tc}$  and tests of nuclear wave functions for double-  
2878 beta decays, *Phys. Rev. C* 78 (6) (2008) 064317, URL  
2879 <http://link.aps.org/abstract/PRC/v78/e064317>.
- [171] 2880 C. Wrede, S. K. L. Sjue, A. Garcia, H. E. Swanson, I. Ahmad,  
2881 A. Algora, V.-V. Elomaa, T. Eronen, J. Hakala, A. Jokinen,  
2882 V. S. Kolhinen, I. D. Moore, H. Penttilä, M. Reponen,  
2883 J. Rissanen, A. Saastamoinen, J. Äystö, Electron capture  
2884 on  $^{116}\text{In}$  and implications for nuclear structure related to  
2885 double- $\beta$  decay, *Phys. Rev. C* 87 (3) (2013) 031303, URL  
2886 <http://link.aps.org/doi/10.1103/PhysRevC.87.031303>.
- [172] 2887 S. Rahaman, V.-V. Elomaa, T. Eronen, J. Hakala, A. Joki-  
2888 nen, A. Kankainen, J. Rissanen, J. Suhonen, C. We-  
2889 ber, J. Äystö, Double-beta decay Q values of  $^{116}\text{Cd}$   
2890 and  $^{130}\text{Te}$ , *Phys. Lett. B* 703 (4) (2011) 412, ISSN  
2891 0370-2693, doi:10.1016/j.physletb.2011.07.078, URL  
2892 <http://www.sciencedirect.com/science/article/pii/S0370269311008975>.
- [173] 2893 H. Schatz, A. Aprahamian, J. Görres, M. Wiescher,  
2894 T. Rauscher, J. Rembges, F.-K. Thielemann, B. Pfeif-  
2895 fer, P. Möller, K.-L. Kratz, H. Herndl, B. Brown,  
2896 H. Rebel, rp-process nucleosynthesis at extreme tem-  
2897 perature and density conditions, *Physics Reports*  
2898 294 (4) (1998) 167 – 263, ISSN 0370-1573, doi:  
2899 [http://dx.doi.org/10.1016/S0370-1573\(97\)00048-3](http://dx.doi.org/10.1016/S0370-1573(97)00048-3), URL  
2900 <http://www.sciencedirect.com/science/article/pii/S0370157397000483>.
- [174] 2901 K. Peräjärvi, T. Eronen, V.-V. Elomaa, J. Hakala, A. Joki-  
2902 nen, H. Kettunen, V. Kolhinen, M. Laitinen, I. Moore,  
2903 H. Penttilä, J. Rissanen, A. Saastamoinen, H. Toivonen,  
2904 J. Turunen, J. Äystö, Ultra-high resolution mass separator-  
2905 Application to detection of nuclear weapons tests, *Appl.*  
2906 *Radiat. Isot.* 68 (3) (2010) 450, ISSN 0969-8043, URL  
2907 <http://www.sciencedirect.com/science/article/B6TJ0-4XY4JXT-5/2/26228003b371844001fb97e29b545174>.